GEORGIA INSTITUTE OF TECHNOLOGY
OFFICE OF RESEARCH ADMINISTRATION

RESEARCH PROJECT INITIATION

Date: January 9, 1973

Project Title: Excitation and Ionization of Ions by Electron Impact

Project No: E-21-623

Principal Investigator Dr. R. K. Feeney

Sponsor: Atomic Energy Commission, Oak Ridge Operations

Agreement Period: From Sept. 1, 1972* Until Aug. 31, 1973

*Continuation of project A-668 (EES) under Dr. John Hooper since Sept. 1, 1969

Type Agreement:
Modification No. 11 to Contract No. AT-(40-1)-3027

Amount:
$40,894 AEC Funds (E-21-623)
13,847 GIT Contribution (E-21-317)
$54,741 Total Estimated Cost

Reports Required:
Publication Preprints; Publication Reprints; Progress Report; Final Report

Sponsor Contact Person (s): (not designated by contract)
Research Contracts, Procedures & Reports Branch
Contract Division
U. S. Atomic Energy Commission
Oak Ridge Operations
P. O. Box E
Oak Ridge, Tenn. 37830 Phone (615) 483-8611

Defense Priority Rating: DO-E2 under DMS Reg. 1

Assigned to: _____

COPIES TO:

Principal Investigator	Library
School Director	Rich Electronic Computer Center
Dean of the College	Photographic Laboratory
Director, Research Administration	Project File
Director, Financial Affairs (2)	
Security-Reports-Property Office ✓	
Patent Coordinator	Other _____

RA—3 (6—71)

GEORGIA INSTITUTE OF TECHNOLOGY

OFFICE OF RESEARCH ADMINISTRATION

RESEARCH PROJECT TERMINATION

Date: November 28, 1973

Project Title: Excitation and Ionization of Ions by Electron Impact

Project No: E-21-623

Principal Investigator: Dr. R. K. Feeney

Sponsor: Atomic Energy Commission, Oak Ridge Operations

Effective Termination Date: 8/31/73

Clearance of Accounting Charges: 8/31/73*

Contract Closeout Items Remaining: Certified Expenditure Statement by 11/30/73.

* Continuation project (Contract Modification No. 12) is budgeted under account number E-21-635 effective 9/1/73.

School of Electrical Engineering

COPIES TO:

Principal Investigator
School Director
Dean of the College
Director of Research Administration
Associate Controller (2)
Security-Reports-Property Office
Patent and Inventions Coordinator
Library, Technical Reports Section
Rich Electronic Computer Center
Photographic Laboratory
Terminated Project File No. _____
Other _____

E-21-623

REPORT NO. ORO-3027-26

Technical Summary Report

Microwave Transient Response Measurements of Elastic Momentum Transfer Collision Frequency

By D.A. McPherson
R.K. Feeney
J.W. Hooper

Contract No. AT-(40-1)-3027

U.S. ATOMIC ENERGY COMMISSION
OAK RIDGE, TENNESSEE
1 December 1974

School of Electrical Engineering
GEORGIA INSTITUTE OF TECHNOLOGY
Atlanta, Georgia

NOTICE

Printed in the United States of America
Available from
National Technical Information Service
U. S. Department of Commerce
5285 Port Royal Road
Springfield, Virginia 22151
Price: Printed Copy $7.60; Microfiche $0.95

REPORT NO. ORO-3027-26

(TECHNICAL SUMMARY REPORT)

Category No. UC-34a

MICROWAVE TRANSIENT RESPONSE MEASUREMENTS OF ELASTIC MOMENTUM TRANSFER COLLISION FREQUENCY

by

D. A. McPherson

and

R. K. Feeney

Contract No. AT-(40-1)-3027

U. S. Atomic Energy Commission
Oak Ridge, Tennessee

December 1, 1974

PREFACE

This report summarizes the apparatus and techniques used and the results obtained in the course of studies conducted under Research Contract No. AT-(40-1)-3027 from the U.S. Atomic Energy Commission. The report covers the work completed on microwave transient response elastic momentum transfer collision frequency measurements through November 31, 1974.

This report is identical in text to a thesis entitled "Microwave Transient Response Measurement of Elastic Momentum Transfer Collision Frequency," which was submitted by D. A. McPherson to the faculty of the Division of Graduate Studies and Research, Georgia Institute of Technology, in partial fulfillment of the requirements for the degree Doctor of Philosophy in the School of Electrical Engineering. Having completed all other requirements, Mr. McPherson will be awarded this degree at the March, 1975 commencement of the Georgia Institute of Technology.

TABLE OF CONTENTS

Page

PREFACE ii

LIST OF TABLES. vii

LIST OF ILLUSTRATIONS viii

ABSTRACT. ix

Chapter

I. INTRODUCTION. 1

Motivation
Physical Background

Elastic Collisions
Scattering Cross Sections
Collision Frequency
Ramsauer-Townsend Effect
Effective Range Approximation

Discussion of Related Scattering Measurement Methods

Single Beam Scattering Measurements
DC Electron Swarm Scattering Measuring
Microwave Electron Swarm Scattering Measurements
The Microwave Transient Response Technique
Relevant Results of Related Methods

II. EXPERIMENTAL TECHNIQUE 15

Conceptual Basis for the Transient Response Measurements
Practical Experimental Considerations

Magnetic Field Inhomogeneity
Nonuniform Electron Density
Electron-Electron Collisions
Electron Density Temporal Decay
Microwave Pulse Time Duration

Evaluation of Experimental Parameter Relations
Technical Requirements of the Transient Response Measurements

Chapter Page

Microwave Frequency
Microwave Pulse
Attenuation
Isolation
Signal Detection, Amplification, and Processing
Magnetic Field Coil System
Plasma Production
Vacuum System
Pressure Measurement

III. EXPERIMENTAL APPARATUS 32

Vacuum System

Pumping System
Gas System
Pressure Gauges
Plasma Tube Access
Vacuum System Procedures and Performance

Electron Beam Gun and Plasma Tube
Magnetic Field Coil System
Microwave Pulse
Isolation of the Transient Response and the Microwave Pulse
Response Amplification, Detection, and Recording
Overall Sequence of Events

IV. EXPERIMENTAL PROCEDURES AND RESULTS. 49

Calibrations

Pressure Gauge
Microwave Attenuator
Microwave Crystal Detector
Logarithmic Amplifier
Oscilloscopes

Transient Response Measurement Procedures

Initial Preparation of the System
Routine Preparation of the System
Transient Response Measurement Procedures
Calculation of the Transient Response Decay Rate

Experimental Results
Discussion of Experimental Error

Systematic Errors

Chapter Page

Gas Pressure Error
Microwave Crystal Response Error
Logarithmic Amplifier Error
Oscilloscope Display Errors

Random Errors
Total Error

V. MATHEMATICAL ANALYSIS AND RESULTS 66

Discussion of the Averaging Processes

Thermal Speed Distribution
Waveguide Mode Speed Distribution

Calculation of the Transient Response Envelope
Solutions of the Integral Equations

Waveguide Mode Effects Integral Equation
Thermal Effects Integral Equation

Numerical Techniques
Results of the Corrections
Discussion of Analytical and Numerical Errors

Analytical Errors
Numerical Error
Total Error

VI. COMPARISON WITH RELATED MEASUREMENTS 88

Data of Frost and Phelps
Data of Golden
Comparison

VII. CONCLUSIONS 92

Evaluation of the Transient Response Technique
Suggestions for Improvement of the Transient Response Technique
Conclusion

APPENDIXES

I. MATHEMATICAL DERIVATION OF THE TRANSIENT RESPONSE ENVELOPE DECAY RATE RESULTING FROM ELECTRON-NEUTRAL SCATTERING 97

II. EXPERIMENTAL MEASUREMENT OF THE ELECTRON BEAM GUN GENERATED ELECTRON DENSITY 103

Appendix Page

III. MATHEMATICAL DERIVATION OF THE TRANSIENT RESPONSE ENVELOPE TAKING INTO ACCOUNT THE WAVEGUIDE MODE AND THERMAL SPEED DISTRIBUTION 115

IV. A MORE EXACT CALCULATION OF THE RESIDUAL TRANSIENT RESPONSE DECAY 122

V. SOLUTION OF THE WAVEGUIDE MODE SPEED DISTRIBUTION INTEGRAL EQUATION 126

VI. SOLUTION OF THE THERMAL SPEED DISTRIBUTION INTEGRAL EQUATION 129

VII. SAMPLE CALCULATION OF THE TRANSIENT RESPONSE DECAY RATE 132

BIBLIOGRAPHY 136

LIST OF TABLES

Table		Page
1.	Experimental Transient Response Results	60
2.	Results of the Transient Response Corrections	80
3.	Monoenergetic Collision Frequency Results	87

LIST OF ILLUSTRATIONS

Figure		Page
1.	Transient Response Data of Bruce, Crawford, and Harp	13
2.	Collision Frequency Data of Golden and of Frost and Phelps	14
3.	Pictorial Diagram of the Transient Response	16
4.	Residual Transient Response Decay	25
5.	Diagram of the Transient Response Apparatus	33
6.	Diagram of the Electron Beam Gun Assembly	37
7.	Calibration of the Schulz-Phelps Ionization Gauge	52
8.	Calibration of the Microwave Crystal Detector	54
9.	Calibration of the Logarithmic Amplifier	56
10.	Transient Response Results	61
11.	Velocity Space Representation of Transient Response	67
12.	Fundamental Waveguide Mode Excitation	70
13.	Transient Response Data with the Least Squares Polynomial Fit	75
14.	Results of the Transient Response Corrections	79
15.	Monoenergetic Collision Frequency Results	86
16.	Comparison with Frost and Phelps and with Golden	90
17.	Phase Angle Diagram	98
18.	Diagram of the Electron Density Measurement Apparatus	105
19.	Coordinate System for Density Calculation	108
20.	Results of the Electron Density Measurements	114

ABSTRACT

An experimental facility and the associated techniques have been developed for the microwave transient response measurement of the elastic momentum transfer collision frequency of electrons in gases. The apparatus and methods are applied to the determination of the electron collision frequency in argon gas as a function of electron energy in the energy range from 0.08 eV to 4 eV. This research represents the first successful measurement of the electron collision frequency in argon near the Ramsauer minimum using the microwave transient response technique.

The microwave transient response is the electromagnetic response of a weakly ionized gas, immersed in a uniform magnetic field, to a short pulse of microwave energy at the electron cyclotron frequency. Under the proper experimental conditions, the decay rate of the transient response envelope is a direct measure of the electron momentum transfer collision frequency averaged over the electron velocity distribution. The monoenergetic collision frequency is derived from the experimental data through the solution of those integral equations which analytically describe the collision frequency averaging process. The experimental error of the transient response measurements is estimated to be $\pm$ 10-15 percent. The overall error in the monoenergetic collision frequency results is estimated to be $\pm$ 25 percent.*

*The error very near the Ramsauer minimum may be substantially greater.

The collision frequencies determined in the transient response measurements agree, to within the estimated error limits, with the data derived from previous dc electron swarm measurements in the electron energy ranges on either side of the argon Ramsauer minimum. In the vicinity of the Ramsauer minimum, the transient response results agree more closely with the collision frequencies derived from the data calculated using a modified effective range theory analysis of total elastic scattering cross section measurements. The transient response measurements support the hypothesis of a lower lying Ramsauer minimum for argon than has previously been accepted.

CHAPTER I

INTRODUCTION

The primary objective of the research presented here has been to develop an experimental facility and the associated techniques for the microwave measurement of elastic scattering rates of electrons by atoms in a weakly ionized gas. The apparatus and methods have been applied to the determination of the electron-neutral atom momentum transfer collision frequency in argon gas. The collision frequency has been determined as a function of electron energy in the range from approximately thermal energy to several electron volts.

This research represents the first reliable measurement of electron momentum transfer scattering rates in argon in the electron energy range below about 1 eV using the microwave transient response technique.

Motivation

A quantitative knowledge of elastic scattering rates of electrons by atoms and molecules is basic to the understanding of the physical properties of a gas or a plasma containing neutral particles. The accurate calculation of fundamental transport parameters such as drift velocity and the diffusion and mobility coefficients require a detailed knowledge of electron scattering.[1] The energy dependence of low energy electron scattering is of particular interest in the study of electromagnetic wave propagation in the upper atmosphere[2] and in

tenuous laboratory plasmas.[3] The measurement of low energy scattering of electrons by inert gas atoms is of considerable importance as a test of the theoretical models used in the quantum physics of scattering. Substantial differences exist in experimentally measured data[4,5] which need to be resolved.

This research was undertaken to develop further the relatively new microwave transient response technique as a tool for the measurement of low energy electron scattering in gases. This technique, when developed to its fullest potential, should be a reliable, independent check of the established techniques for the determination of the electron scattering properties of gases. The measurement of elastic scattering rates in argon provides a severe test of the capabilities of the microwave transient response technique.

Physical Background

As a preface to the discussion of this research, a brief account of some important concepts and terminology from the physics of atomic collisions is presented, followed by an outline of related measurement techniques with which the present research must be compared.

Elastic Collisions

A collision between an electron and an atom is classified as elastic if the internal energy of the atomic system remains unaltered throughout the collision process. Otherwise, the collision is classified as inelastic. Inelastic processes in general can occur only when the electron energy exceeds a threshold value. For electron energies below the minimum threshold value, only collisions of the elastic type are possible. For example, in a collision between an

electron and an argon gas atom, only elastic scattering can occur for electron energies below 11.55 eV. For electron energies above this value, the atomic system may be excited to a higher energy state.

Scattering Cross Sections

The fundamental measure of the probability of the occurrence of a collision between an electron and an atom is the cross section, σ, which has the units of the area and which varies with the relative speed of the two colliding particles. The cross section is the basic link between theory and experiment. It is the most fundamental quantity which can be rigorously defined both in the classical and quantum theories of scattering and in terms of the observable parameters of an experiment.

The total elastic scattering cross section, σ_t, is the effective area presented by an atom for changing the direction of movement of an impinging electron by any amount. The elastic scattering cross section for momentum transfer, σ_m, is the effective area presented by an atom for changing the momentum of an impinging electron.

The difference between the two cross sections is, essentially, that σ_t is independent of the electron scattering angle distribution, while σ_m is not. For the case in which all scattering angles are equally probable, $\sigma_m \equiv \sigma_t$. When the scattering is predominantly small angle in nature, $\sigma_m < \sigma_t$; when the scattering is predominantly large angle, $\sigma_m > \sigma_t$.

Collision Frequency

The quantity associated with a cross section which gives the rate at which scattering occurs is the collision frequency, ν, which

has the units of sec^{-1}. The collision frequency is related to the cross section by the formula

$$\nu = N\sigma v, \tag{1}$$

where N is the number density of scatterers and v is the speed of the scattered particle relative to the scattering particle.

It is the momentum transfer collision frequency which enters directly into the calculation of the transport properties of a gas and is, therefore, from a practical standpoint, the most interesting parameter to measure experimentally. Unfortunately, the momentum transfer collision frequency and cross section have not been amenable to precise, direct measurement as have the total scattering quantities, and, as a result, there remain important uncertainties in the momentum transfer data.

Ramsauer-Townsend Effect

The first total and momentum transfer cross section measurements in argon and other heavy inert gases revealed a sharp minimum in the cross section which was unexplained by the classical theory of scattering.[6,7] This minimum was named for its co-discovers, C. Ramsauer and J. S. Townsend. The anomalous minimum was subsequently explained by the quantum theory of scattering as a destructive interference among scattered electron wave functions.

This phenomenon is most simply demonstrated by modeling the inert gas atom as a sharply defined potential well.[8] The sharpness of the well barriers is a result of the closed shell electronic configuration of the inert gas atom. If a monoenergetic beam of

electrons, with energy greater than the energy defined by the top of the well, is allowed to impinge on the well, part of the beam will be reflected by the well barriers, while the rest of the beam is transmitted. For certain combinations of well barrier strengths and beam energies the reflections at the two well barriers will destructively interfere, resulting in total transmission. This condition corresponds to the Ramsauer-Townsend effect.

Effective Range Approximation

A more sophisticated method of analyzing low energy electron scattering is the method of partial wave expansion in the effective range approximation.[9] The effective range approximation, which is valid for low electron energies, consists of expanding a transcendental function of the phase shift of the scattered electron wave function in terms of the incident electron beam momentum eigenvalue. The first two coefficients involve two parameters, called the scattering length and the effective range, which, essentially, describe the potential well approximation for the scattering atom in the presence of a perturbing beam of electrons. The problem then reduces to one of selecting a set of effective range parameters which, in some sense, best fits the potential well.

This quantum mechanical approximation has been used to convert total cross section data to momentum transfer data.[10,11] The effective range parameters are calculated from the total cross section data and used in a subsequent expansion for the momentum transfer cross section. The application of this technique is discussed in the following section and in Chapter VI.

Discussion of Related Scattering Measurement Methods

There are three major categories of electron scattering measurement techniques which have been used in the past to obtain total elastic scattering cross sections, elastic momentum transfer cross sections, and elastic momentum transfer collision frequencies in gases.

Single Beam Scattering Measurements[12]

The first category is the single beam method for measuring the total elastic cross section. The first experiment of this type was reported by C. Ramsauer in 1921.[6]

The Ramsauer technique consists of confining a low energy electron beam to a circular path by means of a magnetic field directed normally to the electron path. A monoenergetic beam of electrons is obtained by placing a series of apertures on the circular path. The radius of the circular trajectory of an electron varies with the electron energy, and so the apertures along the path of the electron beam serve as energy selectors, passing only those electrons which have energies in a range determined by the aperture size and the magnetic field strength.

The resulting, nearly monoenergetic beam is allowed to interact with the target gas in a collision chamber and is collected as it exits the chamber. The current to the collision chamber walls, which is produced by electrons scattered out of the beam, is compared to the current at the beam collector. The total cross section is calculated from the measurement of this current ratio as a function of target gas pressure.

This technique has yielded consistent results ($\pm$ 10 percent)

when used by different experimental groups for measurements at electron energies in the range from 1 eV to the energies at which inelastic processes become significant. In the earlier works, electron reflections at the apertures were determined to be a significant source of error for electron energies below 1 eV. Other errors include the effects of the variation of cathode emission properties with gas pressure, the incomplete theoretical analysis of the experiment because of the presence of the magnetic field, and incorrect pressure measurements made in those systems employing a directly connected McLeod gauge.

Most of these errors have been eliminated or mitigated in the recent Ramsauer type experiments conducted by Golden and Bandel.[13] These experiments have incorporated modern vacuum techniques and beam technology to obtain measurements down to 0.1 eV.

While the beam technique produces precise monoenergetic total cross section results, these data must be converted to momentum cross section data to be useful in practical calculations. Such a conversion has been done, earlier by O'Malley[10] using the beam data of Ramsauer and Kollath,[14] and more recently by Golden,[11] using the beam data of Golden and Bandel. The method involved in each case is to calculate the effective range parameters, described earlier in this chapter, from the total cross section and to use the parameters to calculate the momentum transfer cross section. Although the total cross section data may be accurate to within a few percent, considerable doubt is cast upon the derived cross section because of the questionable validity of the approximations involved in the

conversion process. This problem will be discussed in further detail in Chapter VI.

DC Electron Swarm Scattering Measuring[12]

The second category of elastic scattering measurements is the dc electron swarm method. This method was originated by Townsend and Bailey[7] for the measurement of momentum transfer cross sections, and was introduced almost concurrently with the work of Ramsauer. The general technique is to measure the transport characteristics of a swarm of electrons drifting through a gas under the influence of a weak electric field. Such transport characteristics are the drift velocity, diffusion and mobility coefficients, and the lateral spread of the swarm. The measured values of these quantities are compared with theoretical values computed using an assumed energy dependent momentum transfer cross section. Adjustments are made in the cross section until the calculated quantities agree with their corresponding measured values to within the experimental error.

This method has been highly refined in recent years, principally by the groups of Phelps[15] and Crompton.[16] Precise results for the momentum transfer cross sections have been reported to extremely low electron energies (0.003 eV). The basic defect in the technique is that the electron velocity distribution is not directly observable but must be calculated. The cross section which best fits the experimental data is critically dependent on the calculated electron velocity distribution.

The swarm method is especially suited to measure cross sections which vary slowly with electron energy. The error limits of the

measurements in this case are considered to be less than a few percent. When the cross section varies rapidly, however, as in the case of argon and other heavy inert gases at low electron energies, the error has not been satisfactorily determined and may be substantially greater.

Microwave Electron Swarm Scattering Measurements[12]

The third category of scattering measurements is the microwave swarm method. Microwave techniques for scattering measurements were first introduced by Brown[17] and his students in the late 1940's. The microwave method has not been highly refined and may be considered still in the developmental stage. In the typical microwave experiment,[18] a plasma is formed by periodically breaking down a gas enclosed in a microwave cavity with a high level microwave field. The ratio of the real to the imaginary parts of the complex conductivity of the afterglow plasma is obtained from experimental impedance measurements. The momentum transfer collision frequency, ν_m, is calculated by unfolding an integral expression, derived by Margeneau,[19] for the conductivity ratio in terms of the collision frequency, the microwave frequency, and the isotropic part of the electron velocity distribution, f_0. It is assumed that f_0 is the Maxwellian distribution corresponding to the temperature of the background gas. The resulting calculation yields ν_m averaged over the velocity distribution, f_0. The energy dependence of ν_m is obtained by expanding ν_m in a power series in electron speed and solving for the first few terms. The energy range over which ν_m may be calculated is varied by increasing or decreasing the temperature of the gas. Typical values

for electron energies range from 0.04 to 0.75 eV.

Some problems associated with most microwave experiments are listed below.

1. The electron loss from the microwave cavity must be taken into account, forcing the use of theoretical ambipolar diffusion calculations of uncertain validity.
2. The electric discharge method of producing the plasma introduces uncertainties in the initial electron number density distribution in the microwave cavity, in the physical makeup of the afterglow plasma, and in the excitation state of the gas atoms.
3. The exact form for f_0 is uncertain in many instances. The lack of the achievement of equilibrium has cast doubt on the results of many of the earlier experiments.
4. The value of the peak electron density necessary to obtain sufficient signal strength is generally high enough so that electron-ion and possibly electron-electron scattering cannot be ignored.
5. The simple analytical form chosen for ν_m may cause difficulties if there are actually rapid variations of ν_m with electron energy.

In addition to the measurement of the conductivity ratio, a microwave method has been introduced by Tice and Kivelson[20] for obtaining collision frequency data in the energy range around 0.005 eV from the collisional broadening of the electron cyclotron resonance. The validity of these results has been questioned because of

uncertainties introduced by the flowing gas technique employed and the effects of inelastic collisions.[12]

The Microwave Transient Response Technique

In 1967 at the Stanford Institute for Plasma Research, a more direct microwave method for measuring electron-atom momentum transfer collision frequencies in gases was originated by Bruce, Crawford, and Harp[21] which avoids many of the problems associated with the standard microwave methods. This method became known as the microwave transient response. The electron energy range for which measurements can be made extends from about thermal energy to several eV.

The original Stanford research, which led to the discovery of the microwave transient response, was directed toward the observation of the temporal plasma echo. This echo is the electromagnetic response of a plasma, immersed in a slightly inhomogeneous magnetic field, to two or more short microwave pulses near the electron cyclotron frequency. In the course of those studies, it was observed that when a single pulse was applied to a weakly ionized gas in a highly homogeneous magnetic field, the envelope of the response is a decaying exponential. The researchers recognized that the time constant of the decay is related to the electron collision frequency in the gas, and that by varying the input microwave pulse strength, it is possible to obtain measurements of the collision frequency as a function of electron energy.

Preliminary data obtained by the Stanford group for argon and neon at electron energies above 1 eV were in good agreement with the data derived from the dc electron swarm experiments of Frost and

Phelps.[15] The data below 1 eV indicated that further refinements in the apparatus were necessary. The results for argon are shown in Figure 1. A more refined experiment,[22] however, failed to significantly improve the low energy results.

The present research began as an effort to establish the capability for transient response measurements at Georgia Tech, and if possible, to accomplish the refinements necessary to produce accurate scattering data in the energy range below 1 eV.

Relevant Results of Related Methods

The relevant data for argon with which the results of this research must be compared are shown in Figure 2. The wide discrepancy between the collision frequency curves derived from the data of Frost and Phelps[15] and from Golden[11] in the vicinity of the Ramsauer minimum is typical of the dispersion of experimental measurements in argon and the other heavy inert gases. The data of Frost and Phelps and of Golden were chosen as representing the most reliable and widely accepted of the argon measurements in the energy range of the transient response measurements.

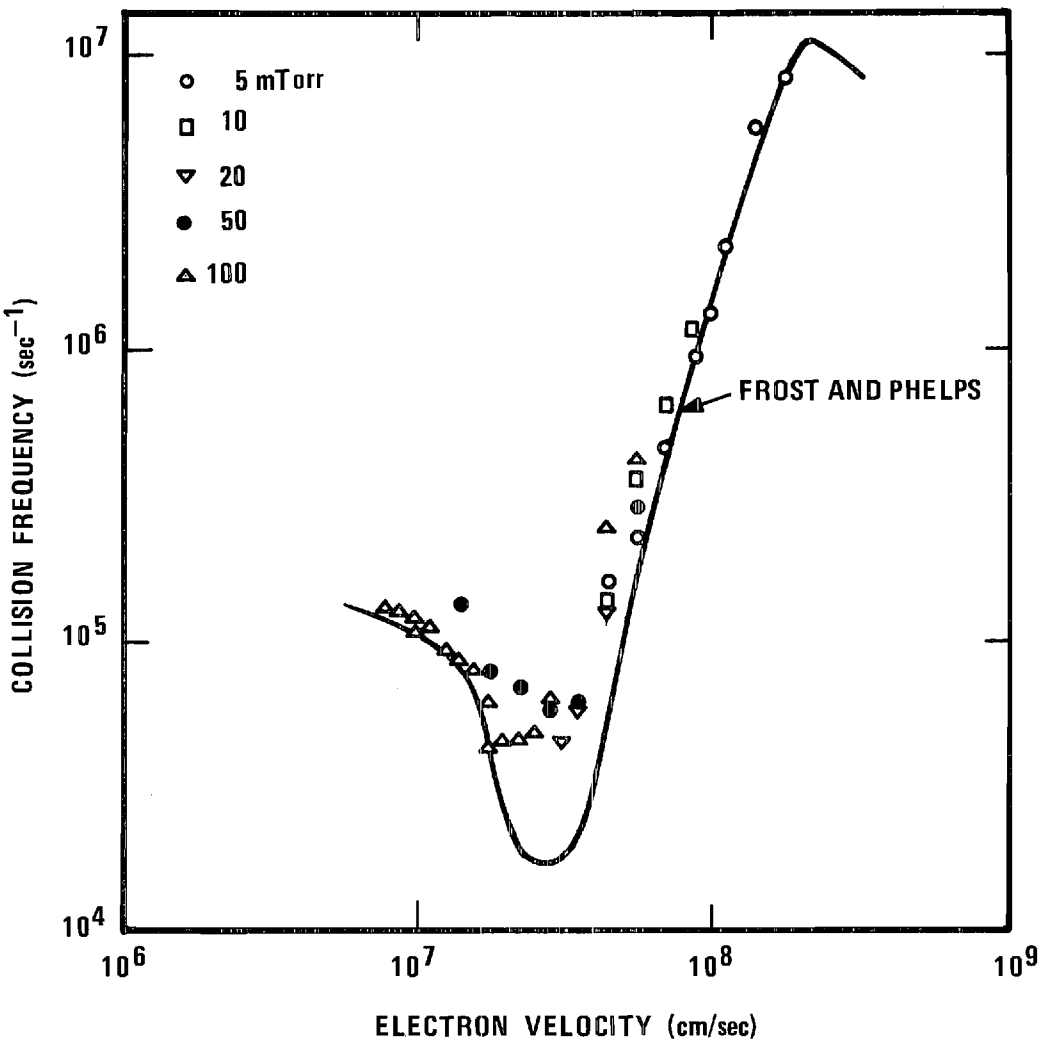

Figure 1. Transient Response Data of Bruce, Crawford, and Harp

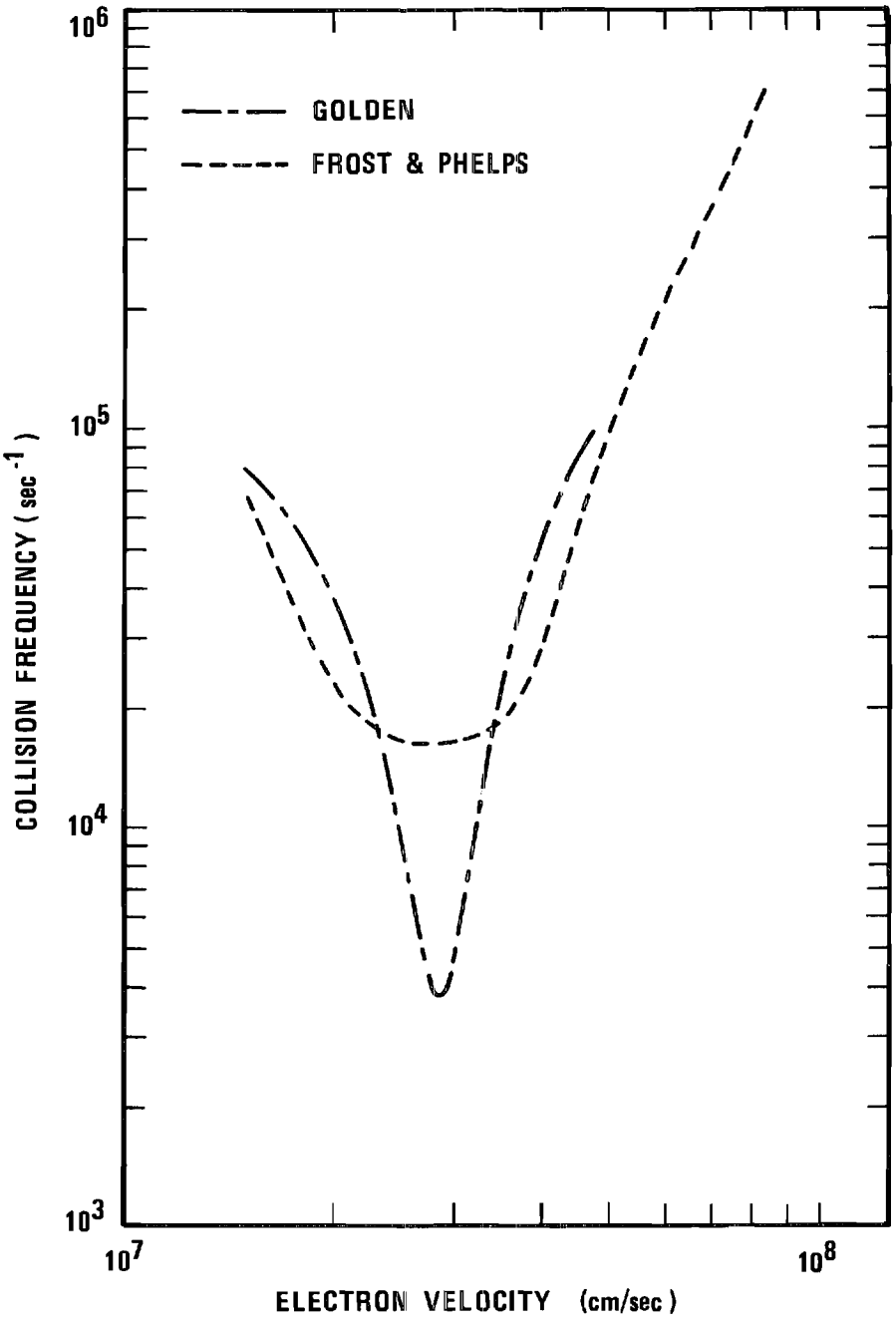

Figure 2. Collision Frequency Data of Golden and of Frost and Phelps

CHAPTER II

EXPERIMENTAL TECHNIQUE

The conceptual basis for the microwave transient response measurement of collision frequency is relatively simple. In this chapter, this basis will initially be discussed in terms of a simple, idealized experiment. In this manner, the salient features of the technique can be emphasized while the presentation remains unhampered by the detailed considerations of a realizable experiment. After the idealized experiment has been described, some nonideal considerations necessary in the design of a practical experiment will be investigated.

In the following discussion, the ionized gas will be characterized as a true plasma, i.e., an ionized gas with zero net charge contained in a volume the smallest dimension of which is large compared to a Debye length. This characterization is completely valid and allows the introduction of the basic equations of plasma dynamics.

Conceptual Basis for the Transient Response Measurements

The microwave transient response is the electromagnetic response of a plasma to a short duration microwave pulse. The plasma is immersed in a uniform, static magnetic field, and the spectrum of the pulse is centered near the electron cyclotron frequency. The physical situation is shown in Figure 3. A uniform microwave pulse is incident upon a plasma of uniform, temporally constant density in a homogeneous magnetic field of flux density B_0. The electron

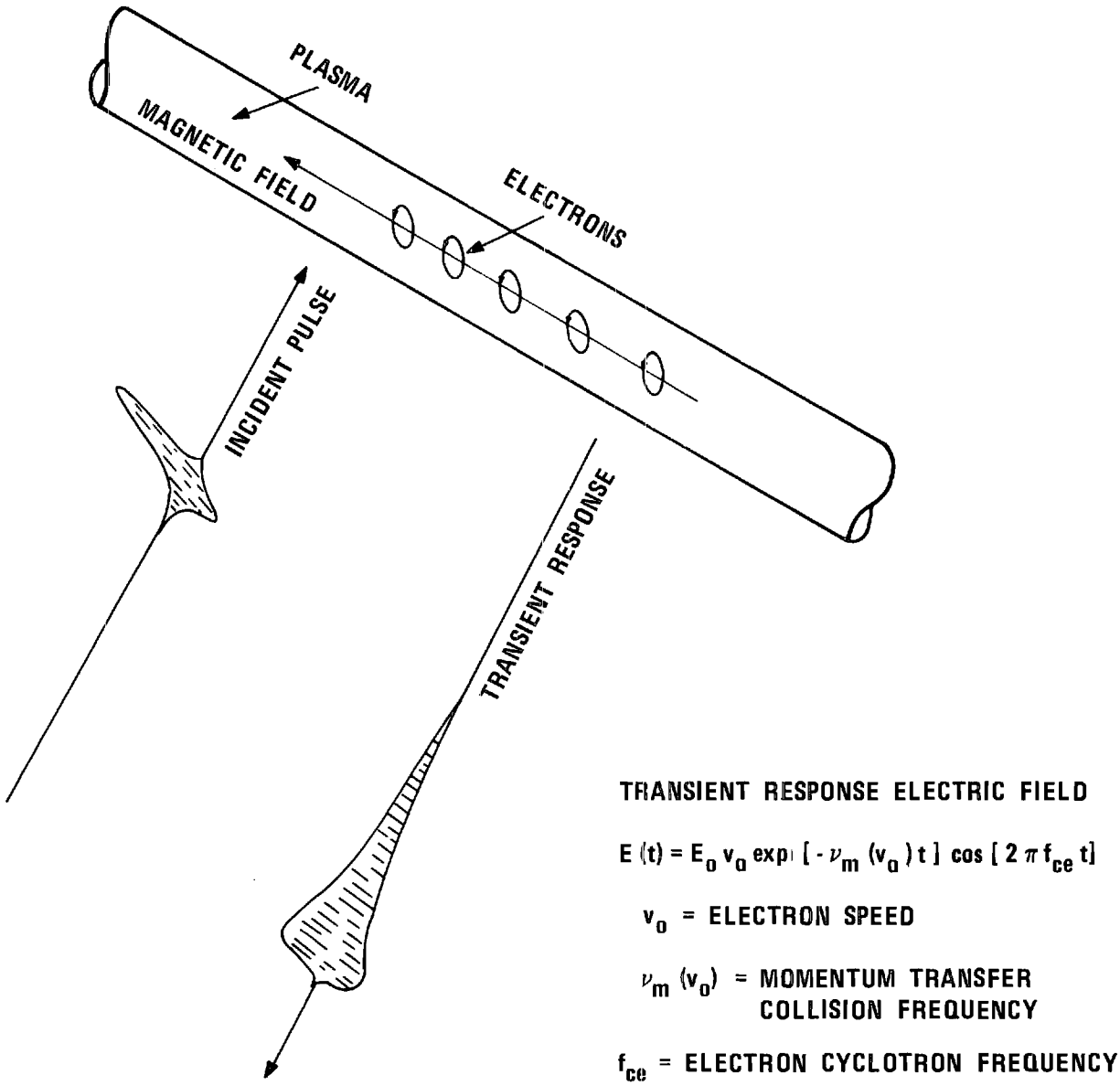

Figure 3. Pictorial Diagram of the Transient Response

cyclotron frequency is given by

$$f = \frac{1}{2\pi} \frac{eB_0}{m} \quad , \tag{2}$$

where e and m are the electron charge and mass respectively. The electric field vector of the microwave pulse is normal to the direction of the static magnetic field.

Microwave energy will be absorbed by the plasma electrons, which are accelerated into resonant oscillations about magnetic field lines with an energy determined by the microwave pulse strength. The ions and neutrals will be relatively unaffected by the pulse. After absorption of the pulse energy, the accelerated motion of the electrons about field lines causes the energy stored during the application of the pulse to begin to be reradiated, at the electron cyclotron frequency, into the surrounding medium.

Initially, the electron oscillations are phase coherent. In the absence of collisions, the electron radiation decays slowly at a rate governed by the radiation damping of the electron motion. As the electrons begin to interact with the other plasma constituents and among themselves through mutual electrostatic forces, the phases of the oscillations become randomized and the amplitude of the resultant radiation from the plasma decreases rapidly. This decaying electron radiation is the microwave transient response of the plasma.

In the present research, the microwave transient response is used to measure the elastic momentum transfer collision frequency of the electrons scattered by atoms in argon gas. Under the proper

experimental conditions, which will be discussed in the following sections, the collision frequency is related to the rate of decay of the transient response in the manner discussed below.

Let time t = 0 be the time at which the applied microwave pulse ceases and the transient response begins. At t = 0 the electrons are oscillating in phase coherent orbits with speed v_0 determined by the applied pulse strength. The frequency of the oscillations is f_{ce}. The atoms and ions are assumed to be at rest, and the electron thermal motion is neglected. The experimental conditions are assumed to be such that the predominant perturbing influence on the electron trajectories is electron-neutral elastic scattering. Departures from these idealized conditions are considered in the following sections and in the appendixes.

It is shown in Appendix I that the envelope of the transient response radiation has a form equivalent to

$$S(t) = S_0 v_0 \exp[-\nu_m(v_0)t] \cos[2\pi f_{ce} t], \tag{3}$$

where S_0 is a proportionality constant, and $\nu_m(v_0)$ is the momentum transfer collision frequency at the energy $mv_0^2/2$. It has been assumed here that the relevant plasma dimensions are small compared to a free space wavelength of the transient response radiation.

Thus, the envelope of the transient response decays exponentially with decay rate $\nu_m(v_0)$. For a monoenergetic group of electrons, the slope of the natural logarithm of the transient response envelope is proportional to the momentum transfer collision frequency. The energy variation of ν_m may be studied by varying the applied microwave

pulse strength. The collision frequency may be measured absolutely by means of a calibrated logarithmic amplifier. For argon gas, the electron energy may be determined by means of a calibrated microwave attenuator, assigning the energy at the Ramsauer minimum the value derived from previous cross section measurements.

Practical Experimental Considerations

In designing a practical experiment and correctly evaluating the resulting data, consideration must be given to departures from the idealized situation assumed in the preceding section. The following analysis presents the effects of the major deviations from the assumptions inherent in the initial discussion of the transient response concept with two exceptions: discussion of the collision frequency averaging effects of the electron thermal velocity distribution and the waveguide mode electric field distribution is delayed until Chapter V. Several key equations are derived which, together with restrictions imposed by the experimental apparatus, allow the calculation of optimum ranges for the values of the important experimental parameters. The procedure will be to calculate the minimum observable transient response decay rate for each effect independently as a function of the experimental parameters. The values of the parameters will be selected so that the greatest of these lower bounds is as small as possible, consistent with practical limitations.

Magnetic Field Inhomogeneity

In a realistic experimental situation, the magnetic field flux density, B_0, will not be completely uniform over the extent of the plasma, but will have a maximum variation, ΔB, from the nominal value.

This variation in field strength will result in a spread in the electron cyclotron frequency over the plasma, resulting in a multi-frequency decay of the transient response. The decay rate resulting from this effect may be conservatively estimated in the following manner.

The minimum bandwidth of the transient response signal, Δf, is approximately given by

$$\Delta f \lesssim f_{ce} \frac{\Delta B}{B_0} \quad . \tag{4}$$

The corresponding minimum observable transient response decay rate, α, is then

$$\alpha \lesssim \frac{1}{2\pi} f_{ce} \frac{\Delta B}{B_0} \quad . \tag{5}$$

A sufficient condition for neglecting this effect in a collision frequency measurement is that the minimum collision frequency measured should be large compared to α.

Nonuniform Electron Density

The experimental plasma will be confined in a circular cylindrical plasma tube with a diameter which is small compared to a free space wavelength of the transient response radiation. This condition implies electron number density variations which are large over a wavelength of the radiation. Such large density gradients lead to a multifrequency decay of the transient response envelope. The origin of this effect lies in the equations of plasma dynamics.

When the mutual electrostatic forces among the electrons and

ions of a plasma are considered, the high frequency resonance of the plasma electrons is found to be shifted from the free electron cyclotron resonant frequency to the "upper hybrid" resonance frequency,

$$f_0 = (f_{ce}^2 + f_{pe}^2)^{\frac{1}{2}} \quad , \tag{6}$$

where f_{pe} is the electron plasma frequency,

$$f_{pe} = \frac{1}{2\pi}\left(\frac{ne^2}{m\varepsilon_0}\right)^{\frac{1}{2}} \quad , \tag{7}$$

n being the electron number density and ε_0, the permittivity of free space.

In a plasma with finite density gradients, there will be a spread in resonance frequencies resulting from variation of the electron density. If it is assumed that the density, n, is a continuous function of position in the plasma tube and vanishes at the plasma tube boundary, and if f_{peo} is the maximum of f_{pe}, where

$$f_{peo}^2/f_{ce}^2 \ll 1 \quad , \tag{8}$$

then the spread in resonance frequencies, Δf_0, over the extent of the plasma may be approximated by

$$\Delta f_0 \lesssim f_{pe}^2/2f_{ce} \quad . \tag{9}$$

In this case, the minimum observable transient response decay rate, β, is

$$\beta \lesssim f_{pe}^2/4\pi f_{ce} \quad . \tag{10}$$

A sufficient condition for neglecting this effect in a collision frequency measurement is that the minimum collision frequency measured should be much larger than β.

A more complete analysis of upper hybrid resonance dephasing effects on transient response decay is presented in Appendix II.

Electron-Electron Collisions

It is now assumed that prior to the application of the microwave excitation pulse, the electron velocities are distributed according to a Maxwellian distribution with absolute temperature $T \simeq 300$ K. Immediately after application of the pulse, the velocity distribution will be displaced from the velocity space origin by the amount of the induced pulse velocity, v_0. The displaced distribution then begins to oscillate about the velocity space origin with frequency $f_0 \simeq f_{ce}$. Because of the spread in electron velocities, each electron, through electrostatic interactions with other electrons, will randomly gain and lose phase with respect to the centroid of the distribution. The random steps in phase result in a random walk of the electron velocities in velocity space along the circumference of the velocity space trajectories. The effect of this movement is to spread the velocities toward a state of uniform phase distribution, and, thus, to diminish the amplitude of the net electron radiation.

To estimate the time required for such dephasing, the approximate formula derived by Spitzer[23] for the "self-collision time" for electron-electron collisions may be used. The formula is

$$t_{ce} = 0.266 \frac{T^{3/2}}{n_0 \ln\Lambda} \quad , \tag{11}$$

where T is the absolute temperature in K, n_0 is the peak electron density in cm^{-3}, and $\ln\Lambda$ is a logarithmic function of n_0 and T and is tabulated by Spitzer.

The minimum observable transient response decay rate, δ, will be

$$\delta \simeq \frac{n_0 \ln\Lambda}{0.266T^{3/2}} \quad . \tag{12}$$

In order to neglect this effect, the minimum collision frequency to be measured must be much greater than δ.

The effect of electron-ion collisions is small compared to that of electron-electron collisions because of the greater relative speeds in the electron-ion case, so that the minimum observable decay rate calculated above will also suffice as a limiting value for electron-ion dephasing.

Electron Density Temporal Decay

In the time interval required to make a collision frequency measurement, the primary mechanism for electron density decay is the thermal streaming of electrons along magnetic field lines, out of the interaction region. The electrons which are lost in this manner are replaced by unexcited electrons, so that no net charge is lost, and the ions are unaffected. The loss of resonantly oscillating electrons does, however, contribute to the decay of the transient response signal.

If all electrons are assumed to have a component of velocity along the magnetic field direction equal to the mean thermal speed,

v_{th}, then, for an interaction region of length L, the density of oscillating electrons will decrease by a factor of two in a time

$$\tau = L/2v_{th} \quad . \tag{13}$$

The minimum observable transient response decay rate, γ, will be

$$\gamma \simeq 2v_{th}/L \quad . \tag{14}$$

In order to neglect this effect, the minimum collision frequency to be measured must significantly exceed γ.

The combined effects of upper hybrid dephasing, electron-electron collisions, and thermal streaming are presented in Figure 4. The dashed line represents the estimated minimum electron-neutral collisional decay rate for argon. The residual transient response decays are calculated for several values of electron density, assuming a mean thermal speed of 1×10^7 cm/sec and an interaction region length of 7 cm. The values of electron densities indicated are averages over a distribution of the form

$$n(r) = n_0\left[1 - \alpha\left(\frac{r}{r_0}\right)^p\right] \quad , \tag{15}$$

where r is the magnitude of the radius vector of the cylindrical coordinate system defined by the plasma tube, r_0 is the plasma tube radius, α and p are parameters assigned values of 0.6 and 2 respectively. The values of α and p are those determined by Vandenplas[24] as best characterizing the electron density variation of a

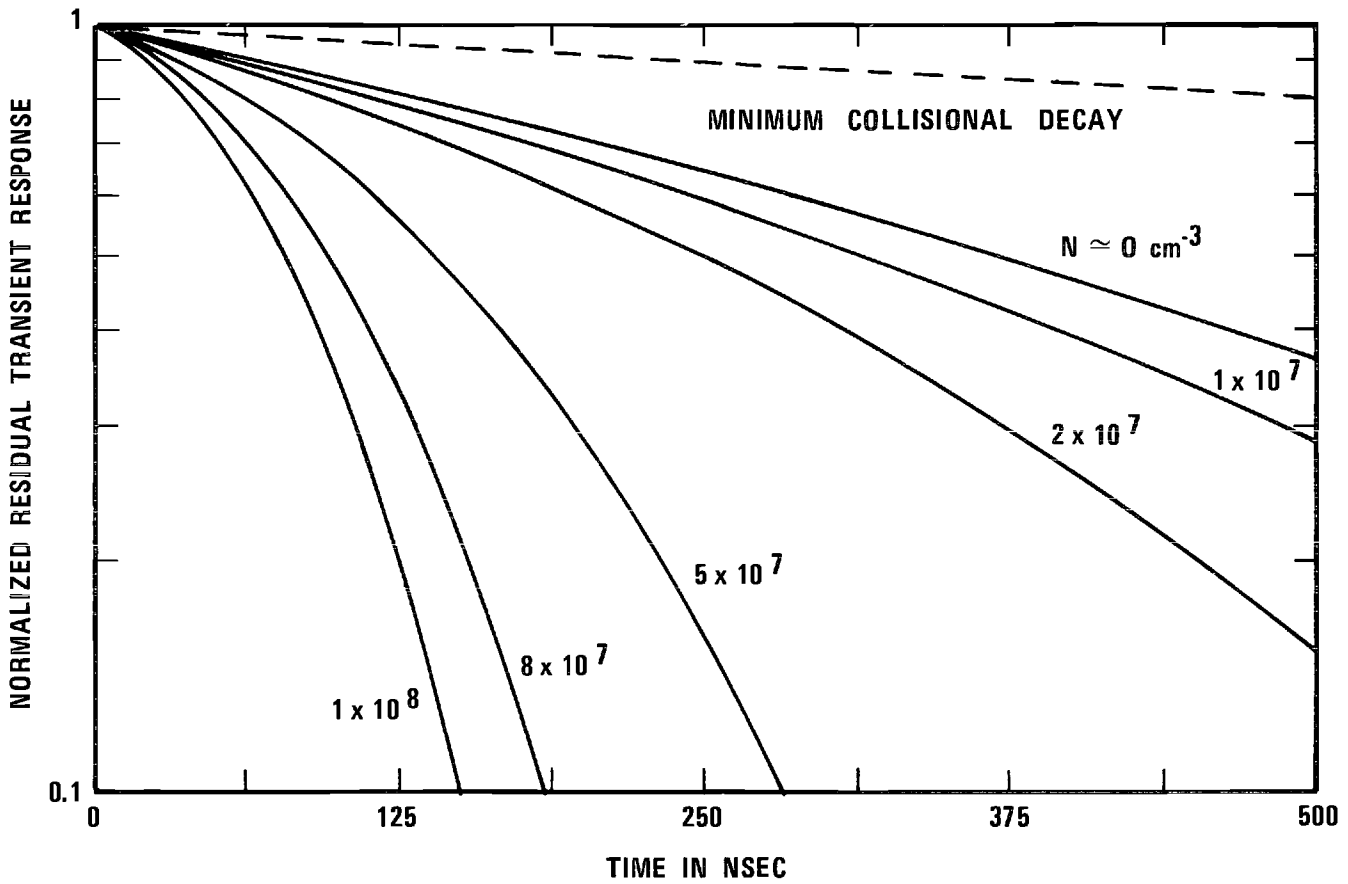

Figure 4. Residual Transient Response Decay

plasma in a cylindrical tube for a variety of electromagnetic scattering experiments.

Microwave Pulse Time Duration

In order to avoid mathematical complications, it is required that the microwave pulse time duration, T_p, be sufficiently small so that collisional dephasing of electron oscillations during the application of the pulse is negligible. If the maximum decay rate to be measured is η, then it is required that

$$T_p << \frac{1}{\eta} \quad . \tag{16}$$

Evaluation of Experimental Parameter Relations

Based on previously reported data, the electron-neutral decay rates to be measured should lie between $1x10^5$ sec^{-1} and $5x10^7$ sec^{-1} for the electron energy and gas pressure ranges appropriate for the present experimental apparatus. Using this range of decay rates, the relations derived in the preceding section can be used to determine limitations on the experimental parameters. The following requirements result from such an analysis:

1. The magnetic field inhomogeneity should be less than 0.02 percent.
2. The peak electron density should be less than $1x10^7$ cm^{-3}.
3. The microwave pulse time duration should be less than 20 nsec.

By limiting these parameters to the specified ranges, the degrading effects of the residual decay mechanisms on the transient response measurements are minimized but are not completely negligible.

The residual decay rates presented in Figure 4 indicate that, even at the very low electron densities, the effects of the residual decay mechanisms cannot be ignored. It is fortunate that the residual decay mechanisms in the transient response measurements of collision frequency are not pressure dependent. This fact allows the direct measurement of the residual decay at gas pressures low enough so that electron-neutral collisional decay is negligible. The residual decay rate may be subtracted from the total decay rate to determine the rate of electron-neutral collisional decay.

In addition to the limitations on the experimental parameters discussed above, there remains a limitation on the electron energies for which valid elastic scattering measurements are possible. The upper limit of electron energies is fixed by the onset of inelastic collision processes. For argon, this limit occurs at about 11.55 eV,[25] the energy of the first excitation level of the argon atom. The lower limit for electron energies is set by the mean thermal energy of the electrons. At room temperature this limit lies at about 0.04 eV.

As a practical matter, however, the upper electron energy limit is set by the maximum power available for the microwave excitation pulse, and the minimum is set by the maximum sensitivity of the transient response measurement system.

Technical Requirements of the Transient Response Measurements

In this section the rather unique and stringent technical requirements associated with the microwave transient response

measurement of collision frequency will be discussed. The experimental apparatus designed to realize these requirements, as nearly as possible, will be described in the next chapter.

Microwave Frequency

The microwave operating frequency for the transient response measurements must be sufficiently high so that standard waveguide components may be used, and so that the frequency dependent residual decay errors in the transient response signal will be small. The frequency must be low enough so that the waveguide size is convenient and the magnetic field coil design is practical. The frequency selected is 2.8 GHz, corresponding to a 2.8 cm x 7.6 cm waveguide cross section and a 1.0 kG magnetic field.

Microwave Pulse

The transient response measurements require a microwave excitation pulse with a peak power of several watts and a time duration of about 10 nsec. These specifications impose rather severe requirements on the switching characteristics of the pulse source and on the impedance matching and bandwidth characteristics of the associated microwave circuits to minimize reflections while conserving the pulse power.

Attenuation

The microwave pulse amplitude must be precisely and continuously variable in order to study the rapid variations in collision frequency around the Ramsauer minimum of argon. The relative calibration of electron energies requires that the attenuator be calibrated over the attenuation range of interest.

Isolation

The most formidable technical requirement of the microwave circuit is the isolation of the large amplitude input microwave pulse from the small amplitude transient response signal. It is estimated that a 1.0 W microwave pulse will produce 10 μW peak transient response signal. For the pulse and the response to be received at the measurement circuit with equal peak power, an isolation of 50 dB is required. This isolation is necessary over approximately a 100 MHz bandwidth.

Signal Detection, Amplification, and Processing

The microwave transient response signal power ranges from about 0.1 μW to 10 μW. This low level rf signal must be amplified to a sufficient level to be detected. The detection system must be calibrated so that the true envelope of the transient response signal may be recovered. The detected signal must be amplified to a high enough level for display on an oscilloscope. The total bandwidth of the receiving system must be about 100 MHz.

The amplified transient response envelope must be processed to obtain its natural logarithm. The frequency response limitation of the logarithmic element requires that the transient response envelope information be stored and retrieved for processing at a rate compatible with the logarithmic processor.

Magnetic Field Coil System

The magnetic field coil system must be capable of producing a 1.0 kG field with a homogeneity over a 1.3 cm diameter by 7.6 cm length cylindrical volume of better than 0.02 percent. The coil

system must be constructed to allow sufficient access for the waveguide components. The power supply for the coils must be regulated to prevent field variations of more than 0.1 percent during the 30 sec time interval of a complete transient response decay rate measurement.

Plasma Production

The transient response measurements require the production of a stable plasma with a density of about 1×10^{7} cm^{-3}. This should be accomplished in such a manner as to produce a minimum electron temperature, to prevent significant excitation of neutral gas atoms, and to prevent the introduction of significant impurity concentrations into the vacuum system.

Vacuum System

The vacuum system must be capable of producing a sufficiently high vacuum to insure that residual impurity concentrations, principally water vapor and vacuum pump oil adsorbed on the vacuum chamber walls during pump down, do not occur at levels high enough to produce erroneous transient response decay rates. The system must also be capable of handling the necessary argon gas loads while maintaining a constant gas pressure during the 30 sec transient response measurement period. The gas supply system must be free of significant impurity concentrations and must allow a precise, continuous control of gas pressure.

Pressure Measurement

Since the calibration of the collision frequency measurement is critically dependent on a precise, accurate knowledge of the gas pressure at the time of the transient response measurement, a highly

reliable, calibrated pressure measurement system is required. The pressure sensing element must be located in the vacuum system so that accurate measurements of the pressure in the plasma tube may be made in the presence of a continuous gas flow.

CHAPTER III

EXPERIMENTAL APPARATUS

The objective of the measurements made with the experimental apparatus to be described in this chapter is to determine the elastic momentum transfer collision frequency for electrons in argon gas as a function of electron energy over the range from approximately 0.08 eV to 4 eV.

A block diagram of the apparatus is shown in Figure 5. Initially, each functional section of the apparatus will be discussed individually. Subsequently the operation of the apparatus as a whole will be described.

Vacuum System

The main vacuum chamber consists of two Varian Associates 7.0 cm stainless steel vacuum cross fittings with copper gasket seals. The two cross fittings are mated in a vertical position providing six access ports. The gas inlet system is connected at the top port, while the pumping system is mounted at the bottom port. The two symmetrical side ports nearest the vacuum pump are used for the low pressure ionization gauge tube and the gate valve access ports. The two symmetrical side ports nearest the gas inlet system are used for the high pressure ionization gauge tube and the plasma tube access ports.

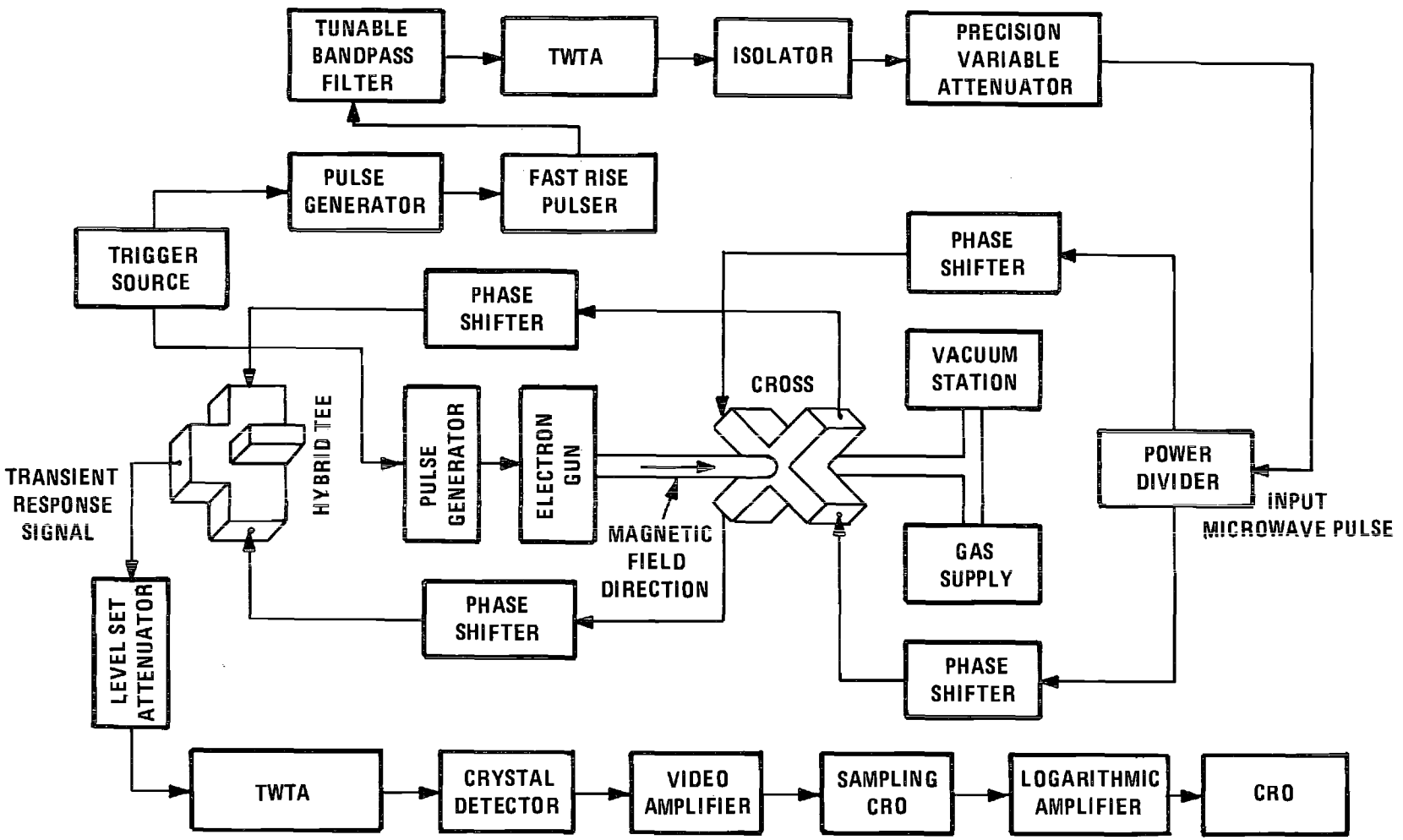

Figure 5. Diagram of the Transient Response Apparatus

Pumping System

The pumping system is composed of a 10 cm oil diffusion pump, Consolidated Vacuum Corporation type PMCS-4B, followed by a freon baffle, Consolidated Vacuum Corporation type BC-40A. The diffusion pump is charged with Dow Corning Corporation type DC-705 silicone diffusion pump fluid. A stainless steel adaptor flange is used to mate the baffle to the cross fitting. All 10 cm flanges are sealed with soft aluminum wire gaskets.

Gas System

Matheson Company prepurified grade argon gas is introduced into the vacuum system through a gas regulator, a Varian Associates high vacuum valve, and a Granville-Phillips Company variable leak valve. During the pump down of the vacuum system, the gas feed line up to the gas cylinder is evacuated to a pressure of less than $1x10^{-3}$ Torr. The line is flushed several times with argon gas, after which the high vacuum valve is closed, and the feed line filled to a pressure of 10 psig. A gate valve throttles the vacuum pump when gas is fed into the system. The gate valve and leak valve are adjusted so that the vacuum chamber is maintained at the proper pressure while a small amount of gas continuously flows through the system. This arrangement allows precise control of the gas pressure and decreases the possibility of significant gas impurity concentrations. The plasma tube and high pressure vacuum gauge tube are located at symmetrical ports, orthogonal to the gas flow, to decrease the possibility of pressure gradients between the plasma tube and the vacuum gauge tube.

Pressure Gauges

The base pressure of the vacuum system is measured with a Veeco model RG-75K Bayard-Alpert type ionization gauge tube located near the vacuum pump port. During the transient response measurements, the argon gas pressure is measured with a Granville-Phillips Company model 224 Shultz-Phelps type ionization gauge tube located at a port symmetrical to the plasma tube access port.

The main vacuum chamber is located a distance of about 50 cm from the magnetic field coil assembly to reduce the influence of the fringe magnetic field on the pressure measurements. The high pressure gauge is situated along the axis of the coil system, so that electron trajectories in the tube are not significantly affected by the field. Both gauges are enclosed with high permeability metal shields. No influence of the magnetic field on the pressure measurements was found.

Plasma Tube Access

A 3.8 cm diameter pyrex tube is connected to the plasma tube access port by means of a Kovar glass-to-metal seal and a flexible stainless steel vacuum coupling. The pyrex tube extends 25 cm, where the diameter is reduced to mate with a 19 mm quartz plasma tube. The pyrex and quartz tubes are joined with a stainless steel vacuum coupling. The seal is accomplished with two Viton O-rings. The O-rings are thoroughly degassed by baking, and a thin coat of ultra-high vacuum sealing compound is applied to each O-ring. The O-ring is necessary for the disassembly of the electron beam gun housing.

Vacuum System Procedures and Performance

The vacuum chamber, including the pyrex tube and the plasma tube seal, is baked with heating tapes to temperatures just over 100°C for a period of 24 to 36 hours during the pump down period. During this period, the electron beam gun is operated to degas the electron beam gun housing and plasma tube. After bakeout, the pressure indicated by the Veeco gauge is $2\text{-}3\times10^{-8}$ Torr with the electron gun operating. The vacuum chamber pressure consistently returns to this range when the argon gas variable leak valve is sealed between transient response measurement periods.

Electron Beam Gun and Plasma Tube

The method selected for ionization of the argon gas in the transient response measurements is the impact ionization of the gas atoms by an electron beam. The beam is directed along the axis of the plasma tube, parallel to the magnetic field direction. The advantages of this method of ionization over the high field breakdown method ordinarily used in microwave experiments are that the initial temperature of the plasma created with the electron beam should be much lower, and there is considerably less chance of creating long-lived excited atomic states. The plasma density required for the transient response measurements is sufficiently low so that plasma-electron beam instabilities, which could lead to enhanced electron scattering, should not be a problem.

A sectional view of the electron beam gun and plasma tube assembly is shown in Figure 6. The cathode is a directly heated spiral filament of tungsten wire. The filament is mechanically

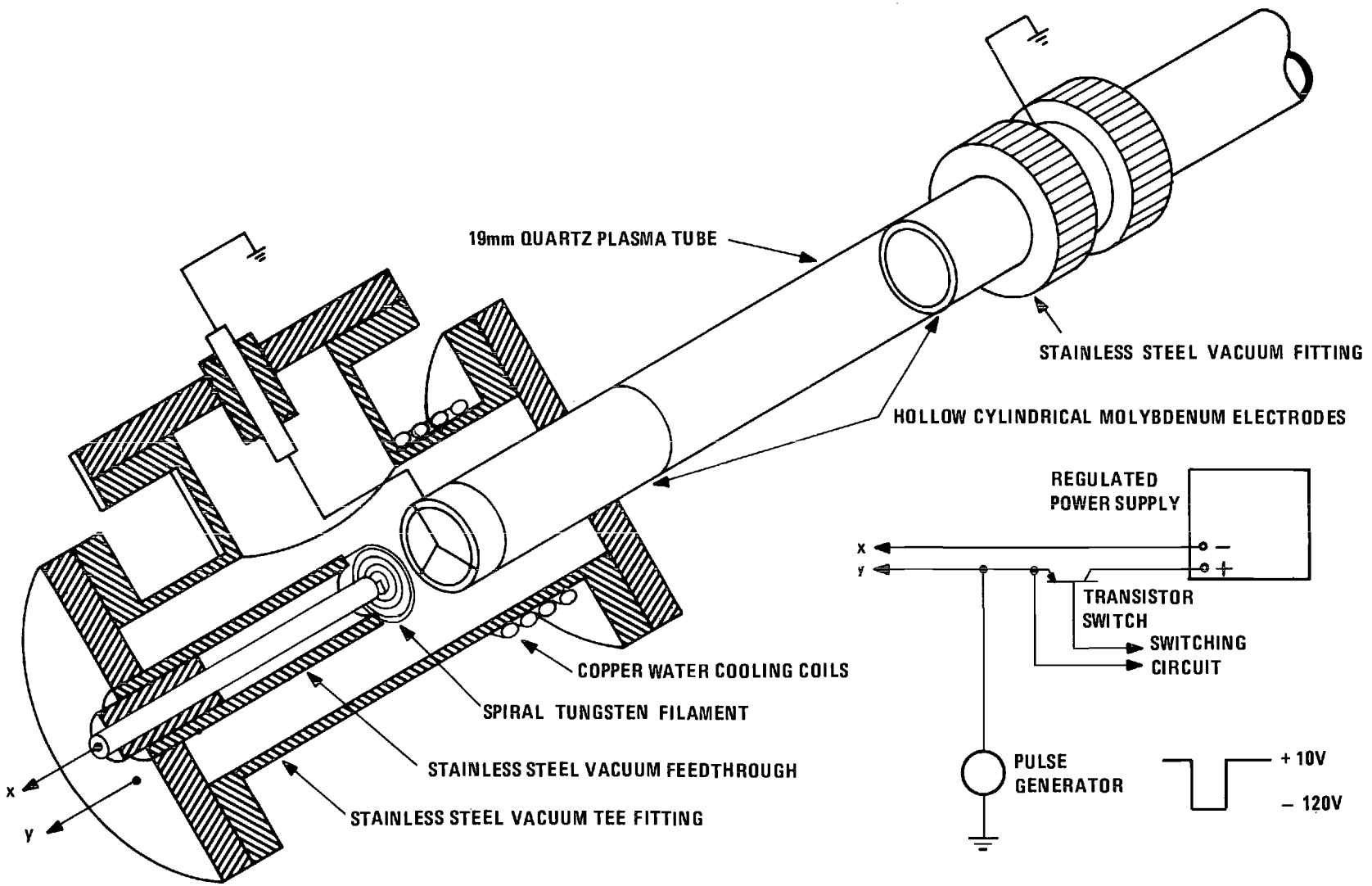

Figure 6. Diagram of the Electron Beam Gun Assembly

attached to a stainless steel vacuum feedthrough. A hollow cylindrical molybdenum anode is located directly in front of the filament and extends into the plasma tube. The anode is approximately 8.0 cm in length and limits the electron beam entering the interaction region to 1.0 cm diameter to insure that the beam edge does not strike the plasma tube wall. A hollow cylindrical collector electrode, similar in structure to the anode, is located 8.0 cm from the end of the anode and is supported by the vacuum union mating the plasma tube to the pyrex vacuum access tube. The electrodes are spaced so that they will extend up to, but do not protrude into, a standard S-band rectangular waveguide section when the plasma tube is inserted through holes in the narrow walls of the guide section. Electrical connection to the collector electrode is made through the vacuum union.

The filament and anode structures are housed in a Varian Associates 7.0 cm stainless steel tee vacuum fitting. The filament current feedthrough and support is mounted on a flange attached to one of the straight through ports of the tee. The anode voltage feedthrough is attached at the perpendicular port. The quartz plasma tube, supporting the anode, is inserted through a flange mounted to the remaining straight through port. The plasma tube is sealed to the flange with ultrahigh vacuum epoxy. The use of a Kovar metal-to-glass seal was avoided because of the detrimental effects of the magnetic Kovar material on the magnetic field homogeneity.

The filament current is supplied by a variable power supply which is regulated against line voltage variations. A transistor

switch in series with the filament supply switches the filament current off during the 1 msec period of a single transient response sample to avoid the effects of stray magnetic fields induced by the filament current.

In the assembled apparatus, the end of the plasma tube extending from the electron beam gun housing is inserted through a rectangular waveguide structure and is connected to the vacuum system. The anode and collector electrodes then are positioned symmetrically on each side of the waveguide, extending up to the walls of the guide. The entire assembly is located on the axis of the magnetic field coil structure, so that the electron beam travels parallel to the magnetic field direction.

The electron beam gun was designed to operate in the following manner. The anode and collector electrodes are maintained at ground potential. In the "off" state, the filament potential is 10 V positive. In the "on" state, the filament is switched to 120 V negative so that electrons are drawn off the filament and are directed, along magnetic field lines, down the axis of the plasma tube and through the waveguide structure. The beam travels through the collector electrode and into the pyrex tube connecting the plasma tube to the vacuum system. In the course of the operation of the electron gun, the pyrex tube quickly accumulates a negative charge because of the intersection of the tube walls with magnetic field lines. The resulting electric field tends to turn the electrons around and to direct them back, along magnetic field lines, toward the anode. As the electrons reach the anode, the filament potential repels the electrons

and redirects them back through the plasma tube. In this manner, the electrons oscillate through the plasma tube until, by collisions with gas atoms, they diffuse across magnetic field lines and are collected at the anode or collector electrodes.

In actual operation, it was found that the electron density magnitude and repeatability could be improved by allowing the anode electrode to float electrically. This arrangement appears to eliminate stray electric fields from the plasma region which cause enhanced decay of the electron density.

A detailed account of the experimental measurement of electron density produced by the electron gun is presented in Appendix II. The results of those measurements are presented in Figure 20.

Magnetic Field Coil System

The magnetic field coil system was designed and constructed at the Oak Ridge National Laboratory. The objective of the design was to produce a coil system capable of providing a 1.0 kG magnetic field, homogeneous over a 1.3 cm diameter by 7.6 cm length cylindrical volume on the axis of the system. The result of the design is an eighth order, air core coil system composed of four separate coils, each carrying the same current. A computer analysis of the system predicts a field inhomogeneity of less than 5×10^{-4} percent over the volume.

The coils are mounted on an aluminum and stainless steel support structure in such a manner that each coil may be independently raised, lowered, or canted in a vertical plane normal to the coil system axis. The horizontal position of each coil is fixed by

aluminum spacers between each pair of coils. Each coil is independently water cooled by a water channel at the inner diameter of the coil and by cooling coils attached to the outer diameter and to the back of the coil enclosure. Access to the axial magnetic field is provided at each end and through the sides of the coil structure.

The coil system produces a magnetic field of 1.0 kG for a coil current of approximately 210 A. The coil current is supplied by a Rapid Electric Company model S-585 three phase rectifier power supply. No internal regulation is provided. The magnet voltage is regulated in the following manner: the three phase ac voltage into the power supply is unbalanced by means of transformers; two phases are set at the nominal operating voltage, while the third is set lower. A single phase regulator is connected in series with the low voltage phase so that its output adds to the phase voltage, boosting that phase to approximately the same value as the other two phases at the input to the power supply. The voltage sensing connection of the single phase regulator, which normally receives a sample of the regulator output voltage, is disconnected, and an appropriately scaled sample of the magnet voltage variation is connected in its place. In this manner, any change in the magnet voltage is reflected in an amplified change in the regulator output, tending to reduce the change in the magnet voltage. This regulation scheme holds the magnetic field constant to within approximately $\pm$ 0.1 percent. Such variations are sufficiently small to permit reproducible transient response measurements. During the transient response measurement, the field variations are visually monitored to detect any variation which would render the

measurement unreliable.

In addition to the voltage regulation, some current regulation is provided by a high current choke coil connected in series with the magnet coils.

The magnetic field spatial homogeneity was measured with a nuclear magnetic resonance gauss meter. A special technique for the spatial measurement is required because of small time variations of the magnetic field caused by line voltage fluctuations. In its orthodox operation, the NMR probe adds a small sinusoidal component to the field being measured in order to generate a repetitive oscilloscope trace displaying the peak of the resonance curve. A shift in the position of the trace indicates a change in the value of the measured field. The time variations in the magnetic field of the present system cause the trace to move about in a random fashion so that no repetitive trace is possible. To overcome this problem, an incremental Hall effect gaussmeter, F. W. Bell, Incorporated model 640, is used to sample the time variations of the field. The recorder output of the Hall effect gaussmeter is applied to the X axis of the NMR gaussmeter oscilloscope. In this way, the sweep of the oscilloscope occurs in a random manner, but the resonance curve trace remains stationary on the screen. Thus, by moving the NMR probe along the axis of the magnetic field coil system, any spatial variation of the field is reflected in a shift of the resonance curve as seen on the oscilloscope. This technique proved to be highly satisfactory in measuring the axial inhomogeneity of the magnetic field. The measured inhomogeneity is less than 0.016 percent.

Microwave Pulse

The microwave pulse requirements imposed by the transient response measurements are beyond the capabilities of ordinary modulation methods. The bandwidth and power output requirements preclude the use of built-in modualtion circuits of the available microwave oscillators and amplifiers. In directly accessing the oscillator or amplifier tube grids, power output is sacrificed to obtain the necessary pulse speed. The method selected for obtaining the microwave pulse is to create a high level, fast rise time voltage pulse and to bandpass filter this pulse to obtain a short duration microwave pulse at the desired frequency. The microwave pulse is then amplified to the required power level.

A 600 V pulse with a rise time of approximately 0.5 nsec is obtained with a Spencer Kennedy Laboratories, Incorporated model 503A fast-rise pulse generator. The output of the pulser is filtered with a Texscan Microwave Products Corporation model 5VF2000/4000-10AA variable center frequency bandpass filter. The bandpass of the filter is 200 MHz. The variable filter allows an optimum center frequency to be chosen for maximum output power. The microwave pulse is amplified with a Hewlett Packard model 491C traveling wave tube amplifier. The microwave pulse derived in this manner has a center frequency of 2.8 GHz, a time duration of about 15 nsec, and a peak power of approximately 1.5 W.

A technical problem associated with producing the microwave pulse in the manner described is that the fast rise pulser output is switched with a reed relay. This type of relay has an inherent time

jitter in its operation. The time duration between the trigger and the pulse output varies in a random fashion. The relay drive and repetition frequency were adjusted to minimize this effect. The mimimun time jitter is about 10 μsec at a pulse repetition frequency of 60 Hz. This value is adequate for the transient response measurements, since the electron density measurements indicate that the density variations are small in a 10 μsec time interval at the operating pressures of the transient response measurements. Thus, the residual transient response decay rate and the transient response amplitude should remain relatively constant for repetitive measurements. The transient response decay rate resulting from electron-neutral scattering is independent of electron density.

Isolation of the Transient Response and the Microwave Pulse

As indicated in Chapter II, an isolation of approximately 50 dB between the high level microwave pulse and the low level transient response is necessary to obtain accurate transient response data. Physical limitations in the lateral access of the magnetic field coil structure preclude the employment of the more straightforward techniques for obtaining such a high level of isolation, such as the balanced hybrid tee circuit used in the Stanford experiments.[21]

The spatial limitations of the field coil structure used in the present research dictate that any standard size S-band waveguide components used to apply the microwave pulse to the plasma and to monitor the transient response signal be contained entirely in the central portion of the coil structure and be fed by coaxial lines. Use of

the next smaller size waveguide components, which could be inserted laterally into the coil structure, requires an increase in the microwave operating frequency, which would lower the available microwave pulse power and which would require an increase in magnetic field strength beyond the capabilities of the coil system.

As a result of these limitations, the microwave circuit, to be described here, was designed and implemented to obtain the necessary isolation.

The microwave pulse is passed through a Waveline type 212 precision variable attenuator and applied to the H-port of a waveguide hybrid tee. The tee acts as a power divider, dividing the pulse into two equal amplitude, equal phase components in the balancing arms of the tee. The two pulses are fed by coaxial lines through a pair of constant impedance, adjustable length coaxial lines, General Radio model 874-LK10L, and into two opposing ports of an E-plane waveguide cross, especially constructed for this experiment by Aircom, Incorporated. The cross structure is 14.9 cm, flange-to-flange, and was constructed to obtain the maximum symmetry possible. The waveguide cross is located inside the magnetic field coil structure, with the plasma tube inserted along the symmetrical axis of the cross, parallel to the direction of the magnetic field, through 20 mm diameter holes machined in the narrow wall sides of the cross. The adjustable coaxial lines are used to currect for small phase differences in the two pulse components. Tuned waveguide-to-coaxial line adaptors, Microwave Research model S40-NB, are employed at the critical transition points in the circuit to provide maximum electrical symmetry and

to minimize the reflection of microwave power.

The two pulses traverse the cross arms and are incident, from opposite directions, on the plasma tube, which is located at the center of the cross, coaxial to the line of intersection of the two H-planes of the cross. Mutual cancellation of the two pulses occurs at the orthogonal set of ports, through which the transient response signal is monitored. Small asymmetries in the cross-plasma tube structure prevent complete cancellation of the pulse components at the transient response monitoring ports. Further cancellation is accomplished by passing the two cross output signals through a second pair of adjustable coaxial lines, to adjust for small phase errors, and applying the two signals to the balancing arms ports of a second hybrid tee. The two uncancelled components of the input pulse at the monitoring ports are almost in phase opposition, while the two transient response signal components are in phase coincidence. Thus, when the monitoring port signals are fed into the balancing arms of the hybrid tee, the transient response signal components will add in phase, and the input pulse components cancel, in the H-arm of the tee. The adjustable coaxial lines are used to optimize the isolation.

This technique provides an isolation in excess of 50 dB with no plasma generated in the plasma tube. The isolation appears to increase when a plasma is present to resonantly absorb the input pulse power. Optimization of the isolation with the adjustable coaxial lines is convenient and requires no more than a few minutes.

Response Amplification, Detection, and Recording

The transient response signal is fed from the H-arm of the

hybrid tee, through a level-set attenuator, and is amplified by a Menlo Park Engineeting model 501 traveling wave tube amplifier. The attenuator is used to adjust the amplitude of the transient response to a preselected level, independent of the input microwave pulse strength. The output of the amplifier is detected with a calibrated microwave crystal detector, Hewlett Packard model 423A. The transient response envelope is then amplified with a Hewlett Packard model 460A wide band amplifier and displayed on a Hewlett Packard model 185B sampling oscilloscope with a model 187B plug-in. The transient response envelope is also displayed on a real-time oscilloscope in order to make adjustments in the level-set attenuator and the magnetic field strength. The sampling oscilloscope horizontal deflection is swept slowly to obtain an accurate display of the transient response envelope. The recorder output of the sampling oscilloscope is fed into a logarithmic amplifier, constructed with operational amplifiers and a Teledyne Philbrick Nexus model 4357 logarithmic feedback element module. An offset voltage is added to the input of the amplifier to compensate for the dc component of the sampling oscilloscope recorder output.

The output of the logarithmic amplifier is displayed on a Tektronix model 531A oscilloscope equipped with photographic capability for permanently recording the transient response decay. Photographs of the transient response signal are made with Polaroid Corporation type 107 film.

Overall Sequence of Events

The transient response measurement apparatus operates

repetitively, taking samples of the decay curve at a 60 Hz rate. The sequence of events for obtaining a single transient response sample point is as follows:

1. The electron beam gun filament current is switched off to avoid stray magnetic fields during the measurement period.
2. The electron beam is switched on for 10 μsec to form a plasma in the plasma tube.
3. After a time delay of 500 μsec, the fast-rise pulser is triggered to generate the microwave pulse.
4. The sampling oscilloscope is actuated by an appropriately advanced trigger to obtain a sample point of the transient response signal.
5. The electron beam gun filament current is switched on to heat the filament for the next sample.

The sampling oscilloscope is swept slowly so that approximately 30 sec are required to obtain a complete transient response decay curve. After processing by the logarithmic amplifier, the slope of the decay curve is measured to obtain a data point corresponding to a particular electron energy. The electron energy is changed by incrementing the microwave excitation pulse attenuation.

CHAPTER IV

EXPERIMENTAL PROCEDURES AND RESULTS

In this chapter the experimental procedures developed for obtaining accurate transient response measurements will be described, and the results of the transient response decay measurements will be presented, together with a discussion of the experimental errors. Before beginning the discussion of the main experiment, however, the procedures and results of the calibration experiments performed for the various components of the transient response apparatus will be presented.

Calibrations

In order to obtain meaningful quantitative collision frequency data from the transient response measurements, and to assess the systematic experimental error of the transient response apparatus, it is necessary to calibrate the important component parts of the measurement system against appropriate standards. The components for which it is necessary to obtain calibration measurements are the gas pressure gauge, the microwave attenuator, the microwave crystal detector, and the logarithmic amplifier.

Pressure Gauge

The absolute calibration of the collision frequency is critically dependent on the argon gas pressure measurement. The Schulz-Phelps high pressure ionization gauge used in the transient response apparatus

to measure the operating gas pressure requires calibration against an absolute pressure standard. The primary standard chosen is the McLeod gauge at the Oak Ridge National Laboratory. The procedure for the calibration measurements is to calibrate a capacitance manometer type pressure gauge against the McLeod gauge and then to transfer the calibration to the Schulz-Phelps gauge. This procedure is similar to that used by Golden and Bandel.[13]

The capacitance manometer used is the MKS Instruments, Incorporated Baratron with a 1 mm head. The McLeod gauge is the Consolidated Vacuum Corporation model GM-110. The error of the Baratron in the pressure range of the calibration is reported to be less than $\pm$ 0.15 percent of the reading, while the McLeod gauge error is reported to be no greater than 1.25 percent. The Baratron and the McLeod gauge readings agree to within 1.0 percent over their common range ($1x10^{-4}$ Torr to $1x10^{-3}$ Torr).

The high pressure limit of the vacuum system used in the calibration measurements is $1x10^{-2}$ Torr, so that measurements cannot be obtained in the pressure range used in the transient response measurements ($2x10^{-2}$ Torr to $4x10^{-2}$ Torr). The calibration is accomplished in the pressure range from $1x10^{-3}$ Torr to $1x10^{-2}$ Torr. The calibration curve is then extended to obtain the calibration at the higher pressure.

The conditions for the calibration of the Schulz-Phelps gauge are as follows: argon gas is used for the calibration, and the emission of the Schulz-Phelps gauge is set at the nominal value for argon. The high emission range is used, and the gauge tube is

degassed for approximately an hour preceding the calibration measurements.

The results of the calibration measurements are presented in Figure 7. The pressure error in the Schulz-Phelps gauge is estimated to be approximately + 5.0 percent in the $2x10^{-2}$ Torr to $4x10^{-2}$ Torr pressure range. The nominal pressure readings for the transient response measurements are corrected by this amount in the calculation of electron-neutral decay rates from the transient response data.

Microwave Attenuator

A relative calibration of the electron energies in the transient response measurements is obtained by assuming that the electron energy is directly proportional to the peak power level of the microwave excitation pulse. The pulse power is calibrated, relative to the maximum available power, by using a calibrated precision variable waveguide attenuator, Waveline model 212, to set the pulse level. A calibration curve for the attenuator is provided by the manufacturer. The error in the calibration is reported to be less than $\pm$ 0.2 dB. The calibration frequency is 3.0 GHz. The attenuation versus frequency curve for the attenuator indicates that the difference in attenuation at the calibration frequency and at the 2.8 GHz transient response operating frequency is well within the calibration error limits.

The transient response measurements, for the most part, are made at the 1.0 dB interval calibration points. Near the argon Ramsauer minimum, linear interpolation between the calibration points is used to find the exact location of the minimum.

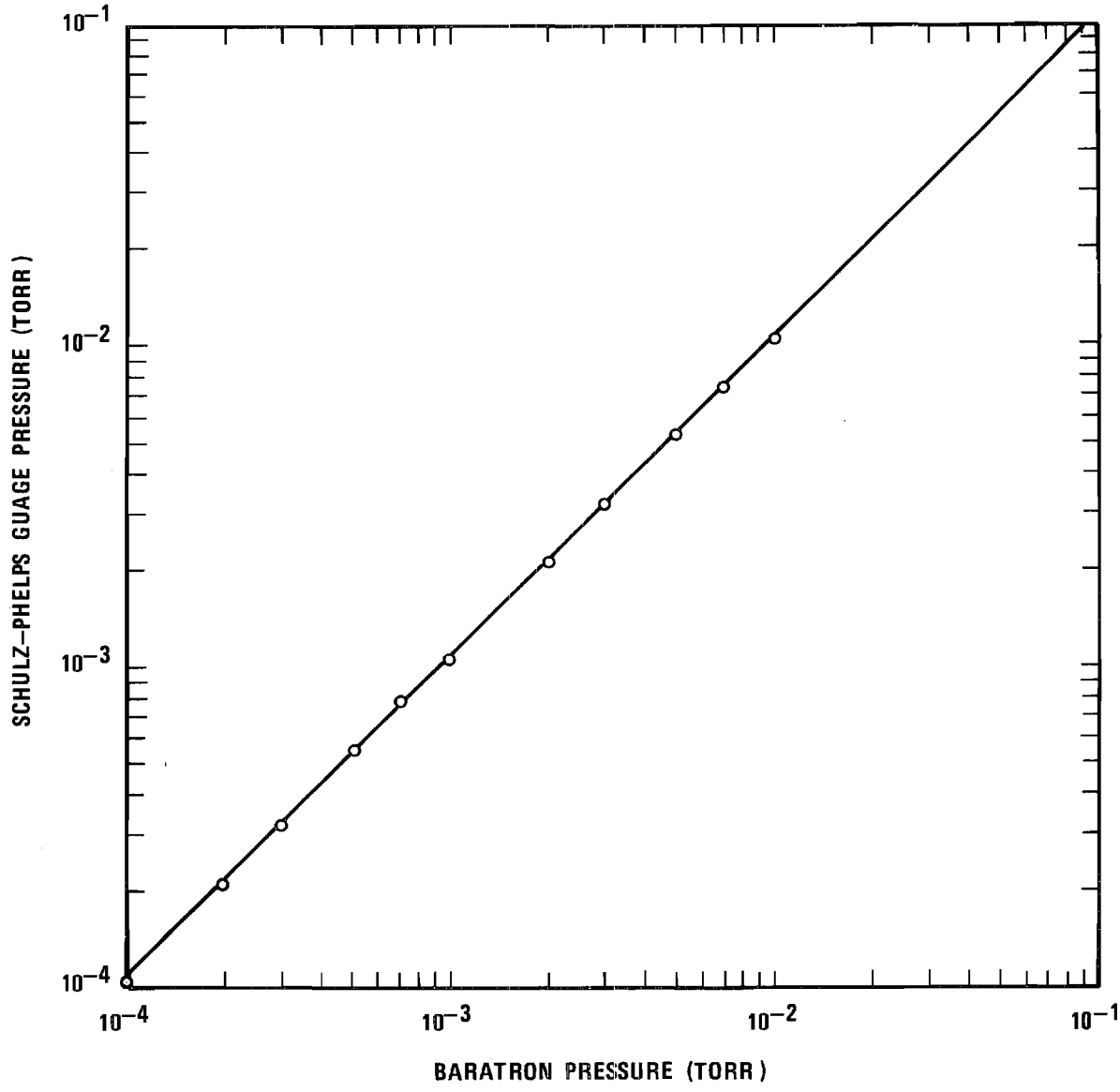

Figure 7. Calibration of the Schulz-Phelps Ionization Gauge

The absolute calibration of the electron energies is accomplished by assigning the value to the electron energy at the argon Ramsauer minimum of the monoenergetic collision frequency curve the value derived from the momentum transfer cross section data for argon reported by Golden.[11]

Microwave Crystal Detector

The recovery of the true shape of the transient response envelope requires the calibration of the nonlinear crystal detector element, which is the Hewlett Packard model 423A microwave crystal detector, used to detect the microwave transient response signal. The calibration is obtained by measuring the dc output voltage of the crystal as a function of input microwave power at the transient response operating frequency.

The procedure used for the detector calibration is to measure the output voltage of the crystal as a function of input microwave power. The microwave power level is varied with the variable attenuator discussed above. The microwave signal is modulated with a 1 kHz square wave, and the crystal voltage is displayed on a calibrated oscilloscope for measurement.

The crystal response curve is shown in Figure 8. To within the calibration error of the attenuator, the crystal has a square-law response when the output voltage does not exceed 20 mV. In the transient response measurements, the signal power level is adjusted so that the peak output voltage of the crystal lies within the square-law response range.

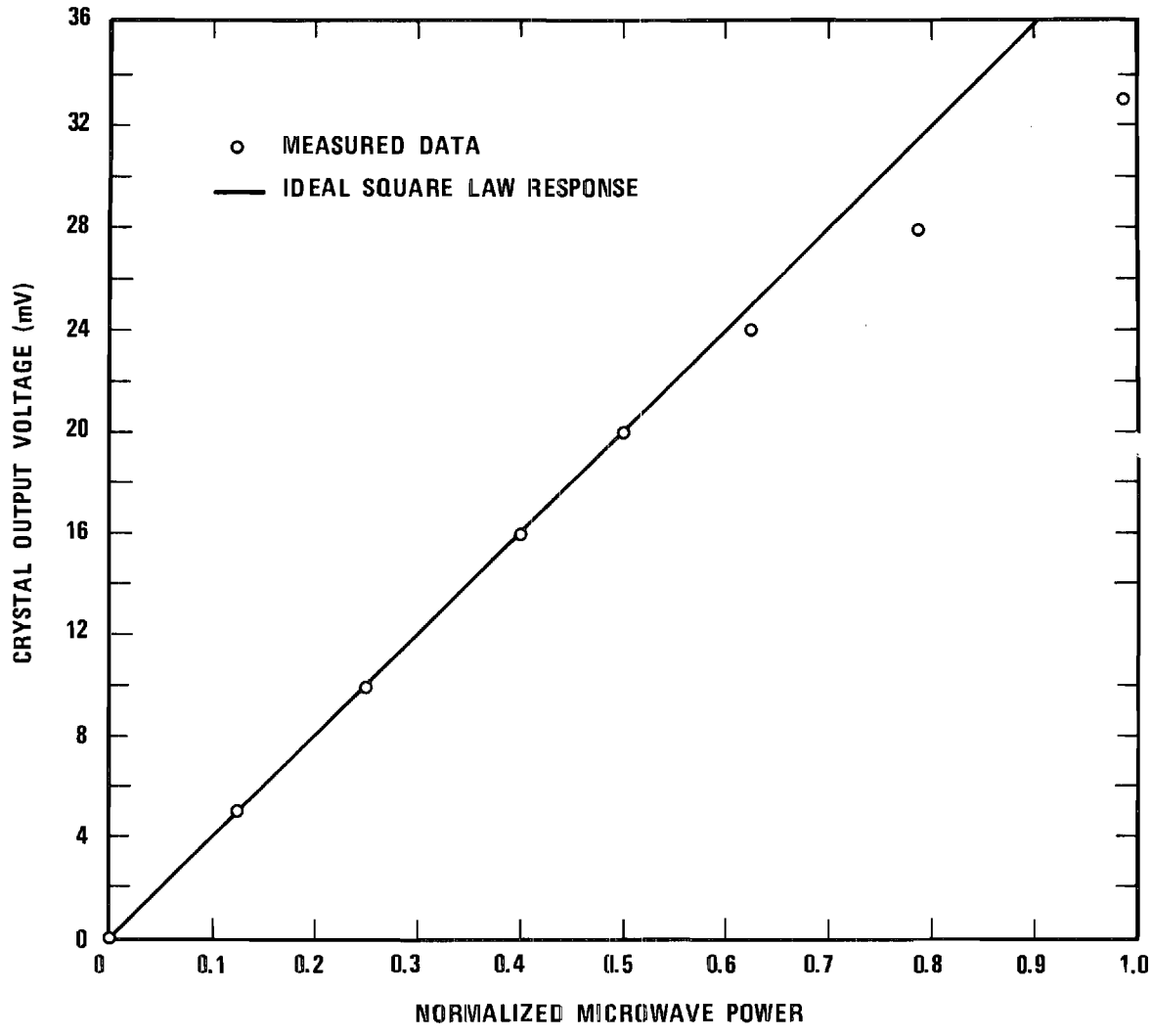

Figure 8. Calibration of the Microwave Crystal Detector

Logarithmic Amplifier

A qualitative check of the response of the logarithmic amplifier, which employs a Teledyne Phibrick Nexus model 4357 logarithmic feedback element, is obtained by applying an exponentially decaying pulse to the input of the amplifier. The amplifier output is displayed on an oscilloscope to check the linearity of the amplifier response. The amplifier exhibits no visible nonlinearity, and the slope of the output voltage trace corresponded to the time constant calculated for the exponential decay within the error limits of the calculation.

An absolute dc calibration of the logarithmic amplifier is obtained by applying a dc voltage to the input and measuring the amplifier output voltage. The input and output voltages are measured with a Hewlett Packard model 3430A digital voltmeter. The calibration curve is shown in Figure 9.

In the transient response measurements, the transient response signal amplitude is adjusted so that the output voltage of the logarithmic amplifier occurs in the range where the amplifier response deviates from a true logarithmic response by less than $\pm$ 1.0 percent.

Oscilloscopes

In addition to the above calibrations, oscilloscope sweep time and vertical amplifier gain calibrations are performed periodically for the real-time and sampling oscilloscopes used in the transient response measurements.

Transient Response Measurement Procedures

This section outlines the general procedures for the transient response measurements. The initial preparation of the system describes

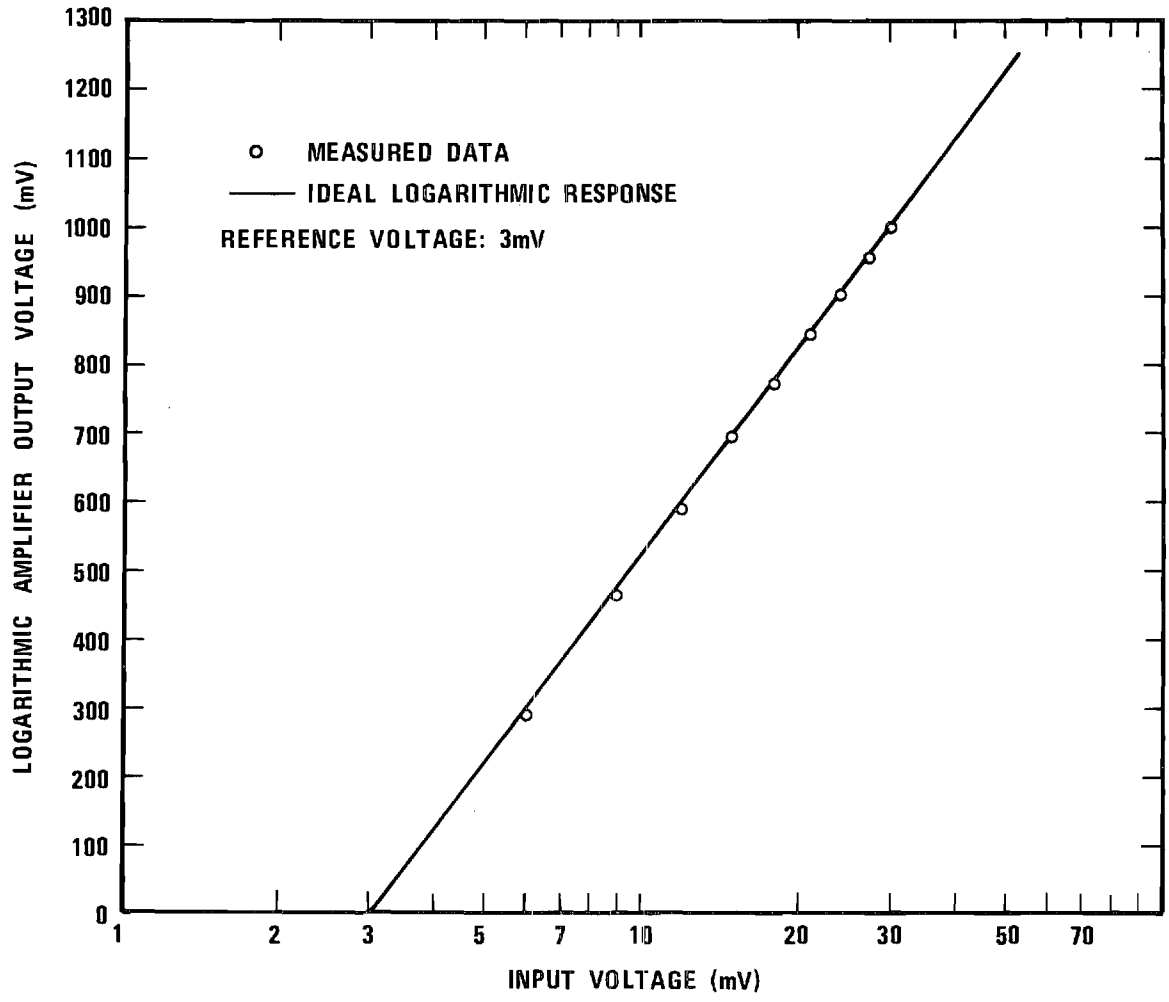

Figure 9. Calibration of the Logarithmic Amplifier

the procedures for activation of the system after being exposed to atmospheric pressure. The routine preparation described is the procedure for activation of the system before each period of data acquisition. At the conclusion of the section, the procedure for calculating the experimental results is described.

Initial Preparation of the System

Prior to the activation of the diffusion pump initiating pumpdown of the vacuum system, the system is flushed several times with argon gas to eliminate any accumulated impurity concentrations in the gas system.

During the 24-36 hour pumpdown and bakeout of the vacuum system, the electron beam gun is activated to allow outgassing and stabilization of the filament temperature to its nominal operating value. Both ionization gauge tubes are outgassed during this period.

After the bakeout period the base pressure of the system reaches $2\text{-}3\text{x}10^{-8}$ Torr with the electron beam gun filament activated.

Routine Preparation of the System

Preceding each measurement period, all electronics of the system, the magnet coils, and the electron beam gun filament are allowed several hours for warmup and stabilization. After the warmup period, argon is admitted into the system and the emission currents of the vacuum gauge tubes are checked for calibration.

Transient Response Measurement Procedures

The argon pressure is adjusted to $5\text{x}10^{-3}$ Torr for the determination of the resonant magnetic field value, and for the residual decay rate measurement. The power level of the microwave pulse is adjusted

to the predetermined value corresponding to the minimum transient response decay rate. At these values of pressure and pulse level, the measured decay rate is independent of $\pm$ 20 percent variations in the gas pressure. The magnetic field strength is adjusted to produce a minimum decay rate and the magnet voltage regulation is activated.

Under these conditions, the measured decay rate corresponds to the residual decay rate resulting from the various decay mechanisms discussed in Chapter II. The residual decay rate is recorded for the subsequent correction of the transient response data.

After measuring the residual decay, the argon gas pressure is adjusted to the transient response operating level of either 2×10^{-2} Torr, used for measurements of the higher decay rates, or 4×10^{-2} Torr, used for measurement of the lower decay rates. The electron beam gun filament current is readjusted to give the same transient response level as in the residual decay measurements. A check is made to insure the independence of the transient response minimum decay rate with respect to small changes in the electron beam gun filament current. After this check, the filament is allowed to restabilize.

The transient response measurements are made by varying the microwave pulse power and recording the corresponding transient response decay rates. The microwave attenuation adjustments are made in both increasing and decreasing attenuation sequences. The gas pressure is adjusted to the high or low value to keep the measured decay rates within an optimum measurement range.

Each individual decay measurement is made by slowly sweeping the sampling oscilloscope while the oscilloscope camera records the

output of the logarithmic amplifier. While the measurement is being made, the magnetic field variation is visually monitored with the incremental Hall effect gaussmeter. Significant variations are reflected in a nonlinear oscilloscope trace of the logarithmic amplifier output.

Before each trace is initiated, a check is made of the dc offset voltage applied to the logarithmic amplifier. The dc component of the sampling oscilloscope drifts slowly so that adjustments must be made occasionally in the dc offset compensation to insure the proper response of the logarithmic amplifier.

Calculation of the Transient Response Decay Rate

The transient response decay rate is obtained from the oscilloscope trace of the logarithmic amplifier output by measuring the slope of the response line. In the event of small deviations of the response from a straight line, the initial slope of the curve is measured. The measured slope is adjusted for the residual decay effects by subtracting the residual decay rate. The resulting slope is multiplied by the appropriate factors to account for the different logarithmic bases involved, the response characteristics of the crystal dectector, and to normalize the transient response decay to 1×10^{-3} Torr and 0°C. A sample of such calculations is presented in Appendix VII.

Experimental Results

The transient response decay rates which were derived from the experimental data in the manner discussed in the previous section are presented in Table 1 and in Figure 10.

The electron velocity absolute calibration is obtained by an

Table 1. Transient Response Data Normalized to 0°C, 1x10^{-3} Torr

Mean Electron Speed (10^7 cm/sec)	Decay Rate (10^4 sec^{-1})	Lower Error Limit (10^4 sec^{-1})	Upper Error Limit (10^4 sec^{-1})
1.50	4.07	3.66	4.49
1.68	3.68	3.31	4.05
1.89	3.41	3.06	3.75
2.12	3.16	2.83	3.48
2.38	2.68	2.40	2.97
2.67	2.37	2.13	2.61
2.99	1.65	1.48	1.82
3.36	2.43	2.18	2.69
3.77	2.70	2.43	2.98
4.23	3.70	3.32	4.08
4.74	5.44	4.89	6.00
5.32	8.50	7.63	9.36
5.97	11.3	10.2	12.5
6.70	18.0	16.1	19.9
7.52	23.7	21.3	26.2
8.44	33.5	30.0	36.9
9.46	47.5	42.5	52.4
10.62	64.8	58.1	71.6

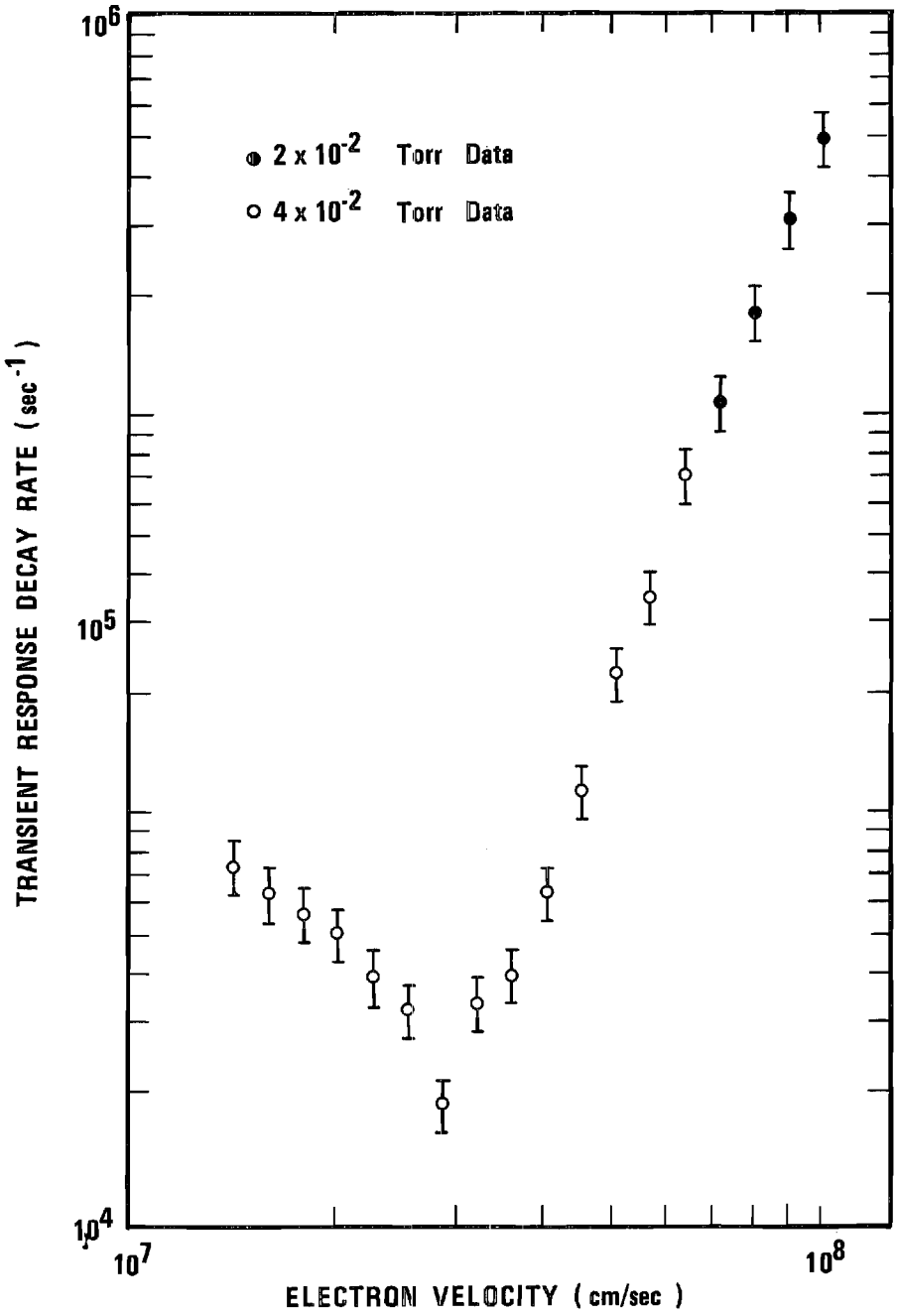

Figure 10. Transient Response Results

iterative procedure involving the mathematical corrections of the transient response data to yield monoenergetic momentum transfer collision frequency results. The calibration procedure and results of the corrections will be presented in Chapter V.

The error limits indicated by the vertical bars in Figure 10 are obtained for each data point as the sum of the estimated systematic experimental error and the 90 percent confidence limits.[26] The confidence limits are calculated from the random distribution of measured values obtained for each value of average electron speed. The data points represent the average of at least five independent measurements. The data values represented by open circles indicate measurements at 4×10^{-2} Torr argon gas pressure; those represented by solid circles indicate measurements at 2×10^{-2} Torr. Overlapping measurements at the two operating pressures indicate no significant pressure dependence of the transient response data.

The data points of Figure 10 represent the mean value of the momentum transfer collision frequency averaged over a velocity distribution determined by the electric field variation of the microwave excitation pulse over the waveguide section and the random thermal motions of the electrons. The Ramsauer-Townsend effect in argon is evident in the sharp minimum around an electron velocity value of 3×10^{7} cm/sec. The sharpness of the minimum in the averaged data indicates the presence of an extremely sharp minimum in the monoenergetic collision frequency curve.

The averaged data presented here will be unfolded to yield the monoenergetic data by the methods presented in Chapter V.

Discussion of Experimental Error

The errors in the transient response measurement are separated into two categories: random error and systematic error. The systematic errors are those due to the deviation of the performance the individual apparatus components from the ideal. These errors are not readily evident in the data but must be estimated from the calibration measurements and from manufacturer specifications. The random errors are those caused by the statistical fluctuation of the experimental conditions and by the unmeasurable interaction among apparatus components which vary as a function of the experimental conditions.

Systematic Errors

The major sources of systematic errors in the transient response measurements are those components for which the calibration measurements, outlined in the first section of this chapter, were obtained.

Gas Pressure Error. The argon gas pressure measured by the Schulz-Phelps high pressure ionization gauge is corrected according to the calibration measurements described earlier. The error in calibration is determined by the errors of the McLeod gauge, the capacitance manometer, and the estimated system error. The calibration error is conservatively estimated to be $\pm$ 3.0 percent. The accuracy of the Schulz-Phelps gauge pressure measurements, when corrected by the extended calibration curve of Figure 7, is estimated to be $\pm$ 5.0 percent.

Microwave Crystal Response Error. The calibration measurements of the microwave crystal response indicate that, for the transient response signal levels measured, the crystal follows the ideal square

law response to within the error of the calibration measurements. The calibration error is dominated by the error limits of the calibrated attenuator used in the crystal calibration. The error limits of the attenuator calibration points assigned by the manufacturer are ± 0.2 dB, corresponding to an amplitude measurement error of ± 4.7 percent. The total error of the crystal response calibration is estimated to be ± 5.0 percent.

Logarithmic Amplifier Error. The calibration measurements of the logarithmic amplifier response indicate that, for the transient response signal levels measured, the amplifier follows the ideal logarithmic response to within the error of the calibration measurements. The calibration error is the error of the digital voltmeter used to measure the input and output voltages of the amplifier. This error is conservatively estimated to be ± 1.0 percent.

Oscilloscope Display Errors. To obtain an estimate of the total systematic error, the rms average of the individual component errors is taken. This procedure is based on the assumption of the independence of each of the component errors. The resulting error obtained in this manner is ± 9.3 percent. The total systematic error assigned to the experimentally measured points is ± 10 percent.

Random Errors

Statistical fluctuations in the experimental conditions are reflected in a random distribution of data values measured at a given value of electron velocity. The estimated error from these statistical fluctuations is assigned using the 90 percent confidence limits[26] calculated from the scatter of the experimental data.

Total Error

The total experimental error at each data point is calculated as the sum of the estimated systematic error and the 90 percent confidence limits. The upper and lower error limits are listed in Table 1.

CHAPTER V

MATHEMATICAL ANALYSIS AND RESULTS

The transient response data presented in Chapter IV represent the elastic momentum transfer collision frequency averaged over a distribution of electron energies. The purpose of this chapter and the associated appendixes is to present a mathematical analysis of the collision frequency averaging and to discuss the techniques developed for the recovery of the monoenergetic collision frequency data from the averaged data.

Discussion of the Averaging Processes

The electron velocity distribution of the transient response plasma is described by a Maxwellian velocity distribution function with a nonzero mean velocity, $\vec{v}_0$, induced by the transient response microwave excitation pulse as depicted in Figure 11. During the time interval of the transient response signal, the magnitude of $\vec{v}_0$ is assumed to be constant; the direction of $\vec{v}_0$ changes harmonically with time as the electrons oscillate about magnetic field line guiding centers.

In the transient response experiment, the magnitude of the induced mean velocity of the electron distribution varies in a sinusoidal manner over the extent of the transient response plasma as a result of the fundamental waveguide mode electric field spatial distribution of the microwave excitation. This analysis begins by treating the thermal and waveguide mode distributions separately. The two distributions

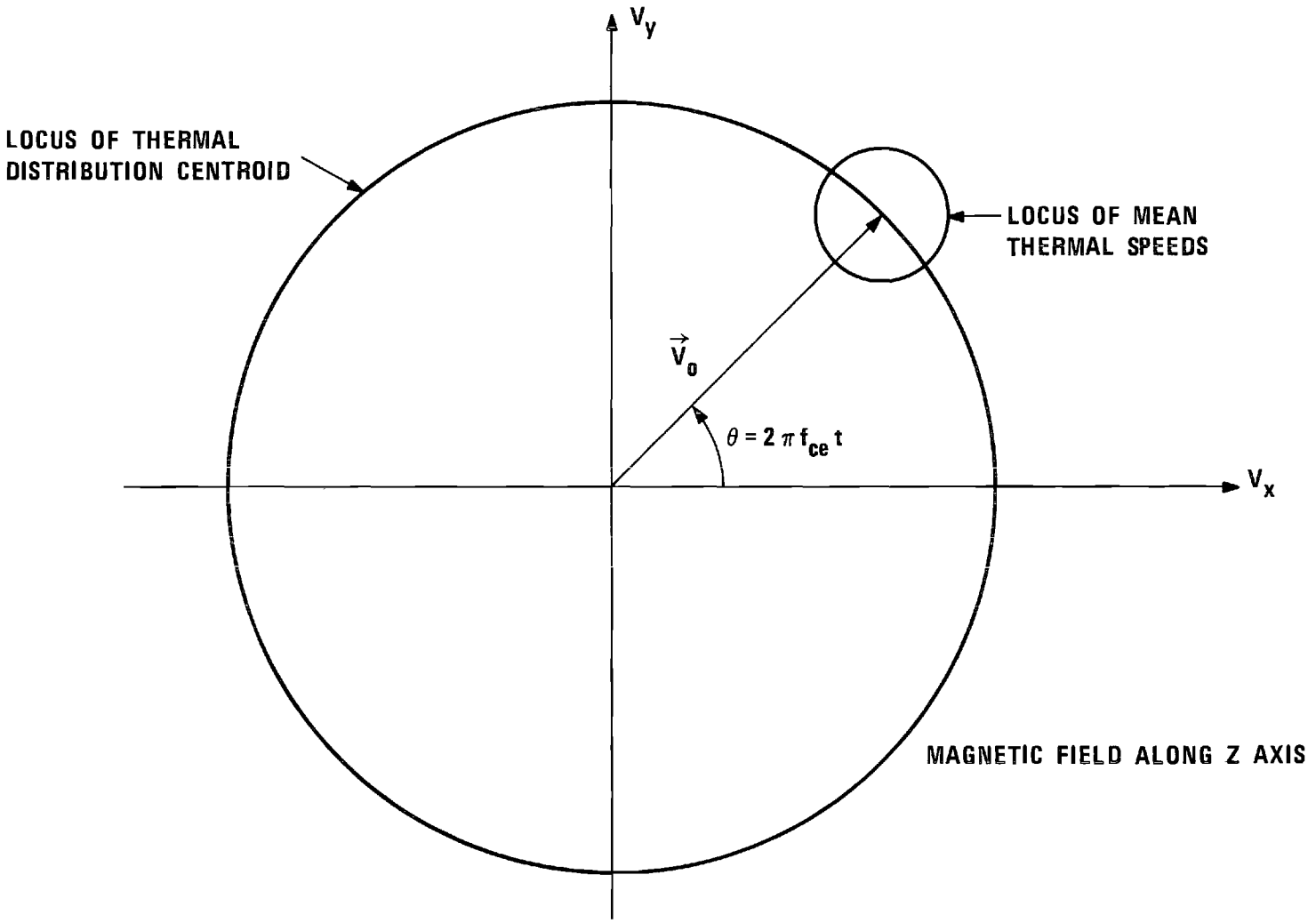

Figure 11. Velocity Space Representation of Transient Response

are then combined to calculate the transient response envelope.

Thermal Speed Distribution

Consider a tenuous plasma immersed in a uniform magnetic field, in thermal equilibrium with the background gas, and with absolute temperature T. The velocities of the plasma electrons will be distributed according to the Maxwellian velocity distribution:

$$f(v_\perp, v_{||})dv_\perp dv_{||} = \frac{1}{2\pi\sigma^2} \exp[-(v_\perp^2 + v_{||}^2)/2\sigma^2]dv_\perp dv_{||} \quad , \qquad (17)$$

where $\sigma = (\frac{kT}{m})^{\frac{1}{2}}$, k is Boltzmann's constant, m is the electron mass, $v_{\perp,||}$ are the components of velocity perpendicular and parallel, respectively, to the static magnetic field direction.

An impulsive electric field is applied to the plasma of such magnitude that an electron, which was at rest prior to the application of the pulse, is accelerated to a speed v_0 by the pulse. The speed distribution after application of the pulse is[27]

$$F_{v_0}(v)dv = \frac{v}{\sigma^2} \exp[-(v^2 + v_0^2)/2\sigma^2] \; I_0\left[\frac{vv_0}{\sigma^2}\right]dv, \; v > 0 \quad , \qquad (18)$$

where $I_0(x)$ is the modified Bessel function of the first kind, order zero.

Waveguide Mode Speed Distribution

In the transient response experiment, the plasma is contained in a cylindrical volume, the axis of which is parallel to the static magnetic field direction. The plasma volume is enclosed by a rectangular waveguide structure in such a manner that the fundamental mode

electric field is perpendicular to the static magnetic field direction, and the magnitude of the electric field varies sinusoidally across the guide section, vanishing at the narrow dimension guide walls. The plasma tube orientation is shown in Figure 12. The diameter of the plasma volume is small compared to a free space wavelength of the transient response radiation.

Let the z axis of a rectangular coordinate system be defined along the axis of the plasma volume with the origin at one narrow dimension guide wall, as shown in Figure 12. The speed of an electron, which was initially at rest at position $z = z_0$, after application of a short-duration microwave will be

$$v_0 = v_p \sin\left(\frac{\pi z_0}{a}\right), \quad 0 \leq z_0 \leq a \quad , \tag{19}$$

where v_p is the maximum pulse speed, and a is the waveguide broad dimension.

It is shown in Appendix III that the appropriately weighted distribution function for electron speeds after application of the microwave pulse, neglecting electron thermal motion, is

$$G_{v_p}(v_0)dv_0 = \frac{1}{v_p} \frac{dv_0}{(v_p^2 - v_0^2)^{\frac{1}{2}}}, \quad 0 \leq v_0 \leq v_p \quad . \tag{20}$$

Calculation of the Transient Response Envelope

Equations 18 and 20 may be combined to calculate the envelope of the transient response signal. The result, which is derived in Appendix III, is

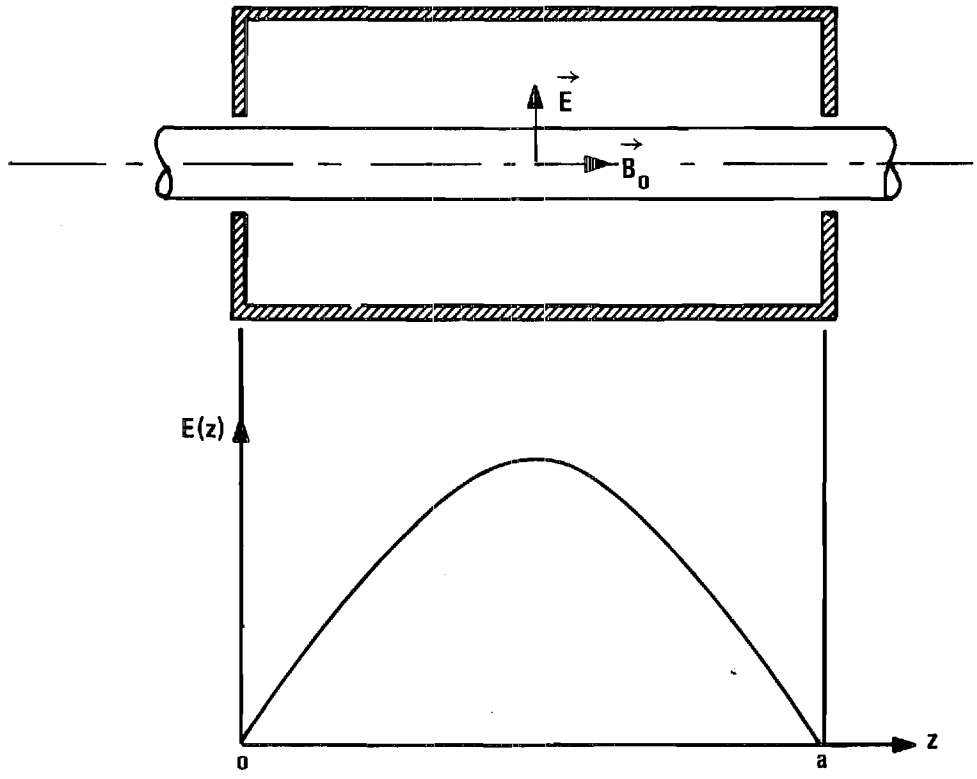

Figure 12. Fundamental Waveguide Mode Excitation

$$R_{v_p}(t) = \int_0^{v_p} G_{v_p}(v_0) \int_0^{\infty} v_\perp F_{v_0}(v) \exp[-\nu_m(v)t]dvdv_0, \quad t > 0 \quad . \tag{21}$$

The experimentally measured quantity is the slope of the logarithm of the square-law response output of the microwave crystal detector at t = 0,

$$M(v_p) = -\frac{d}{dt}\left[\log_{10}\{R^2_{v_p}(t)\}\right]\Bigg|_{t=0} \tag{22}$$

$$= -\frac{2}{\ln(10)} \frac{R'_{v_p}(0)}{R_{v_p}(0)}$$

In order to make Equation 22 mathematically tractable, it is necessary to make the following assumptions:

1. $v_\perp \simeq v$,
2. $\int_0^{\infty} vF_{v_0}(v)dv \simeq v_0$.

These assumptions are valid whenever v_0 sufficiently exceeds σ, the standard deviation of the thermal velocity distribution. The assumptions begin to become invalid at $v_0 \simeq 2\sigma$.

It is convenient to define $T(v_0)$ as

$$T(v_0) = \frac{1}{v_0} \int_0^{\infty} \frac{v^2}{\sigma^2} \nu_m(v) \exp[-(v^2 + v_0^2)/2\sigma^2] I_0\left(\frac{vv_0}{\sigma^2}\right) dv \tag{23}$$

Then,

$$S(v_p) = \frac{1}{v_p} \int_0^{v_p} \frac{v_0 T(v_0)}{(v_p^2 - v_0^2)^{\frac{1}{2}}} \, dv_0 \quad , \tag{24}$$

where

$$S(v_p) = \frac{1}{2} \ln(10) \, M(v_p) \quad . \tag{25}$$

Solutions of the Integral Equations

Equations 23 and 24 are the integral equations which must be solved to determine the monoenergetic elastic momentum transfer collision frequency, $\nu_m(v)$, from the transient response experimental data, $M(v_p)$.

Waveguide Mode Effects Integral Equation

Equation 24 is a Volterra integral equation of the first kind for the unknown function $T(v_0)$ in terms of the known function $S(v_p)$. This equation is amenable to an iterative solution, providing a boundary condition for $T(v_0)$ can be found at $v_0 = 0$.

To derive this boundary condition, Equation 23 must be examined for the case in which v_0/σ is small. In this case, the thermal speed distribution, $F_{v_0}(v)$, is relatively insensitive to changes in v_0, and, hence, $T(v_0)$ is relatively constant for small values of v_0. From Equation 24, it is evident that the constant value approached by $T(v_0)$ as $v_0 \to 0$ is given by $S(0)$.

Since the experimental data is not available to determine $S(0)$, it is necessary to extend a curve, fitted to the experimental points,

in a reasonable fashion to $v_p = 0$. The slow variation of $T(v_0)$ as $v_0 \to 0$ implies that $S(v_p)$ also varies slowly as $v_p \to 0$. Thus, the experimental curve for $S(v_p)$ may be appropriately extended using a least squares polynomial fit to the experimental data points, providing the fit curve exhibits the proper smoothness near $v_p = 0$.

It should be noted that the solution for $T(v_0)$, for $\frac{v_0}{\sigma} > 2$, is relatively insensitive to the values of $S(v_p)$ for small v_p. The value of $T(v_0)$ is determined primarily by the values of $S(v_p)$ and its derivatives, as determined by the least squares fit curve, in a relatively small v_p interval near v_0, and the portion of the $S(v_p)$ curve for $v_p > 2\sigma$ is insensitive to the value chosen for $S(0)$.

The iterative solution for $T(v_0)$, which is derived in Appendix V, is obtained by dividing the range $0 \leq v_0 \leq v_p$ into small increments in which $T(v_0)$ is assumed to be constant. The solution is

$$T(v_p) = \frac{1}{(v_p^2 - v_{p-1}^2)^{\frac{1}{2}}} \left[v_p S(v_p) - \sum_{i=0}^{p-1} T(v_i)\{(v_p^2 - v_{i-2}^2)^{\frac{1}{2}} - (v_p^2 - v_{i-1}^2)^{\frac{1}{2}}\} \right], \tag{26}$$

$$p = 1,2,3,\ldots,N,$$

where v_N corresponds to the maximum value of v_p attained in the measurements.

The implementation of Equation 26 on a digital computer requires that a sufficiently smooth function be obtained to fit the experimental data values for $S(v_p)$. The fitted curve is required to possess continuous derivatives to all orders, since the solution is sensitive to abrupt changes in derivative values. The seventh order

least squares polynomial fit to the transient response data is shown in Figure 13. The order of the fitting polynomial is selected by a subjective judgment of the accuracy and smoothness of the fit. Lower order fits fail to sufficiently fit the individual data points, while higher order fits exhibit oscillations between data points.

It is evident that the polynomial fit of Figure 13 is not exact in the region near the transient response data minimum; the fitting curve does not reflect the true sharpness of experimental data minimum. This fit, however, is considered to be the best analytical representation available for the measured data over the complete experimental range. The values calculated for the monoenergetic collision frequency near the Ramsauer minimum, using the fit curve of Figure 13, must be considered as estimates which probably exceed the true value, assuming the measured transient response data is correct, within the estimated error limitation, in this region. Further consideration of the errors incurred by the use of the polynomial fit will be considered in the section of this chapter dealing with analytical and numerical errors.

Thermal Effects Integral Equation

After the solution of Equation 24 has been obtained, the values calculated for $T(v_0)$ may be used in the solution of Equation 25 for $\nu_m(v)$, the monoenergetic elastic momentum transfer collision frequency. Equation 25 is a Fredholm integral equation of the first kind, and its solution is derived in Appendix VI.

The solution is

$$\nu_m(v) = \frac{1}{v} H_{vx} \left\{ \exp[\sigma^2 x^2/2] \; H_{xv} \; \{vT(v)\} \right\} \quad . \tag{27}$$

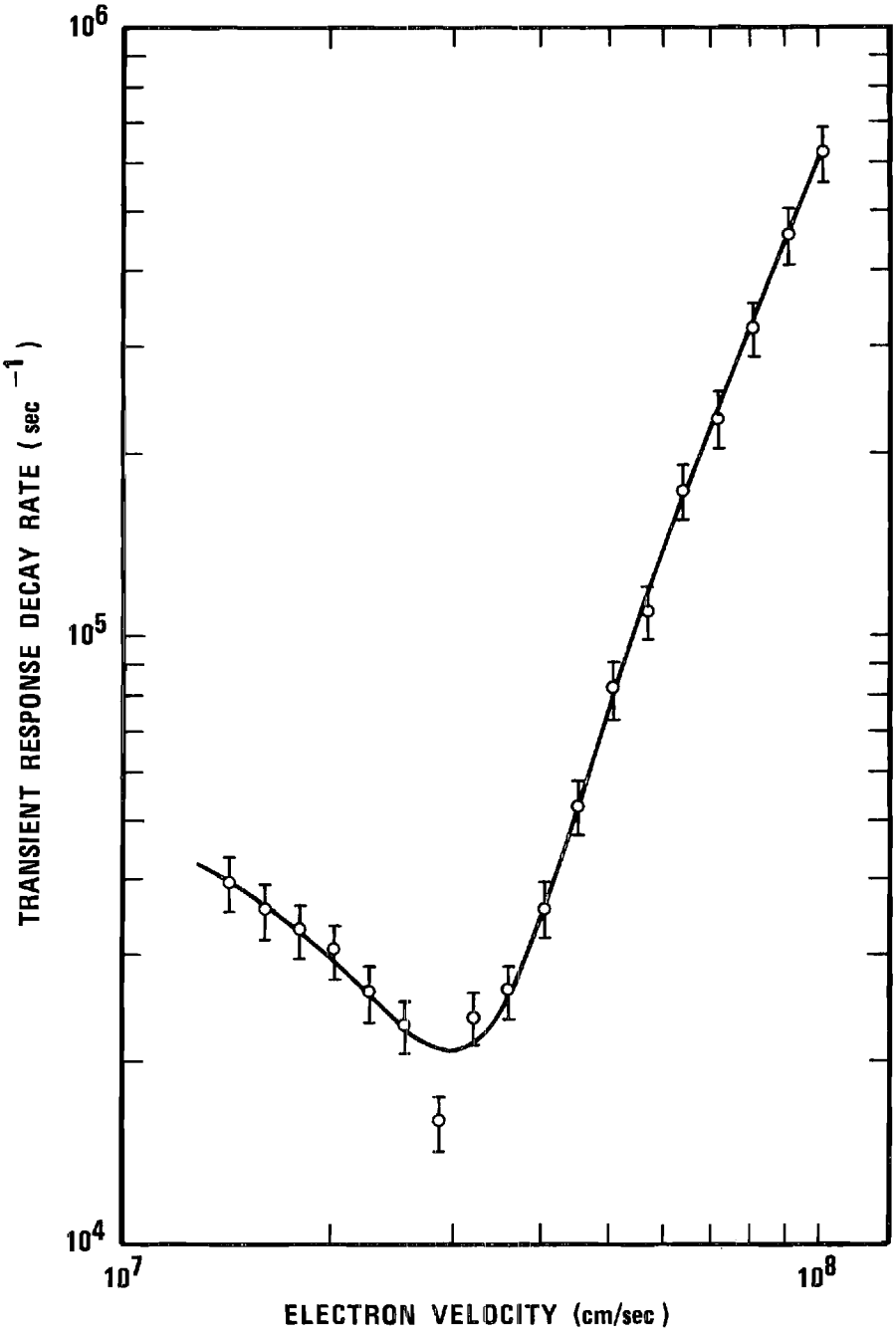

Figure 13. Transient Response Data with the Least Square Polynomial Fit

$H_{xy}\{f(y)\}$ is the Hankel transform of f(y) given by

$$H_{xy}\{f(y)\} = \int_0^\infty yf(y)\ J_0(xy)dy \quad , \tag{28}$$

where $J_0(u)$ is the Bessel function of the first kind, order zero.

Numerical Techniques

The integral equation solutions, Equations 26 and 27, are evaluated digitally, using a Univac 1108 computer. In all cases, single precision arithmetic is used, and the integrals are performed using the trapezoidal integration technique. Various checks are performed to ensure the validity of the numerical techniques involved, such as integrating known functions, varying the integration step size, and performing analytically known integral transformations.

As discussed earlier, the experimental data are analytically represented by a seventh order least squares fit polynomial. The solution of Equation 24, $T(v_0)$ is represented analytically by an eighth order polynomial mean square fit for the evaluation of Equation 27. Again, the order of the fitting curve was selected by a subjective, visual determination of the best available fit. In the case of obtaining a fit for $T(v_0)$, however, the least squares fit curve follows the values calculated for $T(v_0)$ very closely and is considered to be an accurate representation of $T(v_0)$ over its entire range.

The major numerical problem which occurs in the digital evaluation of Equation 27 involves the exponential factor $\exp[\sigma^2x^2/2]$. The Hankel transform spectrum of vT(v) is sufficiently broad so that its product with the exponential becomes very large at large values of x.

Thus, any numerical errors in the calculation of the high frequency components of vT(v) are greatly amplified in the solution for $\nu_m(v)$.

The numerical procedure employed to overcome this problem is to substitute for the exponential factor a factor of the form

$$\frac{\varepsilon + 1}{\varepsilon + \exp[-\sigma^2 x^2/2]} \quad , \tag{29}$$

where ε is a small, positive number. The value of ε is incremented toward increasingly smaller values until errors are detected in the solutions for ν_m. These errors occur in the form of oscillations in the calculated values for ν_m, the amplitude of which increase with decreasing values of ε. It is fortunate that, in the calculations performed, the solution for $\nu_m(v)$ stabilizes before the onset of significant oscillations. The limit for ε in these calculations is $\varepsilon = 0.03$.

The polynomial fit curve obtained for the calculated values of T(v) must be augmented for use in the calculation of Equation 27 by appending an exponentially decreasing tail to the polynomial fit curve. This is necessary for the convergence of the integration of T(v) and for the limitation of high frequency components in the Hankel transform spectrum of vT(v). The procedure is to determine the first value of v, beyond the fitting range, for which the polynomial fit curve takes on zero slope, i.e., the point at which the fit curve begins to decrease. The second derivative of the fit curve is calculated at this point, and a decreasing exponential curve is spline fitted to the polynomial curve, matching the polynomial in amplitude and the values of the first and second derivatives. The polynomial curve, with the appended

exponential curve, is then used in the calculation of Equation 27. The range of integration is extended to a value of v for which the exponential has decreased beyond significance. This procedure has no effect on the values calculated for ν_m, since $\nu_m(v)$ is calculated only for values of v far from the range of influence of the appended portion of the T(v) curve.

The accuracy of both integral equation solutions are checked by performing the respective inverse integrations to obtain the known function in each case from the solution calculated for the unknown function. The results of these checks will be discussed in the section dealing with analytical and numerical errors.

Results of the Corrections

The solutions calculated for Equations 23 and 24 are shown in Figure 14, along with the polynomial fit to the original experimental data. The numerical results are presented in Table 2. All results are normalized to a pressure of 1×10^{-3} Torr and 0°C temperature.

The solution for the waveguide mode effects correction, T(v), exhibits the expected result that the magnitude of the transient response curve is increased where the slope of transient response curve is positive, and decreased where the slope is negative. The thermal effects correction, as expected, predominantly influences the low energy portion of the curve, while the higher energy portion is relatively unaffected.

The calibration of the velocity axis is obtained by iteratively adjusting the transient response data curve along the velocity axis until the minimum of the calculated $\nu_m(v)$ curve coincides with the

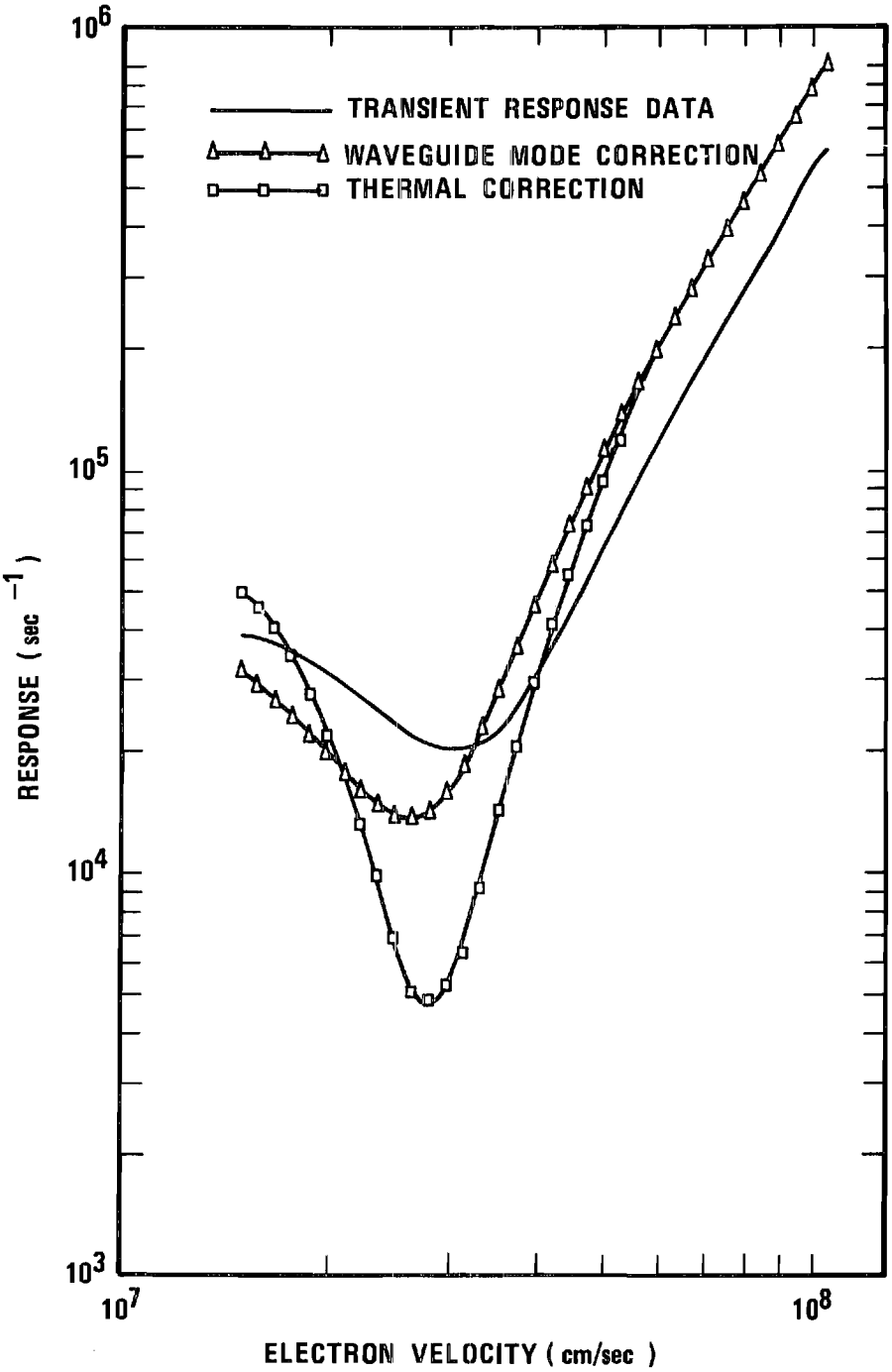

Figure 14. Results of the Transient Response Corrections

Table 2. Transient Response Corrections Normalized to 0°C, 1×10^{-3} Torr

Electron Speed (10^7 cm/sec)	Transient Data (10^4 sec^{-1})	Mode Correction (10^4 sec^{-1})	Thermal Correction (10^4 sec^{-1})
1.50	4.07	3.30	5.17
1.68	3.68	2.78	4.20
1.89	3.41	2.30	2.85
2.12	3.16	1.85	1.76
2.38	2.68	1.53	1.03
2.67	2.37	1.42	0.527
2.83	--	1.48	0.500
2.99	1.65	1.64	0.551
3.36	2.43	2.36	0.959
3.77	2.70	3.75	2.15
4.23	3.70	6.06	4.30
4.74	5.44	9.48	7.60
5.32	8.50	14.3	12.4
5.97	11.3	20.7	20.7
6.70	18.0	29.3	29.3
7.52	23.7	40.7	40.7
8.44	33.5	56.6	56.6
9.46	47.5	78.9	78.9
10.62	64.8	107	107

minimum of the collision frequency curve derived from the cross section data of Golden.[11] A shifting of the final curve obtained for ν_m to obtain the correct minimum position is not sufficient since the calculation of the thermal effects correction must be scaled relative to the mean electron thermal speed, taken to be 1.1×10^7 cm/sec in the calculations. The correct calculation of $\nu_m(v)$ depends on the correct electron speed calibration of the T(v) curve.

The data of Golden were selected for the electron speed calibration because of the sharply defined minimum exhibited by these data and the estimate that experimental apparatus used in their measurement should be capable of accurately determining the position of the minimum.

Discussion of Analytical and Numerical Errors

The errors incurred in the correction of the experimental transient response data for the waveguide mode and thermal electron velocity distribution effects may be divided into two categories. The analytical errors are those resulting from the mathematical assumptions made in the derivation of the integral equations. The numerical errors are those resulting from the digital processing of the analytical equations to obtain solutions.

Analytical Errors

The analytical errors inherent in Equations 23 and 24 stem from the mathematical assumptions made in their derivation. These assumptions are that, for those electrons contributing to the transient response signal, the component of velocity parallel to the magnetic field is insignificant compared to the perpendicular component, and that the value of the mean electron speed is insignificantly different

from the speed induced by the microwave pulse.

The latter assumption is estimated in Appendix V to be in error by less than 10 percent at an induced pulse speed of 1.5×10^7 cm/sec. This error decreases rapidly as the pulse speed increases. However, in the calculation of $\nu_m(v)$ in Equation 27, it is seen that the integration of $vT(v)$ must extend to $v = 0$. From Equation 23, it is seen that $vT(v)$ must be finite at $v = 0$. This effect is accounted for in the numerical calculation of ν_m by replacing $vT(v)$ by $(v_{th} + v^4)^{\frac{1}{4}}T(v)$, where v_{th} is the mean electron speed. The weighting factor multiplying $T(v)$ has approximately the correct value for the entire range of v.

The effect of the former assumption is that the value calculated for $\nu_m(v)$ is in error approximately by the factor $v/v_\perp$. For a thermal speed of 1.1×10^7 cm/sec, this factor represents an error of 6.0 percent at an induced pulse velocity of 1.5×10^7 cm/sec. This error rapidly decreases for increasing pulse velocity.

It should be pointed out that Equation 21 for the transient response envelope neglects the initial electrical phase differences among the incremental contributions of individual oscillating electrons to the total transient response. The initial phase distribution is a result of the thermal distribution of electron velocities. The primary effect of including the phase information would be a more accurate calculation of the initial amplitude of the transient response envelope. In the experimental measurements, however, it is the slope of the transient response envelope, and not the amplitude, which is important. Therefore, the error incurred by omitting the phase information should

not be significant.

As discussed earlier, the accuracy of the resulting mono-energetic collision frequency calculated from the experimental data is limited by the accuracy of the least squares polynomial fit obtained for the experimental data. Small changes in the amplitude and derivative values of the fit curve are amplified in the calculated values for ν_m, especially around the vicinity of the Ramsauer minimum. For example, if the low lying minimum value of the transient response data is assigned zero weight in the mean square fitting process, the fit curve minimum is changed by approximately 10 percent. The resulting shift in the collision frequency curve is approximately 50 percent. It should be pointed out, however, that only those values of collision frequency within $\pm$ 20 percent of the electron speed value corresponding to the minimum are affected significantly.

The significance of the manner in which the transient response data are extended to zero electron speed is primarily reflected in the stability of the numerical solutions. An improper extension results in initial oscillations in the solution at low values of electron speed which propagate into the higher speed range. The values of the solutions, however, are relatively insensitive to the choice of a proper extension.

Numerical Error

The accuracy of the numerical techniques is tested by integrating the solutions of the integral equations to recover the initially known functions which were used to compute the solutions. The solution calculated for T(v) by Equation 26 is inserted into Equation 24 to

calculate $S(v_p)$. The values calculated for $S(v_p)$ differed from the experimental data by less than 1.0 percent. The solution calculated for $\nu_m(v)$ by Equation 27 is inserted into Equation 23 to calculate $T(v)$. These values differed from the original values calculated for $T(v)$ by a maximum of 8.0 percent.

Total Error

The assignment of the total mathematical error is complicated by the failure of the least squares polynomial fit curve to accurately describe the experimental transient response data in the vicinity of the Ramsauer minimum. There is no experimental evidence to warrant the artificial smoothing of the sharp minimum in the measured data. In fact, supplemental measurements made at points around the minimum substantiate the sharpness of the minimum. To accurately fit the experimental data near the minimum would require a more sophisticated curve fitting process than was available for this research.

As a result, the monoenergetic collision frequency curve in the immediate vicinity of the Ramsauer minimum, calculated from the present least squares polynomial fit of the experimental data, must be considered as an approximation which underestimates the true sharpness of the curve and which overestimates the true value of the minimum collision frequency value. The mathematical error quoted here, however, will be based on the assumption that the polynomial fit curve is accurate to within the estimated experimental error.

The total analytical and numerical error is assigned a value of $\pm$ 10 percent. The experimental error has been assigned a value of $\pm$ 10-15 percent. The total error in the collision frequency values,

assuming that the mean square fit of the transient response data is accurate, is conservatively assessed at $\pm$ 25 percent. The mono-energetic elastic momentum transfer collision frequency data, together with the estimated total measurement error limits, are presented in Figure 15 and in Table 3.

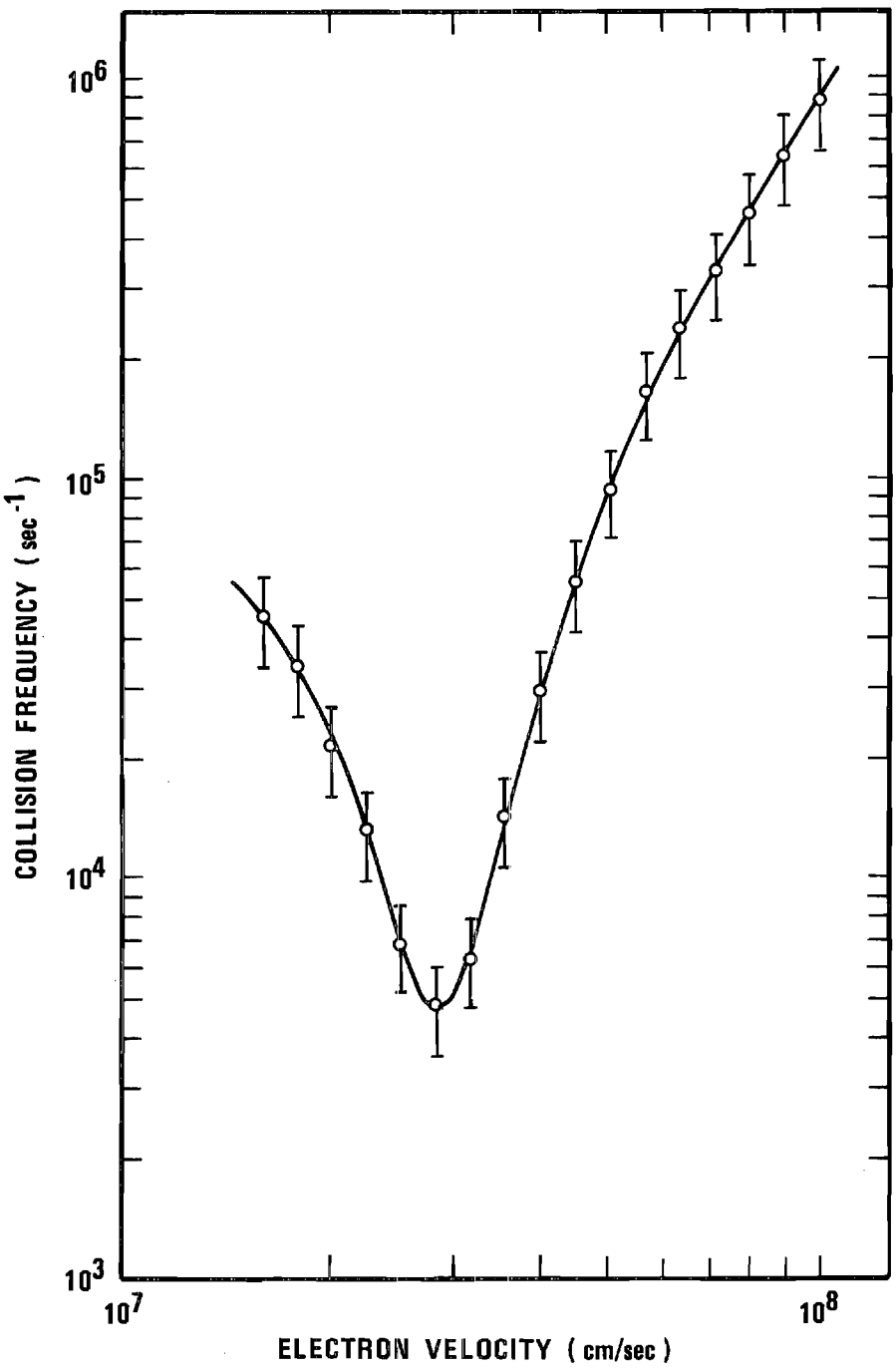

Figure 15. Monoenergetic Collision Frequency Results

Table 3. Collision Frequency Normalized to 0°C 1x10^{-3} Torr

Electron Speed (10^7 cm/sec)	Collision Frequency (10^4 sec^{-1})	Lower Error Limit (10^4 sec^{-1})	Upper Error Limit (10^4 sec^{-1})
1.50	5.17	3.88	6.46
1.59	4.74	3.56	5.93
1.68	4.20	3.15	5.25
1.78	3.55	2.66	4.44
1.89	2.85	2.14	3.56
2.00	2.24	1.68	2.80
2.12	1.76	1.32	2.20
2.24	1.38	1.04	1.73
2.38	1.03	0.773	1.29
2.52	0.714	0.536	0.893
2.67	0.527	0.395	0.659
2.83	0.500	0.375	0.625
2.99	0.551	0.413	0.689
3.17	0.658	0.494	0.823
3.35	0.959	0.719	1.20
3.56	1.49	1.12	1.86
3.77	2.15	1.61	2.69
3.99	3.06	2.30	3.83
4.23	4.30	3.23	4.04
4.48	5.76	4.32	7.20
4.74	7.60	5.70	9.50
5.02	9.80	7.35	12.3
5.32	12.4	9.30	15.5
5.64	17.3	13.0	21.6
5.97	20.7	15.5	25.6
6.33	24.7	18.5	30.9
6.70	29.3	22.0	36.6
7.10	34.6	26.0	43.3
7.52	40.7	30.5	50.9
7.96	48.0	36.0	60.0
8.44	56.6	42.5	70.8
8.93	66.8	50.1	83.5
9.46	78.9	59.2	98.6
10.0	92.6	69.5	115
10.6	107	80.3	134

CHAPTER VI

COMPARISON WITH RELATED MEASUREMENTS

In this chapter, the elastic momentum transfer collision frequency derived from the transient response measurements will be compared with data derived from previous elastic momentum transfer cross section and total elastic cross section measurements. The data chosen for comparison are derived from the experimental measurements of two independent research groups.

Data of Frost and Phelps

In 1964, L. S. Frost and A. V. Phelps reported the measurement of the elastic momentum transfer cross section for electrons in argon gas over the electron energy range from .003 to 30 eV using a dc electron swarm measurement technique.[15] The overall measurement error is estimated by the authors to be $\pm$ 10 percent, although they include the possibility of rapid variations of the cross section, such as that measured for helium,[28] of magnitude greater than the estimated error.

The work of Frost and Phelps is highly respected in the field of atomic collisions, and their argon measurements have become a standard with which all subsequent measurements must be compared.

Data of Golden

In 1966, D. E. Golden reported that calculation of the elastic momentum transfer cross section for electrons in argon gas for electron energies from zero to 0.8 eV. The calculations were based on the total elastic cross section measurements for argon of Golden and Bandel using

a highly refined single beam transmission technique.[13] The calculations were made using the modified effective range theory for low energy elastic scattering,[29] with the effective range parameters determined from the total cross section data. Golden and Bandel estimated their experimental error to be ± 3.0 percent, while Golden estimates the accuracy of the calculated effective range parameters to be within ± 8.0 percent.

Comparison

The momentum transfer cross section for argon calculated by Golden exhibits a much sharper Ramsauer minimum than does the cross section measured by Frost and Phelps, with the minimum of Golden's cross section lying a factor of 4.4 deeper than that of Frost and Phelps. Golden attributes the discrepancy to the inherent inability of the dc swarm measurements to resolve the sharp minimum. Phelps has pointed out, however, that, due to the method by which the cross section is calculated from the experimental data, the swarm measurements should tend to exaggerate the minimum.[12]

The results of the argon elastic momentum transfer collision frequency measurements using the microwave transient response technique are presented for comparison with the data derived from the work of Frost and Phelps and of Golden in Figure 16.

The transient response data agrees, within the estimated error limits, with the data of Frost and Phelps in the electron speed ranges on either side of the Rasmauer minimum. In the vicinity of the Ramsauer minimum, however, the transient response data agrees more closely with the data of Golden. At the extremes of the electron

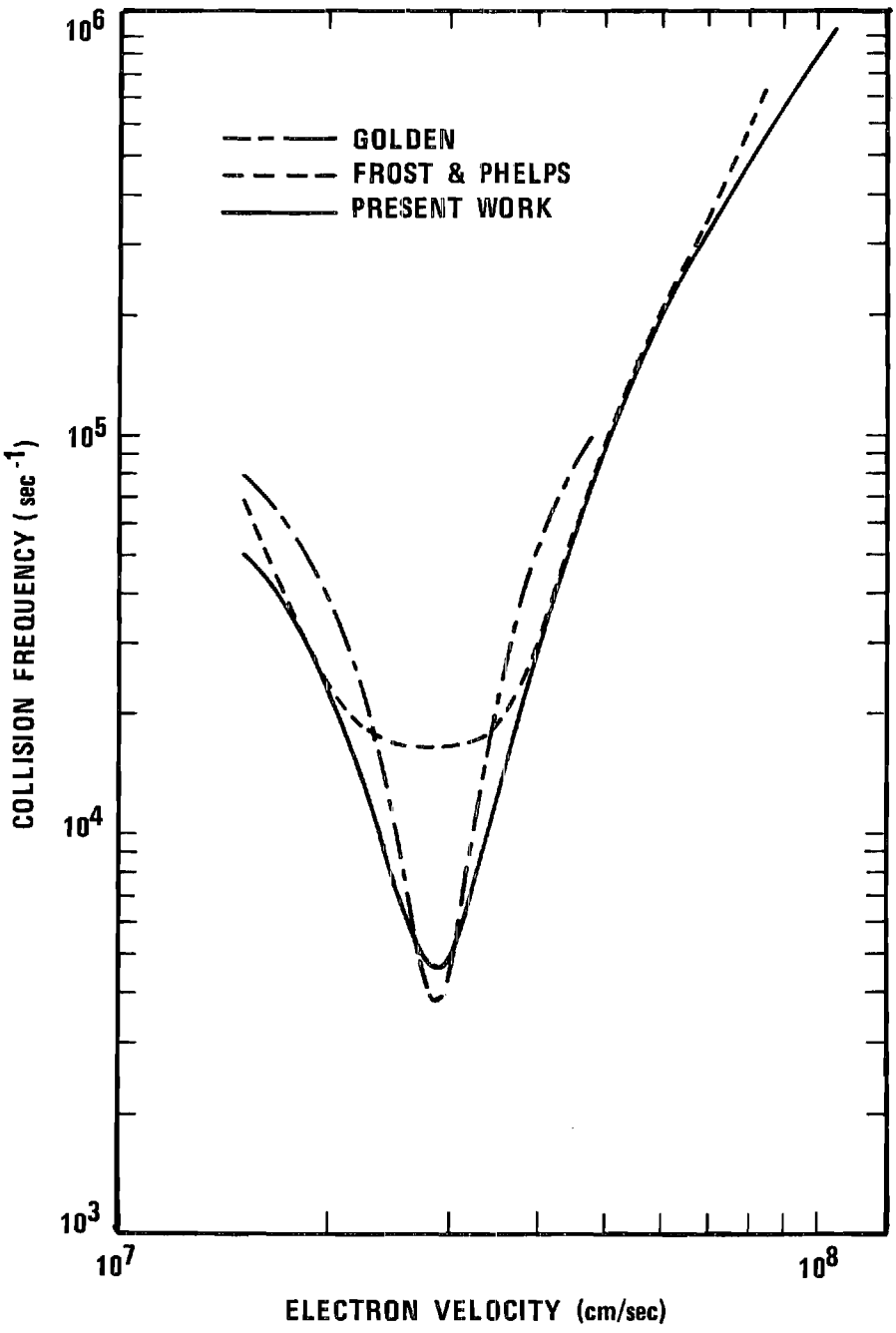

Figure 16. Comparison with Frost and Phelps and with Golden

speed measurement range, the transient response curve is lower than the Frost and Phelps curve. At the lower electron speed values, the effects of the mathematical assumptions used to recover the mono-energetic data from the transient response experimental data would tend to cause an underestimate of the true collision frequency, while, at the high values of electron speed, the effects of the finite time duration of the microwave pulse used in the experimental measurements would tend to lower the measured value of the transient response decay in that range.

It has been pointed out that the error in the transient response collision frequency determinations near the Ramsauer minimum may exceed the estimated error. The additional error may result from the inability of the least squares polynomial fit curve, used in the collision frequency calculations, to follow the experimental data points. This additional error, however, should be toward a less exaggerated Ramsauer minimum. It must be concluded, based on the transient response measurements, that the Ramsauer minimum in argon may lie deeper than either the transient response curve or Golden's curve indicate. In order to match the curve of Frost and Phelps in the region around the minimum, the transient response experimental data would have to be much flatter and smoother than that measured. It is considered unlikely that errors of such magnitude exist in the transient response data.

CHAPTER VII

CONCLUSIONS

The primary conclusion inferred from the transient response measurements is that the microwave transient response technique for the measurement of elastic momentum transfer collision frequency in gases is a potentially valuable tool in the field of atomic collisions which has not been sufficiently exploited. It is not presumed that the measurements presented here settle the question of the depth of the Ramsauer minimum in argon. The transient response technique, in its present state of development, cannot claim the precision of the dc swarm or beam experiments. These measurements serve to indicate the potential of the transient response measurements and the need for further refinement and testing of the technique.

Evaluation of the Transient Response Technique

The transient response technique for measuring elastic momentum transfer scattering of electrons in gases has the advantage that the fundamental momentum transfer quantity to be determined bears a more direct relation to the experimentally measured quantity than is the case in dc electron swarm and single beam experiments. When developed to its full potential, the transient response technique should be capable of providing an almost direct measurement of the momentum transfer collision frequency.

The major defect in the present measurements is that large corrections must be applied to the experimental results to obtain the

desired monoenergetic collision frequency. The experimental parameters governing the analytical corrections, such as electric field and electron number density variations in the waveguide and the mean electron thermal speed, have not been directly measured. The residual transient response decay, while directly measured, represents a large correction factor which could be the source of significant errors. The experimental conditions under which these transient response measurements were made were not subject to the precise control of a more refined experiment.

In view of the uncertainties inherent in the present experiment, it would be unrealistic to attribute a high degree of validity to these collision frequency results in the absence of supporting independent measurements. It is encouraging, however, that the transient response technique, in its present, unrefined state, has produced reasonable results. The results indicate that, with an improved apparatus, the technique should be capable of providing direct monoenergetic momentum transfer scattering data with a precision comparable to that of the beam and swarm experiments. Considering the conflicting results obtained by the latter two methods, the development of the transient response technique seems highly desirable.

Suggestions for Improvement of the Transient Response Technique

The most important improvements of the transient response technique are those which lead to a more direct measurement of the monoenergetic collision frequency. Experimental conditions must be refined so that only small corrections need be applied to the experimental measurements to derive the collision frequency.

The most straightforward method to reduce the components of the residual transient response decay resulting from upper hybrid resonance dephasing and electron-electron collisions is to lower the electron density. This would require a transient response signal receiver with improved sensitivity and noise characteristics. Also, a higher degree of isolation between the excitation pulse and the transient response signal would be required. A better receiver could be attained by employing heterodyne techniques, and PIN diode switches could significantly improve the isolation.

The magnetic field homogeneity could be significantly improved, using NMR techniques, to reduce the associated multifrequency residual decay rate.

To reduce the residual decay resulting from thermal streaming, the electron temperature must be lowered to cryogenic temperatures. After ionization of the gas, the electrons must be allowed to reach equilibrium with a cryogenic cooling source. The technical difficulties involved in cooling the electrons and measuring their temperature would be substantial. The cooling of the electrons would also reduce the magnitude of the corrections involved in unfolding the monoenergetic collision frequency from the electron thermal speed distribution.

The corrections associated with the waveguide mode electron speed distribution may be eliminated by using a uniform waveguide coupler, such as that employed by Bruce and Larsen.[22] Alternatively, the plasma tube could be inserted vertically through the waveguide to obtain uniform microwave excitation. In this case, another means

must be found for producing a low temperature electron density in the plasma tube. The transverse magnetic field precludes the ionization of the gas by an electron beam directed along the axis of the tube.

In order to perform truly independent measurements, the electron energy must be absolutely calibrated. This is a difficult problem which, as yet, has not been solved.

Conclusion

The transient response technique, which was originated by Bruce, Crawford, and Harp has been further developed and refined, and the potential value of the technique for measuring monoenergetic momentum transfer collision frequencies has been demonstrated.

The monoenergetic collision frequency results obtained for argon support the hypothesis of a lower lying Ramsauer minimum than has previously been accepted.

APPENDIXES

APPENDIX I

MATHEMATICAL DERIVATION OF THE TRANSIENT RESPONSE ENVELOPE DECAY RATE RESULTING FROM ELECTRON-NEUTRAL SCATTERING

In this appendix the transient response envelope decay rate resulting from electron-neutral scattering will be derived. It is first necessary to show that the angle through which an electron is scattered is equal to the change in electrical phase angle of the electromagnetic radiation produced by the oscillating electron.

Consider an electron oscillating in a magnetic field about a guiding center 0, with velocity $\vec{v}$ as shown in Figure 17a. Suppose that the electron is instantaneously scattered by a collision with a neutral particle. Immediately after the scattering event, the speed and spatial position in the orbital plane of the electron will be unchanged, but its velocity and guiding center will be changed to $\vec{v}'$ and 0' respectively.

Let $\vec{r}$ and $\vec{r}'$ be the radius vectors to the position of the electron from 0 and 0' respectively. Note that $\vec{v} \perp \vec{r}$ and $\vec{v}' \perp \vec{r}'$. The scattering angle is denoted by α, and the change in oscillation phase is denoted by β.

Figure 17b shows the angular relationships among the various vectors when 0 and 0' are brought into coincidence. By geometrical arguments, it can be shown that the angle γ, as defined in Figure 17b, is given by

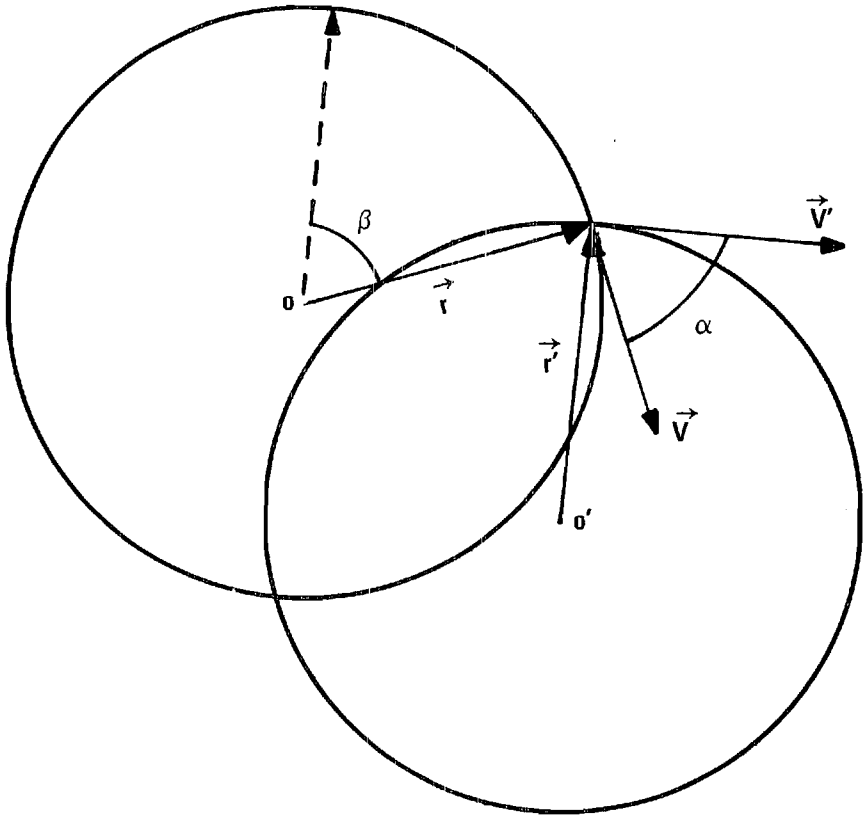

(a)

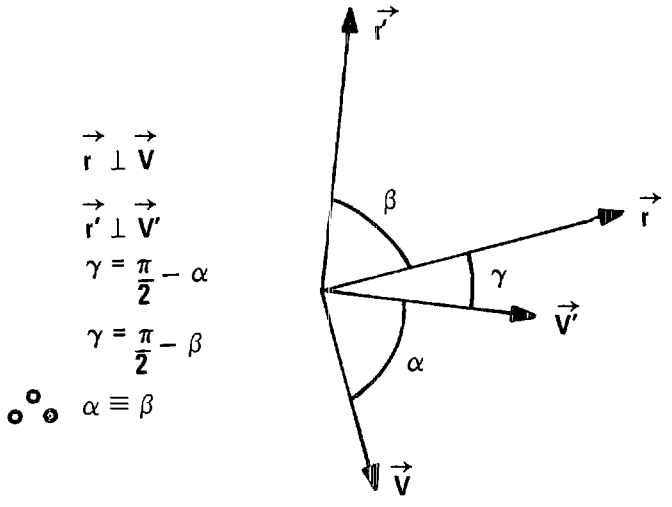

(b)

Figure 17. Phase Angle Diagram

$$\gamma = \frac{\pi}{2} - \beta \quad , \tag{A-1}$$

and

$$\gamma = \frac{\pi}{2} - \alpha \quad , \tag{A-2}$$

so that $\alpha \equiv \beta$.

The electrical phase of the radiation emitted by the oscillating electron measured at a fixed point distant from the electron position bears a fixed relationship to the oscillation phase, so that it has been shown that the scattering angle is equal to the change in electrical phase of the electromagnetic radiation emitted by the electron.

It will now be shown that the decay rate of the transient response radiation from an ensemble of N electrons distributed uniformly and with equal energy and oscillation frequency is equal to the momentum transfer collision frequency.

Let the magnitude of the electric field of the radiation emitted by a single electron be given by

$$e(t) = E_0 \cos(\omega_0 t + \theta) \quad , \tag{A-3}$$

where θ is the phase of the field relative to a fixed phase reference. If the physical extent of the electron ensemble is small compared to a free space wavelength of the radiation, the magnitude of the electric field measured at a point distant from the ensemble will be given by

$$E(t) = \sum_{i=1}^{N} E_0 \cos(\omega_0 t + \theta_i) \quad , \tag{A-4}$$

where θ_i is the phase angle of the radiation emitted by the ith electron.

Let n(t) be the number of electrons which do not experience a collision with a neutral particle in the time interval 0 to t. It is assumed that electron-neutral collisions are the only mechanism by which the phase angle of electron oscillation may be changed, that each electron experiences, at most, one collision in the time interval of interest, and that the phase angle of each electron is zero at t = 0.

Then, at time t, the electric field is given by

$$E(t) = n(t)E_0 \cos \omega_0 t + \sum_{i=n(t)+1}^{N} E_0 \cos(\omega_0 t + \theta_i) \quad , \qquad \text{(A-5)}$$

where $|\theta_i| > 0$ for $n(t) < i \leq N$. Assume, further, that N and n(t) are sufficiently large so that n(t) + 1 may be replaced by n(t) in the sum of Equation A-5.

Let $f(\theta)$ be the probability density function of the scattering angle, that is, $f(\theta)d\theta$ is the probability that an arbitrary scattered electron will have a phase angle between θ and $\theta + d\theta$, where $-\pi \leq \theta \leq \pi$.

The resultant electric field at the point of measurement will be the ensemble average of the electric fields due to the individual electron radiation.

$$\overline{E(t)} = n(t)\, E_0 \cos \omega_0 t + [N - n(t)]E_0 \int_{-\pi}^{\pi} f(\theta)\cos(\omega_0 t + \theta)d\theta$$

$$= [n(t)(1 - \overline{\cos \theta}) + N\, \overline{\cos \theta}]E_0 \cos \omega_0 t \quad , \qquad \text{(A-7)}$$

where

$$\overline{\cos\theta} = \int_{-\pi}^{\pi} f(\theta)\cos\theta d\theta \quad . \tag{A-8}$$

The number n(t) is given by

$$n(t) = N \exp[-\nu_t t] \ , \tag{A-9}$$

where ν_t is the total elastic collision frequency. Then

$$\overline{E(t)} = N[\exp(-\nu_t t)(1 - \overline{\cos\theta}) + \overline{\cos\theta}]E_0 \cos \omega_0 t \ . \tag{A-10}$$

If the resultant field is square-law detected and low-pass filtered, the output of the detector will be

$$S(t) = \langle \overline{E(t)}^2 \rangle = \frac{1}{2} E_0^2 N^2 [\exp(-2\nu_t t)(1 - \overline{\cos\theta})^2 + 2 \exp(-\nu_t t)\overline{\cos\theta}\ (1 - \overline{\cos\theta}) + \overline{\cos\theta}^2] \ , \tag{A-11}$$

where $\langle\ \rangle$ denotes the low-pass filter process, and S(t) is the envelope of the transient response signal.

The measured quantity in the transient response measurements is the time derivative of the logarithm of S(t) at t = 0.

$$r(t)\Big|_{t=0} = \left[\frac{\ln(10)}{\langle \overline{E(t)}^2 \rangle} \frac{d}{dt} \langle \overline{E(t)}^2 \rangle\right]_{t=0} \ , \tag{A-12}$$

where

$$\frac{d}{dt} \langle \overline{E(t)}^2 \rangle \Big|_{t=0} = -\nu_t N^2 E_0^2 (1 - \overline{\cos\theta}) \ , \tag{A-13}$$

and

$$\langle \overline{E(t)}^2 \rangle \Big|_{t=0} = \frac{1}{2} N^2 E_0^2 \ . \qquad \text{(A-14)}$$

Thus

$$r(t)\Big|_{t=0} = -2 \ln(10) \nu_t (1 - \overline{\cos\theta})$$

$$= -2 \ln(10) \nu_m \ , \qquad \text{(A-15)}$$

where $\nu_m \equiv \nu_t(1 - \overline{\cos\theta})$ is the elastic momentum transfer collision frequency.

The measured quantity in the transient response measurements is

$$R = -2 \ln(10) \nu_m \ , \qquad \text{(A-16)}$$

neglecting the residual decay mechanisms.

Therefore, the measured transient response is identical to the response which would be measured if the transient response envelope were given by

$$S(t) = S_0 v \exp[-\nu_m(v)t] \ , \qquad \text{(A-17)}$$

where S_0 is a normalizing constant, unimportant in the experimental measurements, and v is the electron speed. The factor v is included in Equation A-17 to indicate that the amplitude of the transient response signal is proportional to the electron speed.[40]

The equivalent form for the transient response envelope, Equation A-17, will be used in Appendix III.

APPENDIX II

EXPERIMENTAL MEASUREMENT OF THE ELECTRON BEAM GUN GENERATED ELECTRON DENSITY

In this appendix the theory and the experimental apparatus for the time-resolved measurement of the electron density produced by the electron beam gun used in the transient response experiment are described.

The transient response measurements do not require a knowledge of the plasma electron density, since the associated effects which alter the measured transient response decay rate are taken into account in the residual response decay correction. However, it is considered advantageous to determine the performance and operating characteristics of the electron beam gun in order to eliminate the gun as a possible source of error in the transient response measurements.

Relative, Time-Resolved Measurements

The measurement of the relative electron density produced by the electron beam gun in the plasma tube as a function of time in the plasma afterglow is accomplished using an adaptation of the experimental apparatus of Ajmera and Lashinsky.[30] A theory is developed for the calculation of the electron density from the experimental data.

Experimental Apparatus

Ajmera and Lashinsky have developed an open Fabry-Perot type

resonator apparatus for the measurement of electron density as a function of time. The method consists of using the plasma as an impedance element in the low Q resonator. The Q of the resonator is enhanced by a positive feedback loop in which the resonator oscillations at the output are amplified and fed back to the input. The gain of the amplifier in the feedback loop is adjusted to the point at which free oscillations occur. Changes in the electron density of the plasma impedance element are reflected in a shift in the oscillation frequency. A sample of the resonator oscillations is passed through a frequency discriminator and is envelope detected to obtain the experimental data from which the electron density is calculated.

In the present experiment, the open resonator is replaced by a closed resonator consisting of a rectangular waveguide section, designed to resonate at 3.0 GHz. The resonator cavity is terminated at each end by metal plates. Vertical slits are machined in the metal plates to allow the partial transmission of the fundamental mode waveguide field. The plasma tube of the electron beam gun assembly is inserted into the center of the waveguide section through the narrow guide walls, so that its axis is perpendicular to the fundamental waveguide mode electric field direction. A static magnetic field is applied along the axis of the plasma tube. The magnitude of the field is significantly below the electron cyclotron resonance value. A block diagram of the experimental arrangement is shown in Figure 18.

The frequency discrimination of the sampled microwave oscillations is obtained by passing the microwave signal through a cavity type

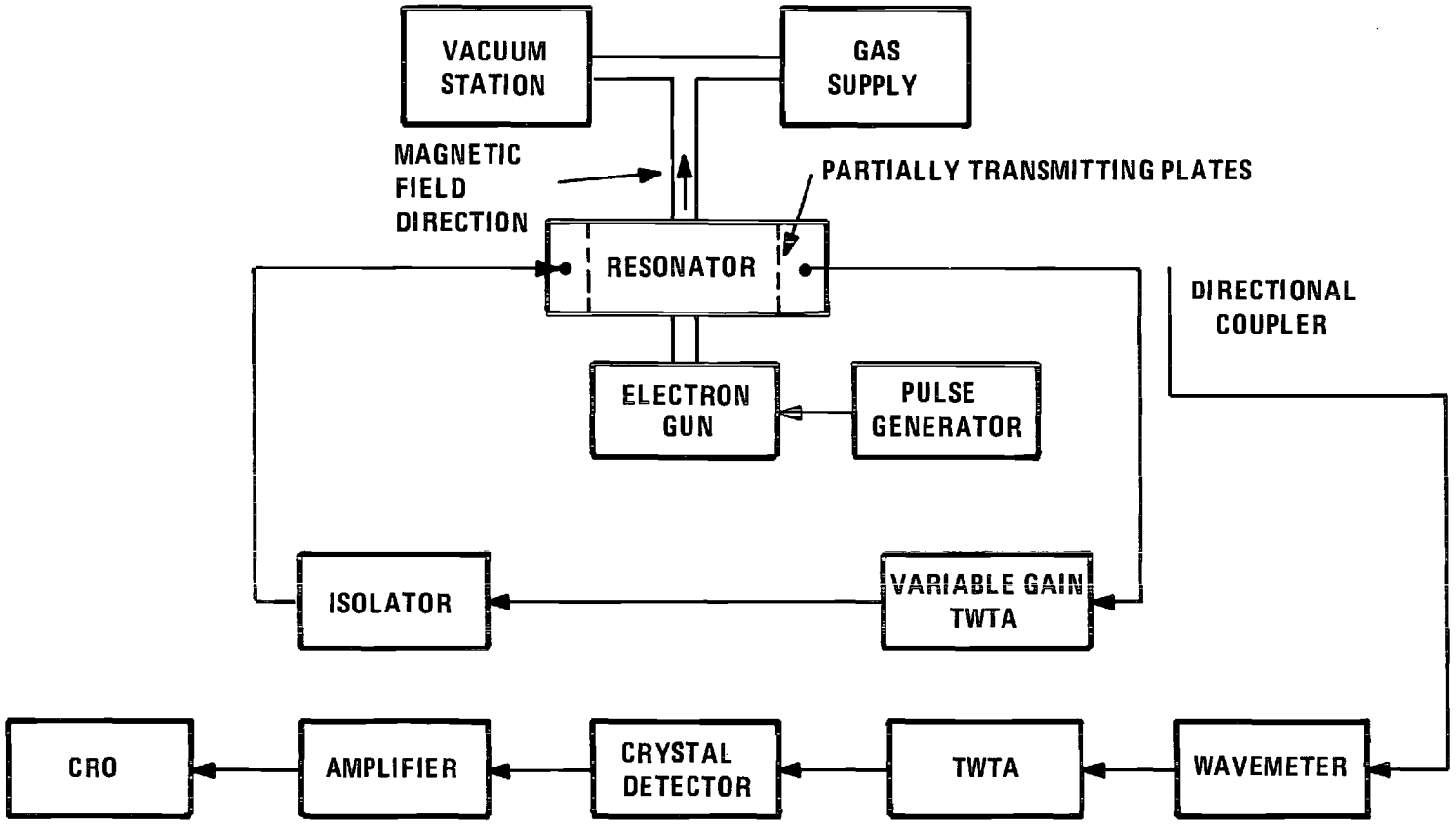

Figure 18. Diagram of the Electron Density Measurement Apparatus

frequency meter which produces a sharply defined 1.0 dB attenuation at the resonant frequency of the meter cavity. The wavemeter is set so that the free oscillations of the density measurement cavity occur at a point near the minimum of the wavemeter frequency response curve. This point is selected so that the change in the oscillation frequency produced by the plasma will result in a linearly proportional change in the amplitude of the output voltage of the microwave crystal detector. The wavemeter frequency characteristics are calibrated to obtain the proportionality constant relating the frequency shift to the crystal output voltage.

The electron gun is operated repetitively, and the measurement signal is displayed on an oscilloscope. Various checks are performed on the apparatus to insure its proper operation. The resonator microwave field is sampled spatially to check for fundamental mode operation. The sampled microwave oscillations are measured in the absence of frequency discrimination to test for amplitude modulation of the resonator field by the introduction of the plasma. The frequency shift is measured as a function of magnetic field strength to check the accuracy of the analytical form assumed for the plasma permittivity.

Mathematical Analysis

The analysis of the relative electron density measurement technique begins with a calculation of the microwave electrid field inside the plasma tube with, and without, a plasma present. The quasi-static approximation is used in the field calculation. This approximation is valid since the plasma tube diameter is small compared

to a free space wavelength of the microwave radiation.

The coordinate arrangement for this calculation is shown in Figure 19. The plasma tube is immersed in a uniform electric field directed normally to the tube axis. The plane containing the plasma tube cross section is divided into three regions as shown in Figure 19. The electrostatic potential has the following forms in each of the three regions:

$$\text{Region I:} \quad \phi_1 = E_0\left(r + \frac{A}{r}\right)\sin\theta, \tag{A-18}$$

$$\text{Region II:} \quad \phi_2 = B\left(r + \frac{C}{r}\right)\sin\theta, \tag{A-19}$$

$$\text{Region III:} \quad \phi_3 = D\, r \sin\theta, \tag{A-20}$$

where E_0 is the magnitude of the uniform field, and A, B, and C are constants to be evaluated.

The dielectric permittivities are denoted by:

Region I: $\varepsilon = \varepsilon_0$, the permittivity of free space

Region II: $\varepsilon = \varepsilon_g$, the permittivity of the glass

Region III: $\varepsilon = \varepsilon_p$, the transverse permittivity of the plasma

It is convenient to denote the permittivity ratios by

$$K_{gp} = \frac{\varepsilon_g}{\varepsilon_p}$$

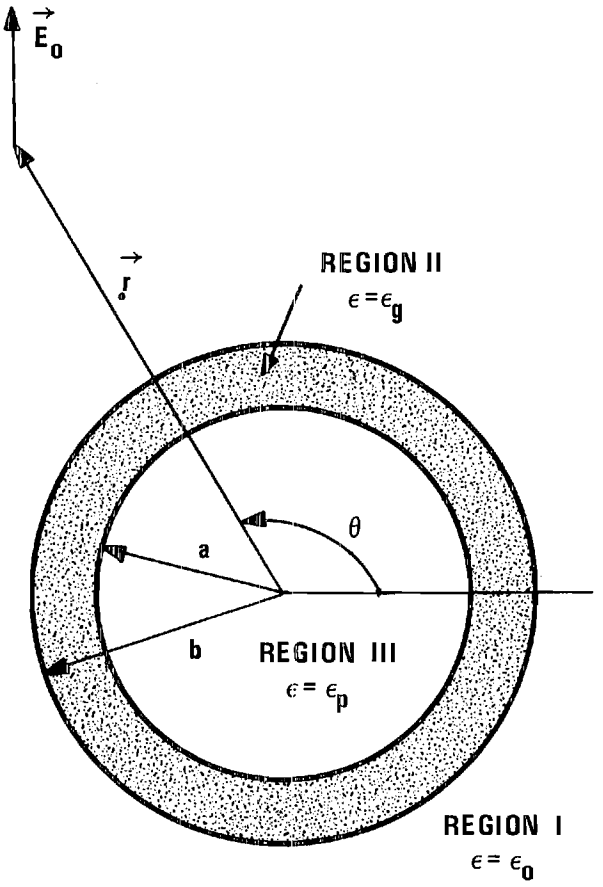

Figure 19. Coordinate System for Density Calculation

$$K_{go} = \frac{\varepsilon_g}{\varepsilon_0}$$

Applying the boundary conditions on the normal and tangential components of the electric fields, the electric field in Region III is calculated to be

$$\vec{E} = E\vec{a}_y \ , \tag{A-21}$$

where

$$E = \frac{4E_0 K_{gp}}{K_{gp}\left[1 + \frac{a^2}{b^2} + K_{go}\left(1 - \frac{a^2}{b^2}\right)\right] + \left[1 - \frac{a^2}{b^2} + K_{go}\left(1 + \frac{a^2}{b^2}\right)\right]} \tag{A-22}$$

In the absence of a plasma in the plasma tube, $\varepsilon_p = \varepsilon_0$ and Equation A-22 reduces to

$$E = \frac{4E_0 K_{go}}{(K_{go} + 1)^2 - \frac{a^2}{b^2}(K_{go} - 1)^2} \tag{A-23}$$

The restriction on the uniformity of E_0 is now relaxed to allow for the fundamental mode sinusoidal variation of the electric field across the waveguide, along the axis of the plasma tube. In Equations A-22 and A-23, E_0 is given by

$$E_0 = E_p \sin\left(\frac{\pi z}{a}\right) \ , \tag{A-24}$$

where a is the waveguide transverse dimension.

The transverse permittivity of the plasma is assumed to be

$$\varepsilon_p = \varepsilon_0\left(1 - \frac{f_{pe}^2}{f_0^2 - f_{ce}^2}\right) , \qquad \text{(A-25)}$$

where f_{pe} is the electron plasma frequency, f_{ce} is the electron cyclotron frequency, and f_0 is the microwave cavity oscillation frequency. Then

$$K_{gp} = \frac{K_{go}}{1 + \Delta K_p} , \qquad \text{(A-26)}$$

where

$$\Delta K_p = - \frac{f_{pe}^2}{f_0^2 - f_{ce}^2} . \qquad \text{(A-27)}$$

For the conditions of the present experiment, ΔK_p is small compared to unity. It is seen in Equation A-22 that the major influence of the plasma upon the electric field magnitude comes from the K_{gp} factor in the numerator. The K_{gp} factor in the denominator contributes only second order corrections. In order to simplify Equation A-22, the K_{gp} factor in the denomitor will be replaced by K_{go}. The equation for E becomes

$$E = \frac{4E_o\ K_{go}\left(\frac{1}{1 + \Delta K_p}\right)}{(K_{go} + 1)^2 - \frac{a^2}{b^2}(K_{go} - 1)^2} = FE_0\left(\frac{1}{1 + \Delta K_p}\right) . \qquad \text{(A-28)}$$

To calculate the frequency shift of the microwave cavity produced by the plasma, the following stationary perturbation formula will be used[31]

$$\frac{\Delta f}{f_0} = \frac{\Delta\epsilon}{2\epsilon_0} \frac{\int_{\Delta V} \vec{E} \cdot \vec{E}_1 \, dv}{\int_V |\vec{E}_1|^2 \, dv} \quad , \tag{A-29}$$

where ΔV is the volume of the perturbing dielectric, V is the total volume of the cavity, and $\vec{E}_1$ is the electric field in the absence of the perturbing dielectric.

The magnitude of $\vec{E}_1$ in ΔV is calculated using Equation A-28; in V, $\vec{E}_1$ is replaced by $\vec{E}_0$. Since $\vec{E}$, $\vec{E}_0$, and $\vec{E}_1$ are all assumed to have the same z dependence, the volume integral ratio of Equation A-29 reduces to a surface integral ratio. The resulting formula for the frequency shift is

$$\frac{\Delta f}{f_0} = - \frac{\Delta A}{A} F^2 \frac{\Delta K_p}{1 + \Delta K_p} \quad , \tag{A-30}$$

where A is the cross sectional area of the waveguide cavity, and ΔA is the cross sectional area of the plasma.

Finally, the formula for the average electron density of the plasma in terms of the cavity resonant frequency shift is

$$\bar{n} = 4\pi^2 \frac{m\epsilon_0}{e^2} (f_0^2 - f_{ce}^2) \left[\frac{\frac{1}{F} \frac{\Delta f}{f_0} \frac{A}{\Delta A}}{1 + \frac{1}{F} \frac{\Delta f}{f_0} \frac{A}{\Delta A}} \right] \quad , \tag{A-31}$$

where

$$F = \frac{4K_{go}}{(K_{go}+1)^2 - \frac{a^2}{b^2}(K_{go}-1)^2} \quad . \qquad \text{(A-32)}$$

In the calculation of the average electron density from Equation A-31, the cross sectional area of the plasma, ΔA, is taken to be the area of the electron beam cross section.

Absolute Calibration

In order to calibrate the initial value of the time-dependent average electron density, a dielectric with a precisely known permittivity is used in a substitution procedure. The dielectric selected for the calibration is the polar gas CH_3Cl.[32] The dielectric constant of this gas has been documented to obey the relation

$$(K - 1)T/293p = 14.3\text{x}10^{-6}\ ^{\circ}\text{K Torr}^{-1} \quad , \qquad \text{(A-33)}$$

where K is the dielectric constant, T is the absolute temperature in K, p is the gas pressure in Torr.

The relation A-33 is reported to be in error by less than 1.0 percent near room temperature and atmospheric pressure, at a measurement frequency of 3.0 GHz. Under these conditions, the gas produces a frequency shift in the density measurement apparatus in the same range as the electron densities measured.

The experimental arrangement used for the calibration is the same as that used for the relative measurements with the exception that the sample of the microwave oscillations is mixed with a suitably

stable 3.0 GHz microwave oscillator, and the difference frequency is determined with a frequency counter. The count error is estimated to be 10 KHz out of 3 GHz.

The experimental procedure is to evacuate the plasma tube to a pressure of less than 1×10^{-3} Torr and to adjust the microwave oscillator to give a zero frequency count. The plasma tube is then refilled with the CH_3Cl gas to atmospheric pressure as measured with an absolute pressure gauge. The resonant frequency shift is read from the frequency counter. This procedure is repeated several times and the results averaged. The frequency shifts obtained in this manner varied by about $\pm$ 1.0 percent. The average frequency shift is 3.14 MHz out of 3.0 GHz.

The calibration is obtained by calculating the change in dielectric constant from Equation A-33 and determining the ratio of the frequency shift to the change in dielectric constant. The calibration is applied to the relative electron density measurements to determine the initial value of the time dependent electron density. The results of the electron density measurements are presented in Figure 20.

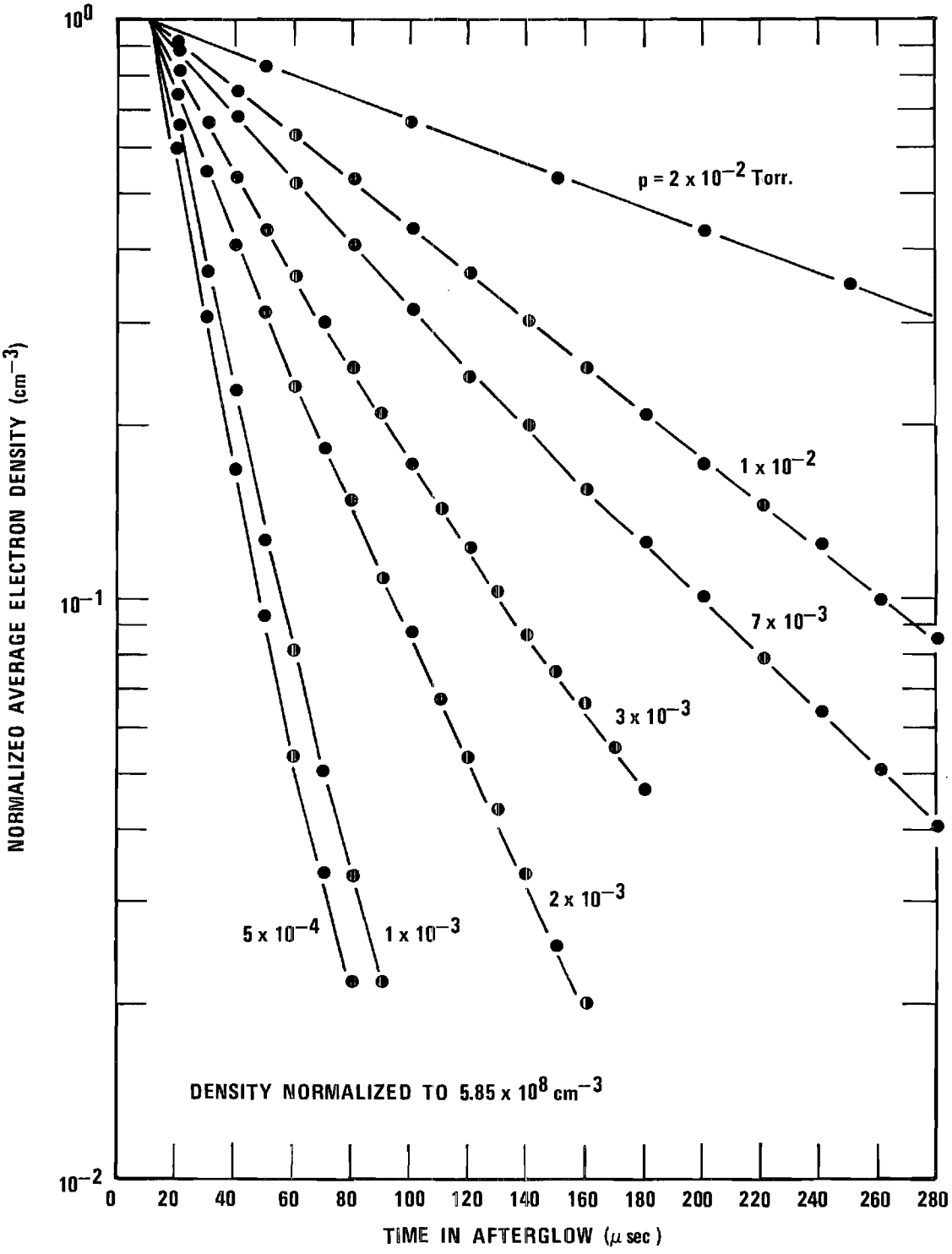

Figure 20. Results of the Electron Density Measurements

APPENDIX III

MATHEMATICAL DERIVATION OF THE TRANSIENT RESPONSE ENVELOPE TAKING INTO ACCOUNT THE WAVEGUIDE MODE AND THERMAL SPEED DISTRIBUTION

It has been shown in Appendix I that the transient response envelope of a uniform density, monoenergetic group of electrons has a mathematical form experimentally equivalent to

$$S(v,t) = S_0 \, v \exp[-\nu_m(v)t] \quad . \tag{A-34}$$

In this appendix, the analytical form of the transient response envelope will be derived, taking into account the nonuniform distribution of electron speeds resulting from the waveguide mode variation of the electric field associated with the microwave excitation pulse, and resulting from the random thermal motion of the electrons.

Waveguide Effects

The microwave pulse electric field which excites the electrons into resonant oscillations about magnetic field lines will be assumed to be distributed across the waveguide in the fundamental waveguide mode as shown in Figure 12. The electron speeds produced by the pulse will be assumed to be proportional to the field strength,

$$v_0(z) = v_p \sin(\frac{\pi z}{a}) \quad , \tag{A-35}$$

where a is the transverse waveguide dimension.

The current in the plasma tube immediately after the microwave pulse application will be

$$J(z) = eN(z)\ v_0(z)\ , \qquad \text{(A-36)}$$

where N(z) is the electron number density.

In the experimental apparatus, the hollow cylindrical electron beam gun electrodes extend up to the waveguide wall. During operation, the quartz plasma tube inside the waveguide becomes charged by scattered electrons to approximately the beam voltage, while the electrodes remain at approximately ground potential. The electric field created by the potential difference causes a charge separation in the plasma in which the electrons tend to concentrate near the electrodes. A calculation reveals that the charge separation at the center of the waveguide is of the same order of magnitude as the average electron density used for the transient response measurements. Thus, the electron density will have a pronounced variation along the plasma tube axis, peaking near the waveguide walls, and having a minimum at the center of the guide.

The electron density has an axial variation which is opposite in nature to the electron speed variation, so that, in the central portion of the waveguide, the product $N(z)\ v_0(z)$ is approximately constant.

For the purposes of this analysis, the current density will be assumed to be a constant across the waveguide. This assumption is justified by the fact that the received transient response signal is

relatively insensitive to the current near the guide walls.

The fundamental mode field produced by the current is[35]

$$E(z) = \int_0^a J(z')\, G(z|z')dz' \quad , \tag{A-37}$$

where

$$G(z|z') = - \frac{j\omega\mu_0}{\alpha\beta} \sin(\frac{\pi z}{a})\sin(\frac{\pi z'}{a}) \quad , \tag{A-38}$$

μ_0 is the permeability of free space, ω is the radian frequency, β is the fundamental mode propagation constant, and $j = \sqrt{-1}$.

As dephasing of the electron oscillations by electron-neutral scattering progresses, the current density at position z will decay exponentially in time,

$$J(z) = eN(z)\ v_0(z)\ \exp[-\nu_m(v_0)t] \ . \tag{A-39}$$

With the assumption that Nv_0 is a constant,

$$J(z) = J_0\ \exp[-\nu_m(v_0t] \ . \tag{A-40}$$

The peak amplitude of the resulting fundamental mode electric field will be

$$E_p(t) = \int_0^a \exp[-\nu_m(v_0)t]\ \sin(\frac{\pi z}{a})dz \quad . \tag{A-41}$$

Substituting

$$\frac{v_o}{v_p} = \sin(\frac{\pi z}{a}) \quad , \tag{A-42}$$

$$\frac{dv_0}{(v_p^2 - v_0^2)^{\frac{1}{2}}} = dz \quad , \tag{A-43}$$

then

$$E_p(t) = \frac{E_0}{v_p} \int_0^{v_p} \exp[-\nu_m(v_0)t] \frac{v_0}{(v_p^2 - v_0^2)^{\frac{1}{2}}} dv_0 \quad . \tag{A-44}$$

The transient response envelope, neglecting electron thermal motion, is

$$R_{v_p}(t) = \int_0^a S(v_0,t)\, G_{v_p}(v_0) dv_0 \quad , \tag{A-45}$$

where

$$G_{v_p}(v_0) dv_0 = \frac{1}{v_p} \frac{dv_0}{(v_p^2 - v_0^2)^{\frac{1}{2}}} \tag{A-46}$$

is the waveguide mode speed distribution.

Thermal Effects

It has been shown in Chapter V that the thermal distribution of electron speeds of a group of electrons with a mean velocity $\vec{v}_0$ is

$$F_{v_0}(v) dv = \frac{v}{\sigma^2} \exp[-(v^2 + v_0^2)/2\sigma^2]\, I_0\left(\frac{vv_0}{\sigma^2}\right) dv \quad . \tag{A-47}$$

The transient response envelope, taking into account electron thermal motions, is

$$R_{v_p}(t) = R_0 \int_0^{v_p} G_{v_p}(v_0) \int_0^{\infty} v_\perp F_{v_0}(v) \exp[-\nu_m(v)t]dvdv_0 \ . \quad \text{(A-48)}$$

The component $v_\perp$ of v is used in Equation (A-48) since $v_{||}$ makes no contribution to the radiated waveguide mode field.

The normalizing factor R_0 may be replaced by unity if the assumptions

$$v_\perp \simeq v \ , \quad \text{(A-49)}$$

$$\int_0^{\infty} v \, F_{v_0}(v)dv \simeq v_0 \quad \text{(A-50)}$$

are made. These assumptions will be made and discussed in the following section.

Measured Transient Response

The experimental quantity measured is

$$M(v_p) = - \frac{d}{dt} \left[\log \left\{ R^2_{v_p}(t) \right\} \right] \Big|_{t=0} \quad \text{(A-51)}$$

$$= - 2 \log(e) R'_{v_p}(0)/R_{v_p}(0) \ ,$$

where

$$R'_{v_p}(0) = - \int_0^{v_p} G_{v_p}(v_0) \int_0^{\infty} v_\perp F_{v_0}(v)\nu_m(v)dvdv_0 \ , \quad \text{(A-52)}$$

and

$$R_{v_p}(0) = \int_0^{v_p} G_{v_p}(v_0) \int_0^{\infty} v_\perp F_{v_0}(v)\,dv\,dv_0 \quad . \tag{A-53}$$

It will now be assumed that $v_\perp$ may be replaced by v, so that

$$R'_{v_p}(0) = -\int_0^{v_p} G_{v_p}(v_0) < v\nu_m(v) >_{v_0} dv_0 \quad m \tag{A-54}$$

and

$$R_{v_p}(0) = \int_0^{v_p} G_{v_p}(v_0) < v >_{v_0} dv_0 \quad , \tag{A-55}$$

where $< >_{v_0}$ denotes averaging over the thermal speed distribution function $F_{v_0}(v)$.

The value of $< v >_{v_0}$ may be analytically evaluated in terms of Whittaker functions. This computation has been made for several values of v_0. The results indicate that the assumption

$$< v >_{v_0} = v_0 \tag{A-56}$$

is in error by approximately -20 percent at $v_0 = 1\text{x}10^7$ cm/sec, (assuming a mean electron thermal speed of $1\text{x}10^7$ cm/sec) and by -5 percent at $v_0 = 2\text{x}10^7$ cm/sec, the error decreasing rapidly as v_0 increases. To facilitate the following analysis, the assumption of Equation A-56 will be made. The effect of this assumption is to weight the low speed contribution to the total transient response by an amount less than that of the exact analysis. This effect is countered by the assumption $v_\perp = v$, which gives more weight to the

low speed contribution than would be given in an exact analysis. In both cases, the assumptions affect only the extremely low portion of the experimentally measured electron speed range.

With the specified assumptions, Equation A-48 becomes

$$M(v_p) = 2 \log (e) \frac{1}{v_p} \int_0^{v_p} \frac{1}{(v_p^2 - v_0^2)^{\frac{1}{2}}} \int_0^{\infty} \frac{v^2}{\sigma^2} \nu_m(v) \times \exp[-(v^2 + v_0^2)/2\sigma^2] I_0\left(\frac{vv_0}{\sigma^2}\right) dv dv_0 \quad . \qquad \text{(A-57)}$$

APPENDIX IV

A MORE EXACT CALCULATION OF THE RESIDUAL TRANSIENT RESPONSE DECAY

In Chapter II, an estimate of the influence on the transient response decay rate of the upper hybrid dephasing of electron oscillations is derived. This appendix presents a more detailed calculation of this effect in order to more accurately determine the residual decay rate for the transient response measurements. The calculated decay rate is compared to the experimentally measured residual decay as a check on the proper operation of the transient response apparatus.

The procedure for the calculation is to determine the natural frequency components of the transient response as a function of electron density. The frequency components of the total transient response are calculated by integrating the incremental response over an assumed electron number density distribution. Finally, the effects of thermal streaming electron loss and electron-electron collisions are added to determine the total transient response residual decay as a function of electron density.

Consider an incremental plasma element consisting of electrons and infinitely massive ions immersed in a uniform magnetic field directed along the z-axis.

At time $t = 0$ the plasma element is subjected to an impulsive electric field directed along the x-axis. The equations for the transverse components of electron velocity are:

$$\frac{d^2v_x}{dt^2} + \omega_c \frac{dv_y}{dt} + \omega_p^2 v_x = \frac{dF(t)}{dt} \quad , \tag{A-58}$$

$$\frac{d^2v_y}{dt^2} - \omega_c \frac{dv_x}{dt} + \omega_p^2 v_y = 0 \quad , \tag{A-59}$$

where $F(t) = \frac{eE_0}{m}\delta(t) = \beta\delta(t)$, $\omega_c = \frac{eB_0}{m}$, $\omega_p^2 = \frac{ne^2}{m\varepsilon_0}$,

e and m are the electron charge and mass respectively, E_0 and B_0 are the magnitudes of the electric and static magnetic fields respectively, n is the electron number density, and ε_0 is the permittivity of free space.

The Laplace transforms of Equations A-58 and A-59 are:

$$(s^2 + \omega_p^2)v_x + \omega_c s v_y = s\beta \tag{A-60}$$

$$-\omega_c s v_x + (s^2 + \omega_p^2)v_y = 0 \tag{A-61}$$

The solution for v_y is

$$v_y = \frac{\omega_c \beta s}{s^4 + (\omega_c^2 + 2\,\omega_p^2)s^2 + \omega_p^4} \tag{A-62}$$

To determine the natural frequencies of the system, which will be the frequencies of the incremental transient response, the denominator of Equation A-62 must be factored. The roots occur in conjugate pairs and are given by

$$s_+^2 = -\frac{1}{2}\omega_c^2\left[\left(1 + 2\frac{\omega_p^2}{\omega_c^2}\right) - \left(1 + 4\frac{\omega_p^2}{\omega_c^2}\right)^{\frac{1}{2}}\right] \quad , \tag{A-63}$$

$$s_-^2 = -\frac{1}{2}\omega_c^2\left[\left(1 + 2\frac{\omega_p^2}{\omega_c^2}\right) + \left(1 + 4\frac{\omega_p^2}{\omega_c^2}\right)^{\frac{1}{2}}\right] \quad , \tag{A-64}$$

where the + and - subscripts refer to the sign of the discriminator. It can be shown that s_+^2 and s_-^2 are both always negative so that the free oscillations are undamped. The oscillation frequency determined by s_+^2 are much lower than that determined by s_-^2, so that only the latter frequency will be of interest in the transient response measurements.

The procedure now is to integrate the incremental transient response given by

$$S(t) = S_0 \cos(\omega_0 t) \quad , \tag{A-65}$$

where

$$\omega_0 = \frac{1}{2}\omega_c^2\left[\left(1 + 2\frac{\omega_p^2}{\omega_c^2}\right) + \left(1 + 4\frac{\omega_p^2}{\omega_c^2}\right)^{\frac{1}{2}}\right]^{\frac{1}{2}} \quad , \tag{A-66}$$

and S_0 is a normalizing constant. The incremental response is integrated over an electron density distribution of the form

$$n(r) = n_0\left[1 - \alpha\left(\frac{r}{r_0}\right)^p\right] \quad , \tag{A-67}$$

where n_0 is the peak electron density, α and p are assigned the

values 0.6 and 2 respectively as discussed in Chapter II.

To include the effect of electron-electron collisions the incremental response of equation A-65 is multiplied by

$$\exp\left[-\frac{t}{t_c}\right] \quad , \tag{A-68}$$

where t_c is the Spitzer self-collision time for electrons,

$$t_c(r) = 0.266 \frac{T^{3/2}}{n(r)\ln(\Lambda)} \tag{A-69}$$

as discussed in Chapter II.

The effect of free-streaming electron loss is included by multiplying the incremental response by the factor

$$\left(1 - \frac{v_{th}t}{2L}\right) \quad , \quad 0 \leq t \leq \frac{L}{v_{th}} \quad , \tag{A-70}$$

where v_{th} is the mean electron thermal velocity and L is the length of the active interaction region.

The total residual transient response is given by

$$S(t) = 2\pi\left(1 - \frac{v_{th}t}{2L}\right) \int_0^{r_0} S_0 \cos[\omega_0(r)t]\exp[-t/t_c(r)]rn(r)dr \quad ,$$

$$0 \leq t \leq \frac{L}{v_{th}} \quad . \tag{A-71}$$

The integration is done numerically, and the results, for various values of average electron number density, are presented in Chapter II.

APPENDIX V

SOLUTION OF THE WAVEGUIDE MODE SPEED DISTRIBUTION INTEGRAL EQUATION

In Chapter V it is shown that the solution for the monoenergetic elastic momentum transfer collision frequency is obtained by the successive solution of two integral equations. The first of these equations is the expression of averaging of the thermally averaged collision frequency over the waveguide mode electron speed distribution:

$$S(v_p) = \frac{1}{v_p} \int_0^{v_p} \frac{v_0 T(v_0)}{(v_p^2 - v_0^2)^{\frac{1}{2}}} \, dv_0 \quad , \tag{A-72}$$

where $T(v_0)$ is the thermally averaged collision frequency, $S(v_p) = \frac{1}{2} \ln M(v_p)$, $M(v_p)$ is the measured transient response decay rate, v_p is one of the set of electron speeds induced by the microwave pulse corresponding to the 1.0 dB interval experimental measurement points. It is required to solve for $T(v_0)$ in terms of $S(v_p)$.

Equation A-72 is a Volterra integral equation of the first kind, which may be solved in an iterative manner providing the proper boundary condition on $T(v_0)$ can be found. The boundary value which is sought is

$$\lim_{v_0 \to 0} T(v_0) \quad .$$

To obtain this boundary value, the second integral equation must be examined in this limit:

$$\lim_{v_0 \to 0} T(v_0) = \lim_{v_0 \to 0} \frac{1}{< v >_{v_0}} \int_0^\infty \frac{v^2}{\sigma^2} \nu_m(v) \exp[-(v^2 + v_0^2)/2\sigma^2]$$

$$\times I_0\left(\frac{vv_0}{\sigma^2}\right) dv \quad , \tag{A-73}$$

where $< v >_{v_0}$ is the electron speed averaged over the thermal speed distribution corresponding to an induced pulse speed of v_0. For small values of v_0/σ, Equation A-73 becomes insensitive to changes in v_0, and $T(v_0)$ is relatively constant. Therefore, for small values of v_p/σ, $T(v_0)$ may be removed from the integration of Equation A-72 and the limit becomes:

$$\lim_{v_0 \to 0} T(v_0) = \lim_{v_p \to 0} S(v_p) \quad . \tag{A-74}$$

The limiting value for $S(v_p)$ may be obtained by smoothly continuing the least squares polynomial curve, fitted to the experimental data points, to $v_p = 0$. The slope and curvature of the curve should be small near $v_p = 0$.

Having determined the boundary condition for $T(v_0)$, Equation A-72 may be iteratively solved in the following manner: represent the integration of A-72 as a finite sum of integrals of the form

$$S(v_p) = \frac{1}{v_p} \sum_{i=1}^{p} \int_{v_{i-1}}^{v_i} \frac{T(v_i)}{(v_p^2 - v^2)^{\frac{1}{2}}} v dv \tag{A-75}$$

The increment $v_i - v_{i-1}$ is chosen small enough so that T(v) can be accurately represented by the constant value $T(v_i)$ in the interval. Thus

$$S(v_p) = \frac{1}{v_p} \sum_{i=1}^{p} T(v_i) \left[(v_p^2 - v_{i-1}^2)^{\frac{1}{2}} - (v_p^2 - v_i^2)^{\frac{1}{2}} \right] \quad . \qquad \text{(A-76)}$$

Equation A-76 may be solved in an iterative manner according to the following pattern:

$$T(v_p) = \frac{1}{(v_p^2 - v_{p-1}^2)^{\frac{1}{2}}} \left[v_p S(v_p) - \sum_{i=1}^{p-1} T(v_i) \left\{ (v_p^2 - v_{i-1}^2)^{\frac{1}{2}} - (v_p^2 - v_i^2)^{\frac{1}{2}} \right\} \right]$$

$$p = 1, 2, 3, \ldots, N \quad , \qquad \text{(A-77)}$$

where v_N is the maximum value attained by v_p. The successive calculation of the $T(v_p)$ is accomplished using a Univac 1108 computer. The results are presented in Chapter V.

APPENDIX VI

SOLUTION OF THE THERMAL SPEED DISTRIBUTION INTEGRAL EQUATION

The solution for the thermally averaged collision frequency is obtained in Appendix V. In this appendix, the monoenergetic collision frequency will be determined from the averaged data. The integral equation to be solved is

$$T(v_0) = \frac{1}{v_0} \int_0^\infty \frac{v^2}{\sigma^2} \nu_m(v) \exp[-(v^2 + v_0^2)/2\sigma^2] I_0\left(\frac{vv_o}{\sigma^2}\right) dv \quad . \quad \text{(A-78)}$$

It is desired to solve Equation A-78 for $\nu_m(v)$ in terms of $T(v_0)$.

Equation A-78 is a Fredholm integral equation of the first kind. The solution is obtained through the use of the definite integral[33]

$$\int_0^\infty x \exp(-\alpha x^2) \, I_\nu(\beta x) J_\nu(\gamma x) dx = \frac{1}{2\alpha} \exp\left[\frac{\beta^2 - \gamma^2}{4\alpha}\right] J_\nu\left(\frac{\beta\gamma}{2\alpha}\right) \quad , \quad \text{(A-79)}$$

where $\mathrm{Re}\{\alpha\} > 0$, $\mathrm{Re}\{\nu\} > 1$, and $J_\nu(x)$ is the Bessel function of the first kind, order ν.

In order to cast Equation A-78 in the desired form, both sides are multiplied by $v_0^2 J_0(\gamma v_0)$ and integrated from $v_0 = 0$ to $v_0 = \infty$. The result is

$$\int_0^\infty v_0^2 T(v_0) J_0(\gamma v_0)\, dv_0 = \int_0^\infty f(v) \int_0^\infty v_0 \exp\left(-\frac{v_0^2}{2\sigma^2}\right) I_0\left(\frac{v v_0}{2\sigma^2}\right) J_0(\gamma v_0)\, dv_0 dv \ , \tag{A-80}$$

where $f(v) = \frac{v^2}{\sigma^2} \nu_m(v) \exp(-\frac{v^2}{2\sigma^2})$, and the order of integration for the left side has been reversed.[34]

Using Equation A-79, setting $\nu = 0$, $\alpha = \frac{1}{2\sigma^2}$, and $x = v_0$, the inner left side integration is evaluated, and Equation A-80 becomes

$$\int_0^\infty v_0^2 T(v_0) J_0(\gamma v_0)\, dv_0 = \sigma^2 \int_0^\infty f(v) \exp\left[\frac{v^2}{2\sigma^2} - \frac{\sigma^2 \gamma^2}{2}\right] J_0(\gamma v)\, dv$$

$$= \exp\left(-\frac{\sigma^2 \gamma^2}{2}\right) \int_0^\infty v^2 \nu_m(v) J_0(\gamma v)\, dv \ . \tag{A-81}$$

It is then noted that both sides of Equation A-81 involve the Hankel transform defined as

$$H_{yx}\{f(x)\} = \int_0^\infty x f(x) J_0(xy)\, dx \ . \tag{A-82}$$

Thus, Equation A-81 may be written as

$$H_{uv}\{vT(v)\} = \exp\left(-\frac{\sigma^2 u^2}{2}\right) H_{uv}\{v\nu_m(v)\} \ . \tag{A-83}$$

The inverse Hankel transform has exactly the same form as the direct transform, so that the solution of A-83 for $\nu_m(v)$ is

$$\nu_m(v) = \frac{1}{v} H_{vu} \left\{ \exp\left[\frac{\sigma^2 u^2}{2} \right] H_{uv} \{vT(v)\} \right\} . \qquad \text{(A-84)}$$

The formal solution of Equation A-84 is straightforward, involving numerical integration. As a practical matter, however, special care must be taken to avoid numerical errors which may lead to large errors in the calculation of ν_m. The functional form of T(v) must be artificially defined for large values of v to insure the convergence of the infinite integral. A discussion of the numerical techniques necessary to obtain an accurate solution for ν_m is presented in Chapter V.

APPENDIX VII

SAMPLE CALCULATION OF THE TRANSIENT RESPONSE DECAY RATE

In this appendix the procedure for calculating the transient response decay rate from the experimental data will be demonstrated.

The following are the experimental conditions of the sample measurement:

Pressure reading from Schulz-Phelps gauge: 4×10^{-2} Torr.

Microwave Pulse attenuation setting: 9.0 dB.

The output of the logarithmic amplifier is described analytically by

$$v_{out} = \log_{10} \left(\frac{v_{in}}{v_{ref}} \right) \quad V \quad .$$

The input voltage has the form

$$v_{in} = v_0 \exp[-2\nu t] \quad ,$$

where ν represents the total decay of the transient response envelope, including the residual decay. The factor 2 comes from the square-law detection process.

Therefore, v_{out} is given by

$$v_{out} = -2\nu t \log_{10}(e) + \log_{10} \left(\frac{v_0}{v_{ref}} \right) \quad .$$

The time derivative of v_{out} is

$$R = \left.\frac{dv_{out}}{dt}\right|_{t=0} = -2 \log_{10}(e)\nu \ ,$$

so that ν is given by

$$\nu = -\frac{1}{2} \ln(10) R$$

$$= -1.1513R \ sec^{-1}$$

The following values of $|R|$ were obtained graphically from the photographs of the logarithmic amplifier output voltage displayed on an oscilloscope:

Run Number	Measured Slope (10^6 V/sec)
1	1.78
2	1.82
3	1.83
4	1.82
5	1.79

The residual decay rate measured at a gas pressure of 5×10^{-3} Torr is 1.01×10^6 sec^{-1}.

The average measured slope is

$$R = \frac{1}{5}(1.78 + 1.82 + 1.83 + 1.82 + 1.79)$$

$$= 1.808 \times 10^6 \ V/sec \ .$$

The correction for the residual decay is

$$R_0 = 1.808 - 1.01$$

$$= 0.807 \times 10^{6} \text{ V/sec.}$$

The transient response decay is

$$\nu = (1.1513)(0.807)$$

$$= 0.929 \times 10^{6} \text{ sec}^{-1}.$$

The pressure correction is

$$p = (0.95)(4 \times 10^{-2} \text{ Torr})$$

$$= 3.8 \times 10^{-2} \text{ Torr.}$$

Normalizing the transient response decay rate to 1×10^{-3} Torr and 0°C:

$$\nu_0 = \left(\frac{1.0 \times 10^{-3} \text{ Torr}}{3.8 \times 10^{-2} \text{ Torr}}\right)\left(\frac{303°K}{273°K}\right)(0.929)$$

$$= 2.7 \times 10^{4} \text{ sec}^{-1}.$$

The electron velocity corresponding to this value of transient response decay is calculated according to the formula

$$v = 10.12 \times 10^{(I/20)} \text{ cm/sec}$$

where I is the value of the pulse attenuation setting. In this example I = - 9 dB,

$$v = 10.62 \times 10^{(-9/20)}$$

$$= 3.77 \times 10^{7} \text{ cm/sec.}$$

BIBLIOGRAPHY

1. E. W. McDaniel, Collision Phenomina in Ionized Gases (John Wiley and Sons, Inc., New York, 1964), Chaps. IX, X.

2. J. M. Anderson and L. Goldstein, Phys. Rev. 100, 1037 (1955).

3. J. F. Denisse and J. L. Delcroix, Plasma Waves (Interscience Publishers, New York, 1963), Chap. I.

4. E. W. McDaniel, op. cit., Chap. IV.

5. H. S. Glick and T. G. Jones, AIAA Journal 7, 4 (1969).

6. C. Ramsauer, Ann. Physik 64, 513 (1921).

7. J. S. Townsend, and V. A. Bailey, Phil. Mag. 43, 593 (1922).

8. David Park, Introduction to the Quantum Theory (McGraw-Hill Book Co., Inc., New York, 1964), Chap. IV.

9. L. I. Schiff, Quantum Mechanics, 3rd ed. (McGraw-Hill Book Co., Inc., New York, 1955), Chap. IX.

10. T. F. O'Malley, Phys. Rev. 130, 1020 (1963).

11. D. E. Golden, Phys. Rev. 151, 48 (1966).

12. B. Bederson and L. J. Kieffer, Rev. Mod. Phys. 43, 601 (1971).

13. D. E. Golden and H. W. Bandel, Phys. Rev. 138, A14 (1965).

14. C. Ramsauer and R. Kollath, Ann. Physik 3, 536 (1929).

15. L. S. Frost and A. V. Phelps, Phys. Rev. 136, A1538 (1964).

16. R. W. Crompton, M. T. Elford, and R. L. Jory, Australian J. Phys. 20, 369 (1967).

17. A. V. Phelps, O. T. Fundingsland, and S. C. Brown, Phys. Rev. 84, 559 (1951).

18. L. Gould and S. C. Brown, Phys. Rev. 95, 897 (1954).

19. H. Margenau, Phys. Rev. 69, 508 (1946).

20. R. Tice and D. Kivelson, J. Chem. Phys. 46, 4743 (1967).

21. R. L. Bruce, F. W. Crawford and R. S. Harp, J. Appl. Phys. 39, 2088 (1968).

22. R. L. Bruce and J. M. Larsen, J. Appl. Phys. 42, 895 (1971).

23. L. Spitzer, J., Physics of Fully Ionized Gases (John Wiley and Sons, Inc., New York), Chap. V.

24. P. E. Vandenplas, Electron Waves and Resonances in Bounded Plasmas (Interscience Publishers, New York, 1968), Chap. I.

25. E. W. McDaniel, op. cit., p. 732.

26. R. S. Burington and D. C. May, Jr., Handbook of Probability and Statistics with Tables, 2nd ed. (McGraw-Hill Book Co., Inc., New York, 1970).

27. A. Papoulis, Probability, Random Variables, and Stochastic Processes (McGraw-Hill Book Co., Inc., New York, 1965), Chap. VII.

28. G. J. Schulz, Phys. Rev. Letters 10, 104 (1963).

29. L. Spruch, T. F. O'Malley, and L. Rosenberg, Phys. Rev. Letters 5, 347 (1960).

30. R. C. Ajmera and H. Lashinsky, Appl. Phys. Letters 13, 96 (1968).

31. R. F. Harrington, Time-Harmonic Electromagnetic Fields (McGraw-Hill Book Co., Inc., New York, 1961), Chap. VII.

32. E. O. Schulz-DuBois, J. Appl. Phys. 44, 2411 (1973).

33. I. S. Gradshteyn and I. M. Ryzhik, Table of Integrals, Series, and Products (Academic Press, Inc., New York, 1966), p. 718.

34. T. M. Apostol, Mathematical Analysis (Addison-Wesley Publishing Co., Inc., Reading, Mass., 1957), Chap. XIV.

35. R. E. Collin, Field Theory of Guided Waves (McGraw-Hill Book Co., Inc., New York, 1960), Chap. V.